THE SPECTRAL ANALYSIS OF THE SPONTANEOUS EMISSION OF MIT'S 8.8 mm, ROOM TEMPERATURE, PULSED FREE ELECTRON LASER MICROWIGGLER

by

James C. Blastos

B.S., United States Military Academy (1985)
MBA, Chaminade University (1991)

Submitted to the Department of Physics
in Partial Fulfillment of the
Requirements for the
Degree of

MASTER OF SCIENCE IN PHYSICS

at the

MASSACHUSETTS INSTITUTE OF TECHNOLOGY

May 27, 1994

Signature of Author _____
Department of Physics
May 6, 1994

Certified by _____
George Bekefi, Professor of Physics
Thesis Supervisor

Accepted by _____
George F. Koster
Chairman, Departmental Graduate Committee

THE SPECTRAL ANALYSIS OF THE SPONTANEOUS EMISSION OF MIT'S 8.8 mm, ROOM TEMPERATURE, PULSED FREE ELECTRON LASER MICROWIGGLER

by

James C. Blastos

Submitted to the Department of Physics
on May 6, 1994, in partial fulfillment of the
requirements for the Degree of
Master of Science in Physics

ABSTRACT

This thesis is the initial study of the spontaneous emission from MIT's microwiggler conducted at Brookhaven National Laboratory on the Accelerator Test Facility's 50 MeV linear accelerator. The microwiggler consists of 70 8.8 mm period electromagnets in a planar array. This study examines the microwiggler's spontaneous emission spectrum, spectral broadening mechanisms, and potential future refinements in technique and equipment, which will ultimately lead to the microwiggler's lasing in the visible and ultraviolet ranges.

Thesis Supervisor: Dr. George Bekefi

Title: Professor of Physics

ACKNOWLEDGMENTS

No man is an island. All good things in life come from the help and generosity of many; this paper - my work at MIT - is no exception. I would not even have made it to the project without the help of CPT Bill Howard during my first year of school. I could not have written this without Dr. George Bekefi's invitation to join this project and his assistance throughout. I could not have produced any of the experimental work without the help of the fine folks at the Accelerator Test Facility at Brookhaven National Laboratory. Many thanks to Dr. X.J. Wang, Marc Montemagno, Bill Cahill, and especially Cyrus Biscardi. Dr. Alan Fisher stands out for his guidance, patience, and devotion to this project.

I tested the patience of many people during this project. My gratitude to Dave Sisson for his help on the conduct and analysis of the data and to Ivan Mastovsky for his technical expertise in the procurement of the supporting equipment.

My highest appreciation goes to Dr. Rick Stoner. From start to finish, he helped me learn the equipment, computer control, basic theory, data analysis, and just about everything else associated with this project. Few people work as hard and as intensely as he does.

An unusual thank you goes to the great people of the United States and to United States Army. For thirty years, they have housed, fed, and educated me. There are no finer people than those with whom I have served and met during my adventures with the Army.

Always there, through thick and thin, is my family - my parents, sister, and relatives, especially, Jean Blastos. Their unwavering encouragement and prodding con-

tinue to propel me. No son has better support and love than I have had.

BEAT NAVY

TABLE OF CONTENTS

CHAPTER I

INTRODUCTION

Free electron lasers are a relative new comer to the realm of laser physics. In 1951, Hans Motz first developed the theory for free electron lasers, though he did not use that term. The theory was an outgrowth of his investigation of spontaneous emissions from relativistic electrons passing through a device of alternating magnet fields[1]. In 1958, Phillips developed the *ubitron*, which was an acronym for *u*ndulating *b*eam *I*nteraction elec*tron* tube[2]. Its significance was that the ubitron created coherent emission from modulation of mildly relativistic electrons, producing radiation in the 10 cm microwave range, and validated the points made by Motz. Most of the interest in free electron lasers faded due to the advent of the laser in the early '60s.

In 1971, Madey developed a theory that an undulator could be an amplifier for visible radiation and coined the term *free electron laser*. The term acted as a mnemonic device to relate the function of the FEL to something already understood. Similar to Dirac and Kapitza's work in 1933 on the Stimulated Compton Effect, Madey argued, through quantum mechanical analysis, that the undulator field and the electrons would interact through stimulated Compton scattering, thus creating an amplifier of coherent radiation.[3]

Around 1976, Stanford researchers created a coherent beam in the 10.6 μm range using a helical undulator. The interest in FELs exploded. The primary advantage of this new type of device is that FELs are widely tunable from microwaves up to, po-

---

[1] Marshall, p. 15.
[2] Luchini, p. 21.
[3] Luchini, p. 23.

tentially, X-rays. For the past twenty years, much work in the field of free electron lasers has been done, with the latest studies focusing on very short wavelength radiation, higher power, and miniaturization of wiggler systems.

There are two main classes of wiggler structures - planar and helical. This experiment uses a planar wiggler in which the alternating sets of magnets are lined up on one side of the beam path with a corresponding row of magnets on the other side.

The term *free electron laser* is somewhat misleading, for the FEL is not a true laser as a solid state physicist would see it. Rather than creating light through the stimulated orbital transition of electrons in atoms, a FEL's coherent radiation originates from the interaction between an electromagnetic wave and relativistic, unbound electrons. While this interaction is still stimulated emission, the process that creates the FEL's interacting electromagnetic field is a variant of synchrotron radiation[4].

Electrons enter into a device, called a wiggler[5], where an arranged, periodically alternating set of magnets cause the electrons to oscillate sinusoidally as they move through the device. When the electrons oscillate, they emit radiation. This radiation is incoherent spontaneous emission for a wiggler. The frequency and angular dispersion of that radiation depend primarily on:

1. the electrons' momentum,
2. the electron beam's cross section and point of application,
3. the device's internal magnetic field, and
4. the angle from which the interaction is observed.

The electron feels the pondermotive force, given by $\vec{F} = \vec{E}_{rf} \times \vec{B}$, causing faster elec-

[4] Sometimes referred to as magnetoBremstaahlung.
[5] The difference between a wiggler and an undulator is a distinction between the K_w between them (or a_w by some authors). K_w is the wiggler parameter, discussed later. An undulator has a value of K_w which is greater, usually much greater, than 1; a wiggler is less that 1.

trons to slow and slower electrons to speed up. The net results is the creation of electron bunches which begin to act as one, emitting coherent light.

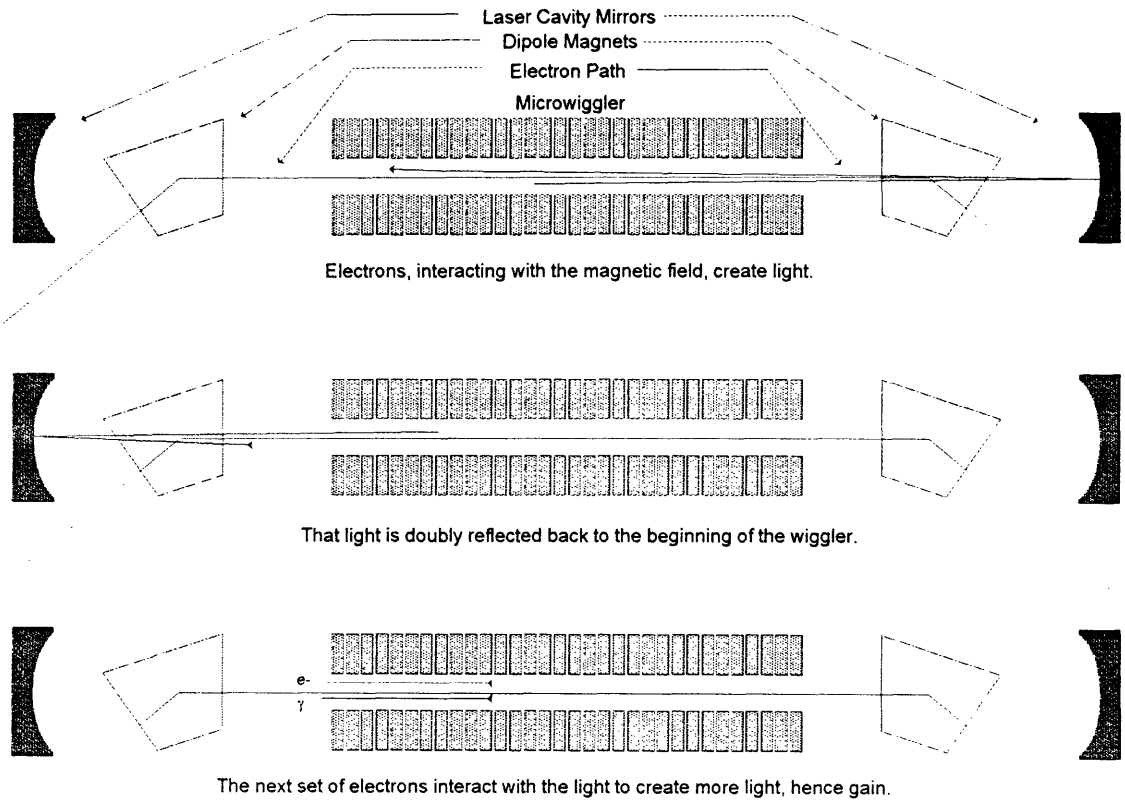

Figure 1 Electron/Wiggler Diagram

To increase the gain of the light, the radiation double-reflects back through the system so that the light is once again going in the same direction of the electrons as seen in Figure 1. Entering into the wiggler simultaneously, the radiation and electrons interact. Repeated a few times, the gain in signal increases quickly.[6] With innovative design, the wiggler can produce higher gain and shorter wavelengths. This is the concept of free electron lasers. This study focuses on the analysis of the spontaneous emission as observed in the absence of the mirrors.

[6] Single pass, high gain FEL's have been made, however, the design of that kind of wiggler is different from the MIT wiggler. So to prevent confusion, I will omit the discussion of high gain systems.

One of the leading-edge areas under study is the short period wiggler. Built by Dr. Richard E. Stoner as a graduate student, the MIT microwiggler, shown in Figure 2, is the focus of this experiment. The wiggler consists of 70 sets of electromagnets, spaced 8.8 mm apart in a planar array. Each magnet is individually tunable to allow for magnet field tailoring for uniformity. It produces a peak on-axis field of 4.3 kilogauss pulsed at 0.5 Hz. A computer controlled charging and firing system provides the wiggler with 14 kiloamps (peak) of current during each pulse. An internal cooling system maintains the wiggler at a constant operating temperature.

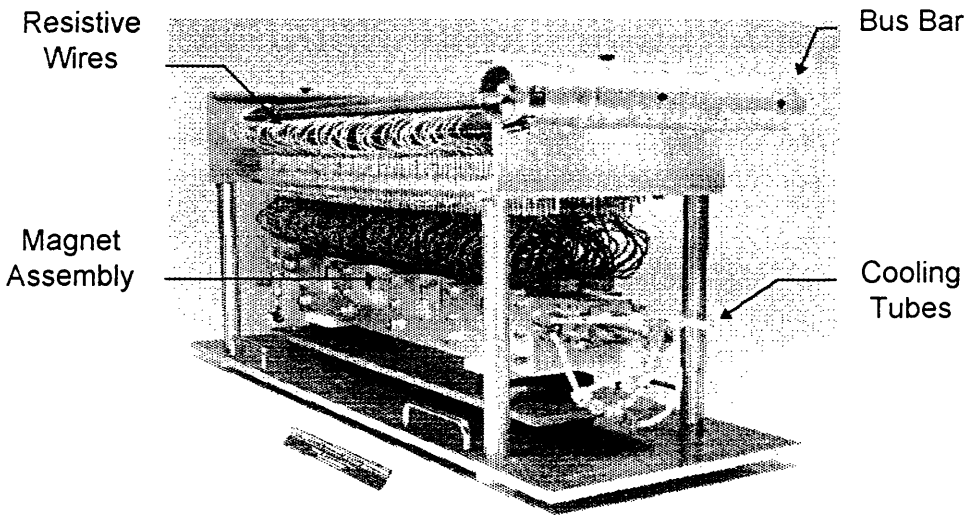

Figure 2 - The MIT Microwiggler

This analysis of the initial spontaneous emission from this device is the first of many studies on the wiggler's road to lasing in the visible and ultimately ultraviolet wavelengths. The enclosed results came from an experiment on January 13, 1994, at the Accelerator Test Facility [ATF] at Brookhaven National Laboratory, Upton, NY.

The ATF is a new high brightness, low emittance linear accelerator. It uses a frequency-quadrupled YAG-laser beam to illuminate a magnesium photocathode in a 100 MeV/m cathode acceleration chamber. The electrons pass through two accelerat-

ing cells to accelerate the electrons to a design momentum of 50 MeV. A series of beam optical controls and dipoles direct the electrons to one of the three available beamlines in the ATF.

For the MIT wiggler, the electrons travel down beamline #3, passing through a turning dipole (directing the electrons into the wiggler's drift tube), through the wiggler, through a second dipole (pulling the electrons out of the optical path), and into a beam dump. The light created by the electrons travels out of the downstream side of the wiggler, through a series of mirrors and lenses, and to a set of measuring devices in another room.

This thesis covers the initial spontaneous emission study from MIT's microwiggler as we prepare to make it into a free electron laser [FEL]. The purpose of the study is in three parts: 1) to determine if the wiggler is acting properly, 2) to use the data for electron beam diagnostics, and 3) to examine the spectral broadening mechanisms. Our conclusions are that the wiggler creates light in the region where it should, that with improvement of beam transport to the wiggler the spontaneous emission could be used to determine the emittance and charge of the electron beam, and that the principal broadening mechanisms in this experiment are the coupled effects of off-axis emission and energy spread.

The following chapters begin with the underlying theory of spontaneous emission of light from the wiggler. Next is an explanation of the experimental setup and transport system, followed by the presentation of the results from the experiment. Later I will analyze the results in reference to different spectrum broadening mechanisms followed by the conclusions from the analysis. Finally, I will examine the next steps towards lasing of this device.

The future is bright for this experiment. The wiggler will most likely lase in the visible range and ultimately in the ultraviolet range. By incorporating the lessons learned in making this FEL lase, future experiments at the ATF will enjoy the fruits of the labor put into this device.

CHAPTER II

EXAMINATION OF THE THEORY[7]

The focus of this chapter is the examination of the theoretical relationships between the emission parameters. In particular, we'll examine the aspects of the parameters that would lead to spectral broadening.

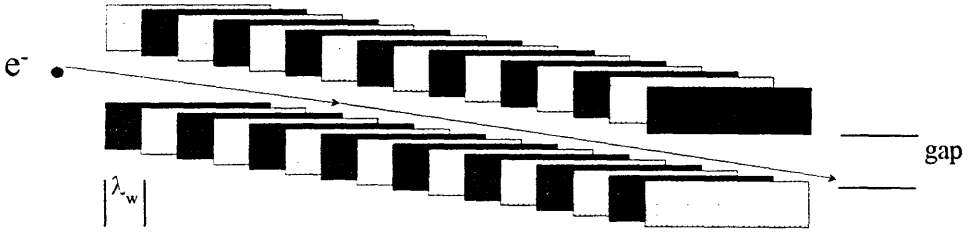

Figure 3 - Wiggler Schematic

Simply stated, due to an electron's forward motion through a fixed array of alternating north-south magnets, the electron feels a force - the Lorentz Force, $\vec{F} = q\vec{v} \times \vec{B}$.

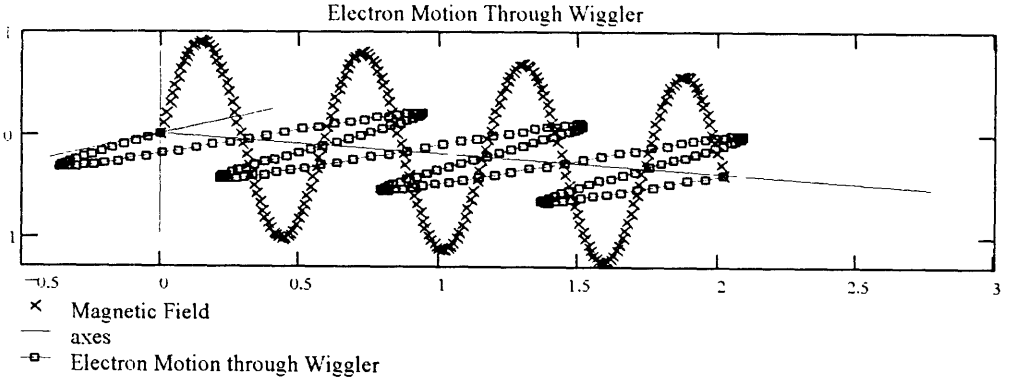

Figure 4 - Electron Motion through the Wiggler

The magnetic field $\vec{B}$ has a vector potential,[8] $\vec{A}_w = \sqrt{2}A_w \sin k_w z\, \hat{x}$ for $0 < z < L_w$. The resultant magnetic field is $\vec{B}_w = \nabla \times \vec{A}_w = \sqrt{2}A_w k_w \cos k_w z$. The Lorentz force causes

[7] All units are in MKS.
[8] Brau, 65.

the electron to oscillate perpendicular to the magnetic field, in this case the X-Z plane. This motion is depicted in Figure 4. The electron's oscillation causes it to emit light tangent to its path in a continuous spectrum, known as synchrotron radiation. The radiation created becomes peaked at one frequency and projected into a $1/\gamma$ narrow cone[9], as in Figure 5. Since the electrons oscillate in the X-Z plane, they project polarized light into the cone.

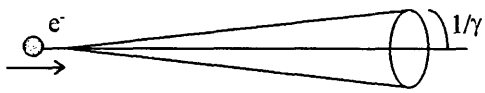

Figure 5 ($1/\gamma$ cone diagram)[10]

This is the spontaneous emission and is the basis for free electron lasers.

We are primarily concerned with the spontaneous emission from the wiggler. JD Jackson's *Electrodynamics* contains the derivation from Maxwell's equations to the spectral fluence equation. The spectral fluence, stated as the energy per unit solid angle for a given frequency range, is[11]

$$\frac{d^2I}{d\Omega d\omega} = \frac{e^2\omega_L^2}{16\pi^2\varepsilon_o c^3}\left|\int_{-\infty}^{\infty}\vec{n}\times(\vec{n}\times\vec{v})e^{i\left(\omega_L t - k_L\vec{n}\cdot\vec{r}\right)}dt\right|^2$$

where $\vec{v}(t)$ is the electron's velocity, $\vec{r}(t)$ is the electron's position, ω_L is the emitted frequency of the radiation, $\vec{n}$ is the unit vector, and k_L is the radiation's wave number. The solution to this equation yields the spontaneous spectrum.

---

[9] JD Jackson, p. 665

[10] where $\gamma = \frac{1}{\sqrt{1-\beta^2}}$.

[11] JD Jackson, *Classical Electrodynamics*, Second Edition (Wiley, New York, NY, 1975), page 671. Adjusted for MKS system.

One of the primary parameters, known as the wiggler parameter, is a_w[12]. It is defined as

$$a_w = a_{w0}\left[1+\frac{(k_w y)^2}{2}\right],$$

where $a_{w0} = \frac{eB_{w0}}{m_e c k_w}$ is the fundamental wiggler parameter, B_{w0} is the magnetic field on axis, y is the displacement from the wiggler's axis, and θ is the off axis observation angle in the coordinate system shown in Figure 6. The term, $1+\frac{(k_w y)^2}{2}$, allows for the variation of B_w with distance y from the axis of symmetry.

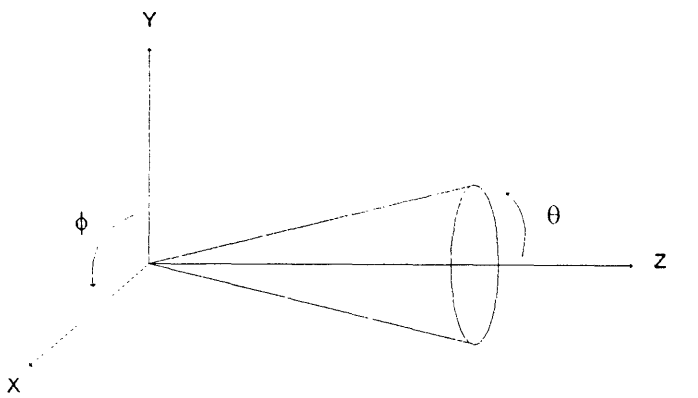

Figure 6 - Reference Coordinate System

The equation for a_w comes from the expression of a_{w0}. The magnetic field inside the wiggler increases approximately as the square of the distance y as we move away from the axis. From the expression,

$$a_w(y=0) = \frac{eB_{w0}}{m_e c k_w} = a_{w0} \text{ and } \bar{B}_w(y) \propto 1+\frac{(k_w y)^2}{2}, \text{ then}$$

[12] Also known as K_w.

$$a_w(y) = a_{w0}\left(1 + \frac{(k_w y)^2}{2}\right).$$

Note that in the expression for a_w, a reduction in the wiggler period must be met with a proportional gain in the magnetic field strength in order to maintain the same value for a_w. Thus, a sub-centimeter wiggler period device, like the MIT microwiggler, requires a large magnetic field. An advantage for a small value of a_w is that the emitted radiation is primarily monochromatic, while wiggler's with a_w larger than 1 tend to be rich in harmonics.[13] However, the big disadvantage is that the FEL gain varies as a_w^2, so at lasing we need a large a_w. The large field requires precise control over the field's uniformity in order to prevent beam steering through the small gap in the wiggler. Such steering would exacerbate betatron oscillations and may lead to electron beam breakup as the beam becomes steered into the walls of the waveguide.

The total path length of the light observed depends on the direction from which it is viewed. As the electron oscillates, the perpendicular component of the electron's

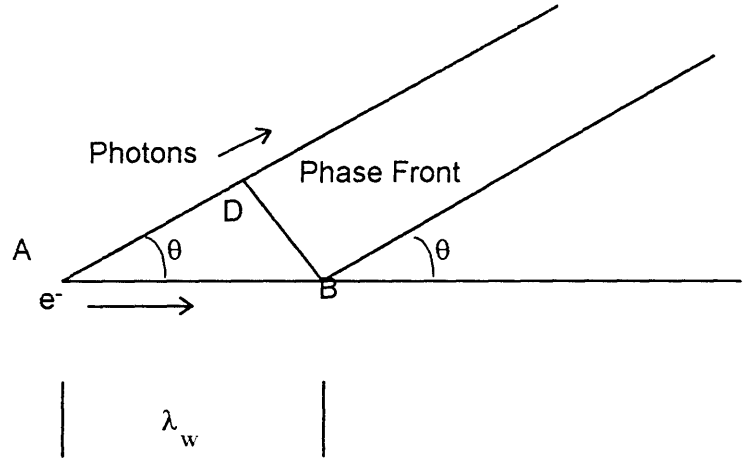

Figure 7 - Angular Dependence of Viewing Angle for Radiation[14]

motion varies. If viewed along the line of propagation of the electron through the wig-

[13] Pelligrini, p.357.
[14] Luchini, p.3.

gler, the radiation is just barely outrunning the electron. Thus, the light observed has a shorter wavelength than if we observe the light off the propagation path.

As the electron proceeds from A to B with the axial velocity of $\beta_{\|} \equiv \frac{v_{\|}}{c}$ and we observe the emitted radiation at the angle of θ, we must consider the formation of a phase front as in Figure 7. The condition for such a front is that the wavelength of light created must be in an integer multiple of the wave period. The path length difference for the Doppler shifted wavefronts becomes

$$\begin{aligned} L &= d_{rad} - d_e \\ &= \frac{N\lambda_w}{\beta_{||}} - N\lambda_w \cos\theta_e \end{aligned}$$

The emitted wavelength becomes

$$\begin{aligned} \lambda_e &= \frac{L}{N}, \text{or} \\ &= \lambda_w \left(\frac{1}{\beta_{||}} - \cos\theta_e \right). \end{aligned}$$

Since $\gamma = \frac{1}{\sqrt{\left(1-\beta^2\right)}}$ and $\beta^2 = \beta_{\|}^2 - \frac{a_w^2}{\gamma^2}$,

$$\lambda_{rad} = \frac{\lambda_w}{2\gamma^2}\left(1 + \frac{a_w^2}{2} + \gamma^2\theta^2\right),$$

where θ is the angle between the direction of observation and the electron's trajectory. Notice that the wavelength is inversely proportional to γ^2. A 1 MeV from a 40 MeV beam shift in momentum results in a 14 nm resonant wavelength shift. Additionally, λ_{Rad} depends on θ^2. The effects are these:

1. a shift in beam momentum will have large impacts on the resonant wavelength,
2. viewing the emitted radiation from other than on axis will cause a quadratic departure in emitted radiation, and
3. moving the beam off axis and propagating the electron parallel to the axis will also cause a quadratic shift in the wavelength.

Both the spread in transverse beam momentum and its physical cross section can be expressed in terms of the emittance ε of the electron beam. It is the phase space volume of the beam in all four dimensions of phase space. Ideally, we want the phase space volume to be as small as possible and will yield a very narrowly peaked spectrum at the resonant frequency.

On the other hand for spontaneous emission, off-axis emission cannot be avoided since we must have a physical collection system for the light. There will be a minimum collection solid cone. When lasing, this problem becomes less of an issue since the cavity will be tuned for a particular wavelength. Thus, spectral narrowing is indicative of gain.

When we examine the effects of viewing the emitted radiation off axis ($\theta > 0$), the spectral fluence (total energy per unit solid angle projected in θ per unit frequency interval) evolves to[15]

$$\frac{d^2W}{d\omega d\Omega} = \frac{e^2 a_w^2 \gamma^2 N_w^2}{2\pi\varepsilon_o c\left(1+\frac{a_w^2}{2}+\gamma^2\theta^2\right)}\left[\frac{\sin\left(\pi N_w \frac{\delta\lambda}{\lambda_R}\right)}{\pi N_w \frac{\delta\lambda}{\lambda_R}}\right]^2 F(\alpha,\xi), \text{ where}$$

[15] Brau, pp. 64 - 73.

$$F(\alpha,\xi)=\left[\sum_{k=-\infty}^{\infty}(-1)^k J_{2k}(\alpha)\left[J_k(\xi)-J_{k+1}(\xi)\right]\right]^2$$

$$\alpha=\frac{2^{1.5}a_w\gamma\theta\cos\phi}{1+\frac{a_w^2}{2}+\gamma^2\theta^2}$$

$$\xi=\frac{1}{2}\frac{a_w^2}{\left(1+\frac{a_w^2}{2}+\gamma^2\theta^2\right)},\text{and}$$

$$\delta\lambda=\lambda_L-\lambda_R$$

The expression for $\delta\lambda$ is the difference in wavelengths between the resonant wavelength as given by $\lambda_{rad}=\frac{\lambda_w}{2\gamma^2}\left(1+\frac{a_w^2}{2}+\gamma^2\theta^2\right)$ and a wavelength in the spectral range under consideration. If the electron beam is monenergetic and on axis (θ=0), the spectrum, depicted in Figure 8, takes on the form of a $\frac{\sin x}{x}$ function centered at the resonant frequency for that beam energy. The full width, half maximum [FWHM] is

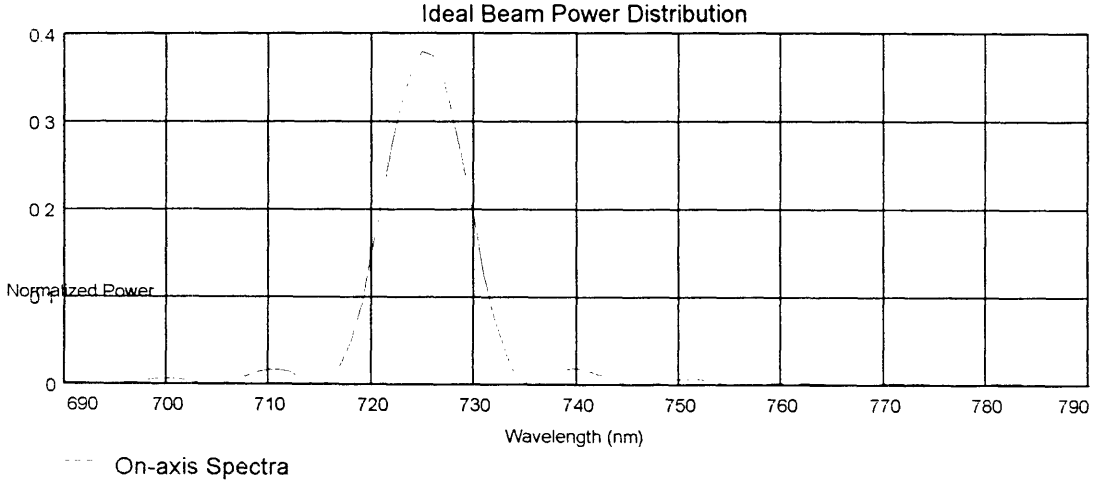

Figure 8 - On-Axis Spectrum at 41 MeV

$\Delta\lambda \approx \frac{1}{N_w}\lambda_{resonant} \approx 10\,nm$ [16], where N_w is the total number of wiggler periods (70). The line broadening is due to the transit time effects resulting from the finite length of time the electron spends in the wiggler.

The effect of off-axis emission is not subtle and in fact is the largest contributor to spectral broadening. In the graph below (Figure 9), we can see the effect of collecting light from on axis to a 4 mrad cone causes tremendous broadening in our area of concern for this experiment.

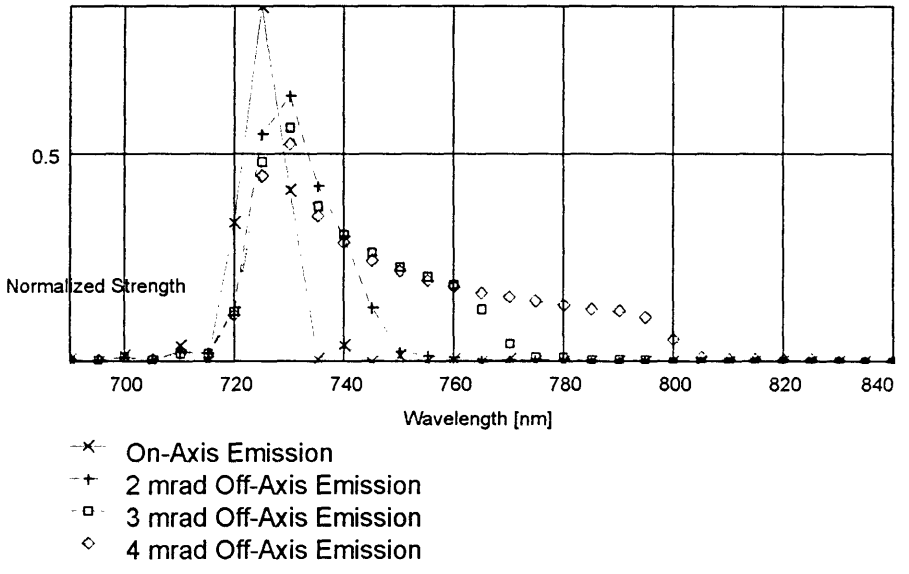

Figure 9 - Spectral Broadening Due to Size of Collection Cone

The red shift originates in the quadratic relations in λ_{rad} and a_w. The shifting occurs as a superposition of $\frac{\sin x}{x}$ spectra where each one has a different value of θ or γ. The effect of emittance and energy spread on the linewidth can be expressed by

[16] Murphy, p. 22.

$$\Delta\lambda = \left[\frac{2\Delta\gamma}{\gamma} + \frac{a_w^2}{1+\frac{a_w^2}{2}}\Delta B + \frac{\gamma^2\theta^2}{1+\frac{a_w^2}{2}} \right] \lambda_{resonant} \approx 60\,nm \,^{17},$$

where $\Delta B=0.12\%$ is the magnetic field error. Chapter IV highlights this effect.

We may wonder how the motion of the electron as it travels through the wiggler may affect the spectrum due to its shifting in the x-z plane due to the Lorentz force. The maximum amplitude of the oscillation for our parameter is

$$x = \sqrt{2}\frac{a_w}{\gamma k_w}\cos k_w z \approx .008\,mm.$$

Clearly the electron moves very slightly in the x-z plane laterally off axis, such that it will not effect a_w.

The matter of emitted power is important from our point of view since it is a direct measure of beam charge, Q. The energy created during the interaction is[18]

$$P = \frac{a_w^2 N_e \gamma^2 I}{\lambda_w}$$

$$E = \int P dt = \frac{a_w^2 N_e \gamma^2 I}{\lambda_w} Q = .511 Q \frac{Joules}{Coulomb}$$

Working backwards through the measuring system, we can estimate the amount of charge in the beam. The spontaneous emission could be used as a diagnostic test to determine, though not as accurately as a Faraday cup, the electron beam charge. Emittance measurements through spectral analysis may also be possible but requires

[17] Pellegrini/USPAS notes.
[18] Stoner

more examination for the relations of the different parameters involved.

CHAPTER III

EXPERIMENTAL SETUP

This chapter outlines the major components of the wiggler experiment. These components are:

1. The Microwiggler
2. The Computer Control System
3. The Electrical System
4. Optical Transport System
5. Measuring System, and
6. The Linear Accelerator.

The experiment was in the Accelerator Test Facility inside the experimental hall. The wiggler, cooler, and capacitor bank were in the experimental hall, and the computer, measuring equipment, and personnel were in the FEL room as shown below in Figure 10.

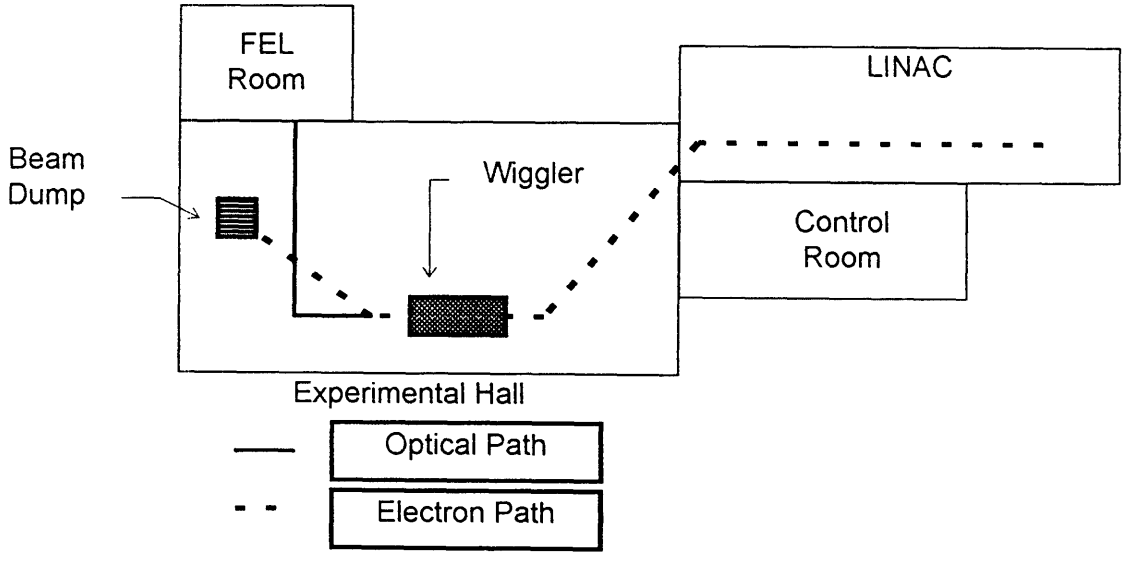

Figure 10 - Experimental Hall Overview

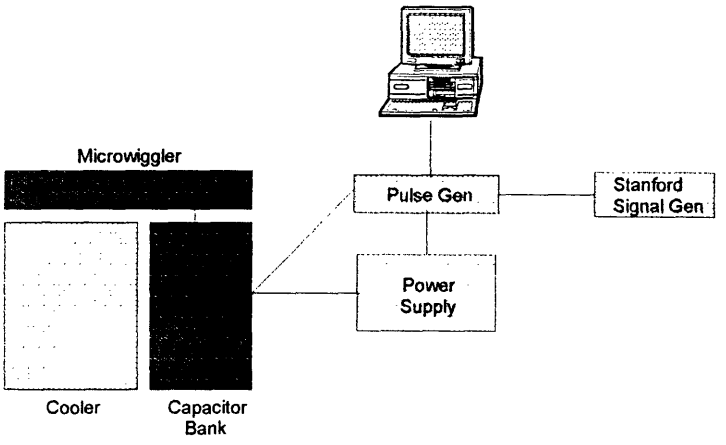

Figure 11 Microwiggler Equipment Diagram

3.1 The Microwiggler

The heart of this FEL system is the microwiggler. Table 1 shows the wiggler's parameters. Built by Dr. Richard E. Stoner, the wiggler [see Figure 2] consists of 70 periods of 8.8 mm period, tunable electromagnets. The magnetic field ends of the wiggler are tapered to allow for smooth electron transition into the wiggler without steering the electrons' path through the system.

Each magnet is tunable via the resistive wires coming from the common bus bar to the individual magnets. By adjusting the length of the resistive wire for each magnet, we can affect the current applied to each magnet. A computer program measures the unadjusted field and calculates the adjustments necessary to obtain a more uniform field. When tuning was complete, this feature allowed the measured magnet field consistency through the wiggler to be made uniform to ±0.12% rms[19].

There is a 3 mm by 5 mm K_a waveguide which runs the length of the wiggler and serves as the bore of the wiggler. Since this is a pulsed system, the wiggler is

[19] Sisson.

cooled via conductive water channels built into the wiggler block. Water circulates through a commercial refrigerating recirculation unit, where the water temperature is kept at 4° C (40° F).

PARAMETERS	VALUE
Magnet Period, λ_w	8.8 mm
Wiggler Length, L_w	.62 m
Peak Magnetic Field	.43 T
Magnetic Field Errors	±.12% rms
Repetition Rate	1/2 Hz
K_w (on axis)	.329

Table 1 - Wiggler Parameters

3.2 The Computer Control System.

The system is computer controlled - from the measurement of the wiggler magnetic field to the control of the wiggler's current during the experimental run. Operated from the wiggler's IBM-compatible 386 computer, the controlling program[20] receives system measurements of current applied to the wiggler (measured by means of a Rogowski coil on one of the bus bars). It portrays the results on the computer monitor as a time function histogram of peak current and actual shot waveform measurements. Using a moving average of peak current applied to the wiggler, the computer controls and adjusts the voltage applied to the pulsing capacitor bank to maintain a consistent magnetic field inside the wiggler with little shot-to-shot jitter. This monitoring and adjust-

[20] written in Pascal by Dr. Stoner,

ing process is important because as the wiggler and capacitors warm up due to resistive heating, the current applied to the magnets changes.

The computer also can measure the magnetic field as a function of position within the wiggler. When the wiggler is not in the beam line, we can insert a B probe into the bore of the wiggler. Attached to a computer controlled stepper motor, the probe, a hand-wound inductive coil on the end of a meter-long rod, travels down the bore of the wiggler while the computer pulses the wiggler. By attaching the probe coil leads to the computer, we can measure the field as a function of position. The computer steps the probe through the entire length of the wiggler taking field measurements along the way. After five complete cycles of field measurements (to help reduce random measurement errors), we put the field data through another computer program which told us how much each of the individual magnet's wire leads needed to be shortened or lengthened to make the magnetic field more uniform. The resistance adjusting program takes into account the fact that by adjusting the strength of one magnet, it effects the field in the adjacent few magnets as well. The adjusting program takes that effect into account via a matrix transformation. We repeated the process until we were satisfied with the field uniformity.

During the tuning process we discovered one of the wiggler's magnets was defective. Period 34's magnet cannot create enough field even with zero tuning resistance. Replacing the magnet required too much time and was not prudent to do so at that time. In order to feed it more current, we connected a direct line to that magnet from the beginning of the bus bar. By bypassing some of the resistivity of the bus bar, we increased the current applied to the magnet. Although this helped, it did not completely eliminate the problem. Accordingly, we adjusted its neighbor to compensate for

the field anomaly so that the steering error induced by the weak field of magnet 34 would not steer the electrons off axis as they pass by.

3.3 The Electrical System

The wiggler's electric system consists of a large bank of capacitors, an inductor, SCR, and bus bar to the wiggler magnets. The capacitor bank consists of four levels of sixteen aluminum capacitors each arranged in parallel. The total capacitance is 10 mF. These aluminum electrolytic capacitors are usually limited to less than 450 volts because they begin to break down at around 500 volts. By arranging the capacitors in parallel, we can operate them at a lower voltage and still draw the nearly 600 volts required for the magnet's operation[21]. Due to thermal limitations, the capacitors can operate no faster than 0.5 Hz, therefore the pulsing rate for the wiggler is also 0.5 Hz.[22] Charged from a commercially made, computer controlled power supply, the capacitor bank receives its cooling from two fans which force air to flow around the capacitors. A computer triggered SCR sets the discharge in motion. The discharge current from the capacitors flows to a torroidal inductor (10 mH) to the bus bar to the wiggler. The LCR circuit allows for a long 880 μsec pulse. The diode leaves the capacitor bank in a positive state so that the power supply does not have to work as hard and to extend the life of the capacitors. The peak current is 14 kiloamps lasting over ≈20 μsec. Future upgrades to the system will eliminate the bulky bank with a new set of four large capacitors, hooked in series, which will provide better shot-to-shot stability, higher repetition

[21] The problem with split level systems such as this one is that the voltage division between levels must be equal, otherwise one set is working harder than another. An imbalance leads to stability problems which we experienced with another capacitor bank. Regardless of our attempts to even the imbalance through resistors, we ultimately had to settle for this bulkier bank with a slower repetition rate.

[22] The ATF's cyclic rate for the accelerator is 3 Hz.

rate, and much smaller size.

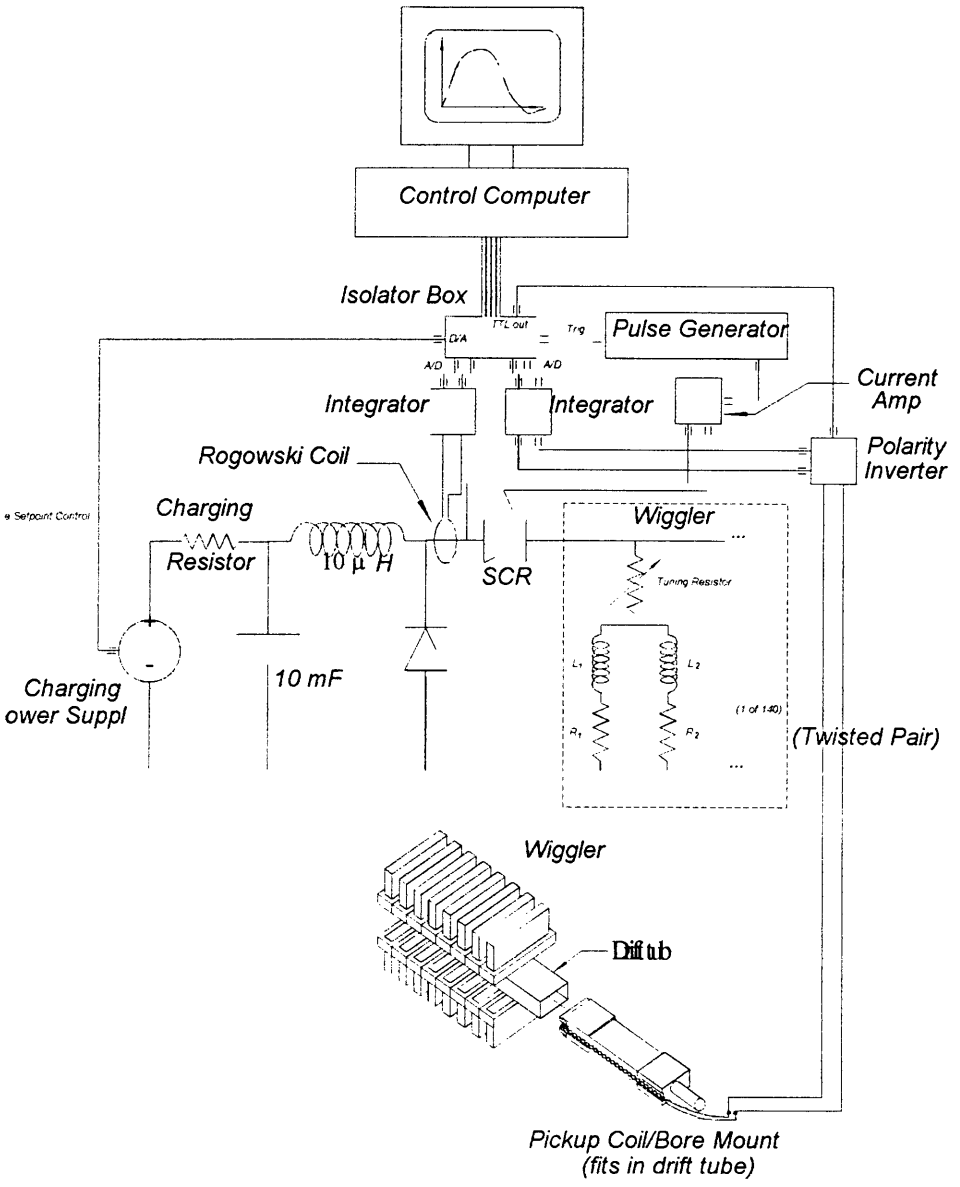

Figure 12 - Wiggler Electrical System[23]

The computer receives its triggering signal either from its own system's pulse

[23] Courtesy of Dr. Stoner.

generator or from an external trigger, usually the ATF's YAG-laser synchronized trigger. A Stanford signal generator permits us to make allowances for the wiggler's pulser lead time (the time required from receipt of trigger until maximum wiggler current) and other timing requirements. Thus, we can sequence events so that the maximum wiggler magnetic field occurs when the electron beam bunch arrives at the wiggler, as shown in Figure 13. Since the peak in the magnetic field lasts on the order of 20 μsec while the electron beam passes in only a few nanoseconds, the timing problems are not very significant.

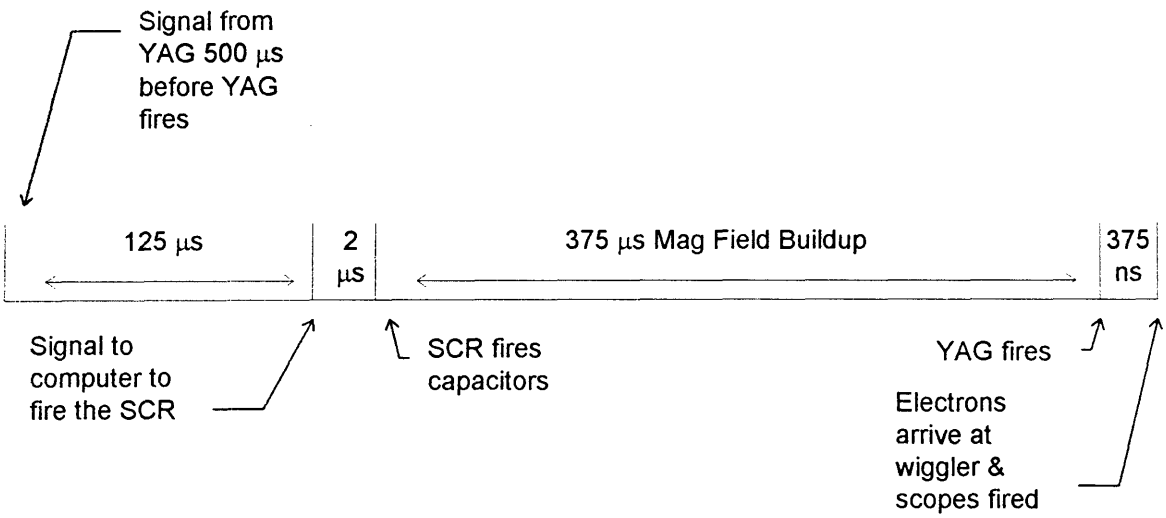

Figure 13 Wiggler Timing Scheme

We can check the accuracy of our timing by displaying the unintegrated current signal from the wiggler versus the ATF's triggering of the YAG, which illuminates the photo-cathode of the ATF's rf gun. The current signal from the wiggler represents the change in the magnetic field $\dot{B}$ in the wiggler. When the signal crosses the zero line, the change in the field is zero, meaning the magnetic field reached its maximum field strength. It is stable there for about 20 μsec during which time the electrons must ar-

rive. Adjusting the pulse generator/timer, we can synchronize the arrival of the electron with the maximization of the magnetic field.

3.4 The Optical Transport System

Because it is not safe to be in the same room as the wiggler when high energy electrons are around, the operator, computer, and spontaneous emission measuring equipment are in the adjacent room to the experimental hall. This gives rise to the optical transport system in Figure 14.

We know that the spontaneous emission comes from the wiggler on the downstream side of the system in an angular width $\cong \frac{1}{\gamma}$ cone (ideally). The problem is to collect as much of that light as possible and transport it into the FEL room for measurement.

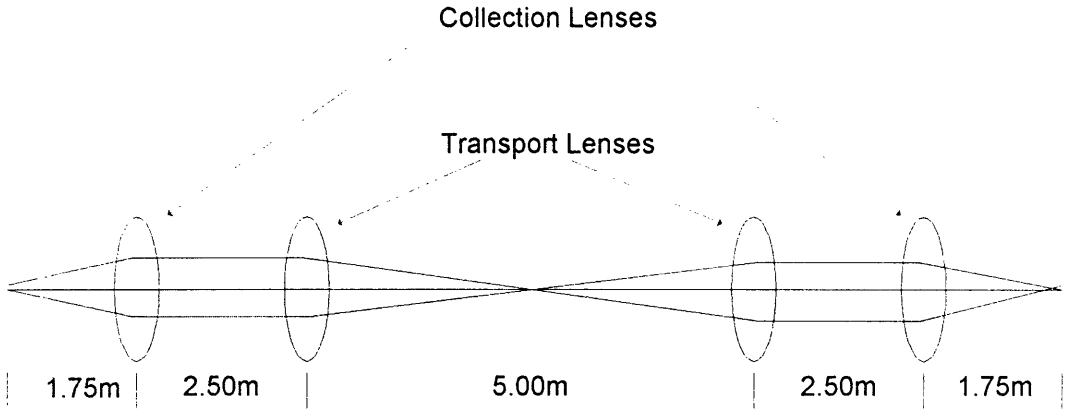

Figure 14 - Optical Transport System

The total path length of the transport is about 12 meters. We designed a transport system as a collection of two-inch lenses: one collecting, two transport, and a final focusing lens. The lenses were custom made by Optics for Research. The two transport lenses had a focal length of 2.5 meters, while the other two had focal lengths of 1.75 meters.

All were coated for broad band antireflection for the visible wavelengths (400 - 690 nm)[24]. We aligned the beam by boresighting a green HeNe laser through the wiggler via two pop-up phosphorous fingers on either side of the wiggler. Each finger assembly is motor driven. In the first setting, the fingers are out of the way; in the second, they protrude into the beam path and are aligned coaxially with the wiggler's axis. When the laser strikes each finger in the center, the laser is also on the axis of the wiggler. By aligning the mirrors with the laser, we can be as sured that the light created by the wiggler will travel down the transport system successfully to the measuring system.

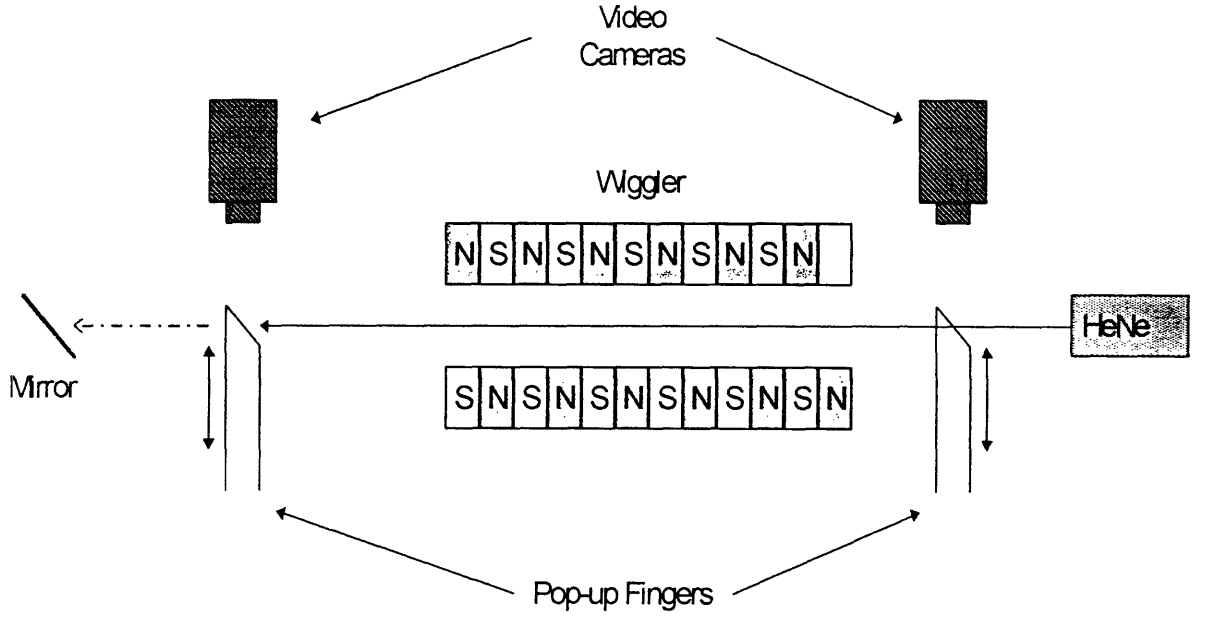

Figure 15 - Optical Alignment Setup

We required the services of a few mirrors as well. All but one were dielectric coated; that one being an aluminum coated mirror. The mirrors were two inches in diameter and made by Newport/Klinger.

[24] This will cause problems later because the beam energy during the experimental run was lower than planned. In turn, that causes the emitted wavelength of the light to be longer than 690 nm, therefore the results must be adjusted accordingly.

The beam energy available at that time (≅ 41 MeV) for this experiment produced a resonant wavelength longer than what the mirrors and lenses were designed to transport. According to the manufacturer of our optics, the coatings are 98% to 99% reflective/transmissive for the range of 400 to 690 nm. Our experimental range of 690 to 840 nm clearly exceeded that. Accordingly we tested each one of the mirrors for its reflectivity in our experimental range.

Schematic of Mirror/Lens Configuration

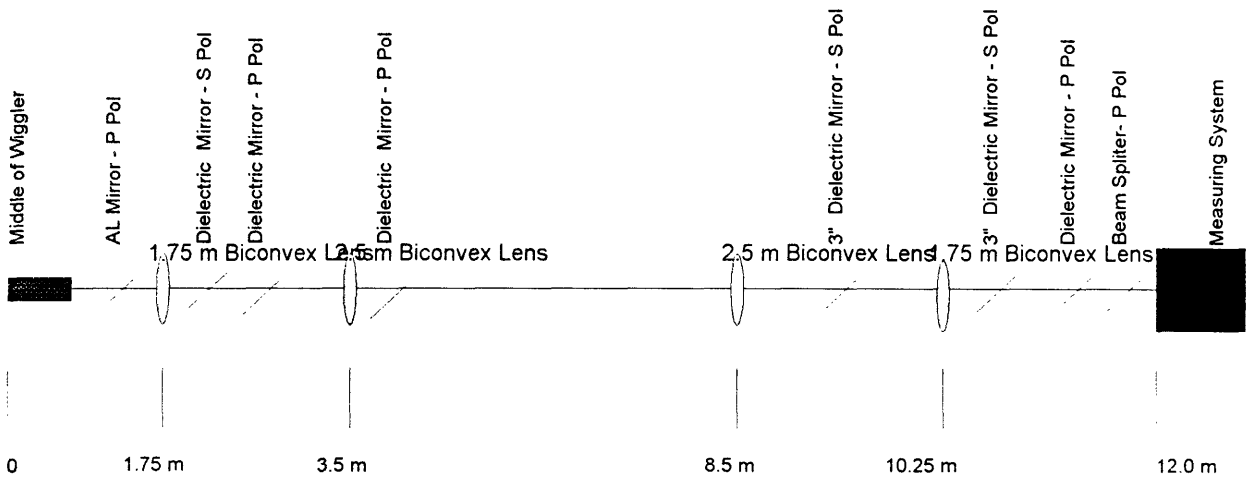

Figure 16 - Optical Design and Path[25]

Each one of the mirrors was positioned to reflect white light 45 degrees from our source into a spectrometer as shown in Figure 17. We knew and took into account each mirror's polarizing orientation, either horizontal or vertical and used a polarizer in the proper orientation for each mirror. As the spectrometer stepped through our experimental range, we took the corresponding voltmeter readings every 5 nm. Using a HeNe laser to reflect off of the test mirror

[25] This schematic only represents the order in which the optics were placed. In reality the optical path via the mirrors becomes reflected through a light-tight system of tubes and boxes at right angle joints.

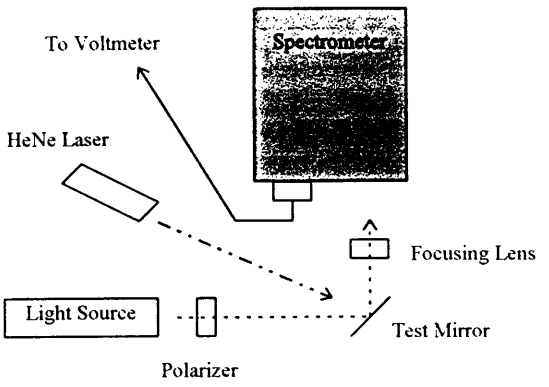

Figure 17- Mirror Reflectivity Test Setup

to a target spot, we can check to see that each mirror is in the same plane as all the others. In order to establish a baseline of spectral information on the white light, we replace our test mirrors with an aluminum one at both vertical and horizontal polarized angles. The aluminum mirror's responses in this range are virtually flat (within a per-cent). Normalizing our test mirrors with the aluminum mirror response, we can relate

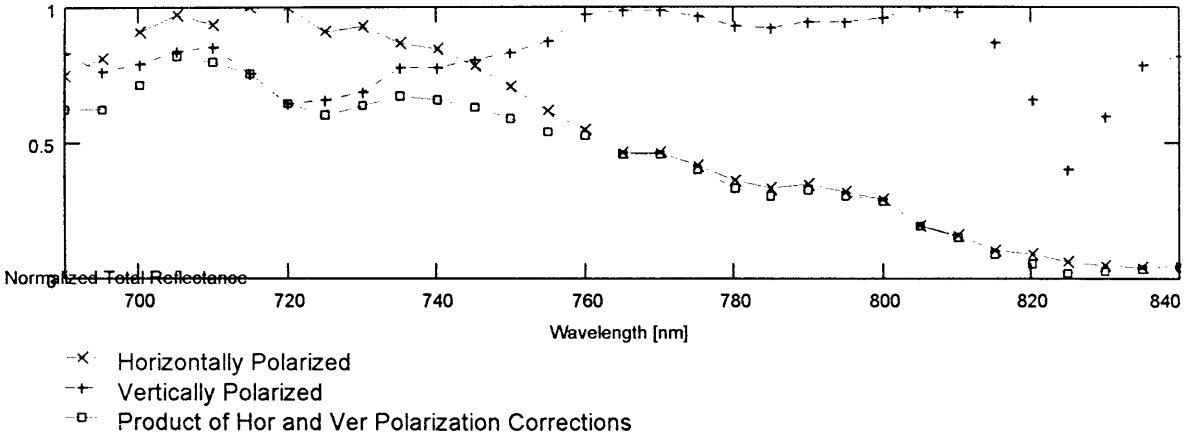

Figure 18 - Mirror Corrections

the reflectivity of our test mirrors throughout our experimental range as shown in Figure 18 and compensate the experimental results accordingly.

Our experience with prior runs also pointed to other light transport problems.

During the initial run of the system, conducted on November 11, 1993, the photomultipliers were located in the experimental hall, directly behind the downstream electron turning dipole.

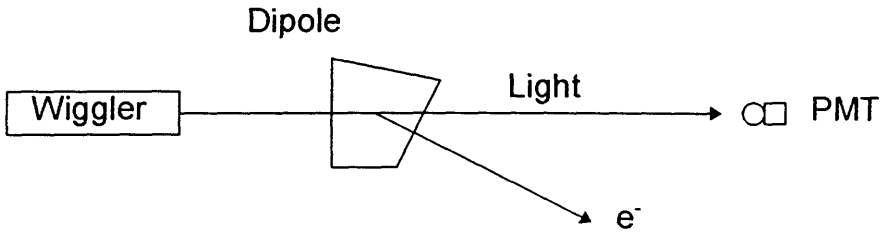

Figure 19 - First Run Setup of PMT

The PMTs showed a large amount of noise when the electron beam pulsed, regardless of whether the wiggler was firing or not. This noise was blocking the signal, if any, that we were receiving. Next we placed the PMTs on the ceiling above the dipole and added a lead glass window in front of the PMT. It proved to work well enough to see a distinct signal due to the wiggler's firing. The interference was most likely due to the Bremstraahlung of the electrons striking a surface inside the chamber. This is primarily a problem in electron beam control because the physical cross section of the beam, either because of momentum dispersion through the dipoles and/or electron gun emittance, was too large to fit cleanly into the wiggler bore.

When we brought the signal into the FEL room, we still had some noise. By placing a series of filters in the light's path, we discovered that the noise was in the shorter wavelength (< 500 nm) range. Therefore, for our experimental run, a low-pass filter was in the light's path to cut off the signal interference. The filter was made by Newport/Klinger with a cutoff at 510 nm, effectively eliminating the noise while retaining 90% to 91% of the spectral signal in the range of concern.[26] The noise seemingly is

[26] Newport supplied information

directly related to the large cross section of the electron beam. A more focused spot should eliminate problems since it appears that the electrons were striking the walls of the system through which they propagated.

We needed to bring the light from the experimental hall to the FEL room. This necessitated the use of an optical transport system. We first assembled a small scale mock-up of the transport path, less the mirrors, to discover if the system would work. We saw that the system produced no magnification and could image an object placed at the focal point quite well at the light's destination. The only problem left was the optical acceptance of the system. Assuming the light created within the wiggler is not well collimated, the light would be aperture stop limited by the waveguide acting as the wiggler's bore. The 5 mm high by 3 mm wide waveguide allowed for a 4 mrad half-angle emerging from the wiggler for light created at the wiggler's midpoint. A two-inch collection lens could easily capture that light and transport it. Further, the beam never exceeds the limits of our two-inch transport lenses.

We also know that the power (brightness) of the light emitted by the wiggler will be quite low. The lack of power comes from that run's low beam charge ($\approx$ 50 pC).[27] The sparse signal requires that the optical path be a light-tight system which encloses all the optics. Through the series of 1/4-inch sheet PVC-sided boxes, 3" black ABS plastic tubing, and foam stripping, we developed such a system and tested it for leaks using bright lights and sensitive photomultipliers.

3.5 The Measuring System

[27] ATF estimate.

At the receiving end, the light hit a 50-50 beam splitter. Half the light went directly to a broad-band Hamamatsu PMT[28]; the other half to a SPEX spectrometer outputting to an identical model PMT. Such an arrangement, shown in Figure 20 allowed us to measure both PMTs' signals and normalize the spectrometer filtered signals since we know the relative gain of both PMTs.

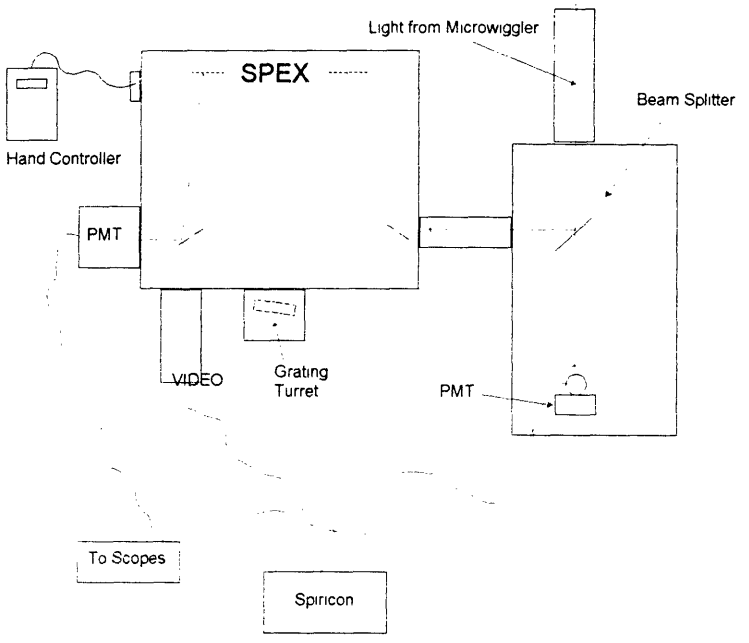

Figure 20- Experimental Measuring System

Prior to the experimental run, we mounted a green[29] light emitting diode [LED] onto a black card shown in Figure 21. On the ground side of the LED, we attached a 100Ω resistor. Attaching the LED to a Stanford timing box, we can light up the LED at nearly any repetition rate and duration we wanted. Additionally, we also attached a fast Tektronix probe spanning the resistor so we could measure the drop in voltage across the resistor over very short pulse lengths.

[28] Hamamatsu PMT Catalog
[29] Green because we anticipated beam energy to be about 45 MeV, which would create light in green (550 nm).

Ultimately, by displaying the probe's voltage vs. time trace across a very fast oscilloscope, we observed the change in voltage across the resistor as the LED lit up and turned off. If we integrate voltage over the charge/discharge of the LED, the net result, when multiplied by the resistance, is the power radiated by the LED.

PMT CALIBRATION SETUP

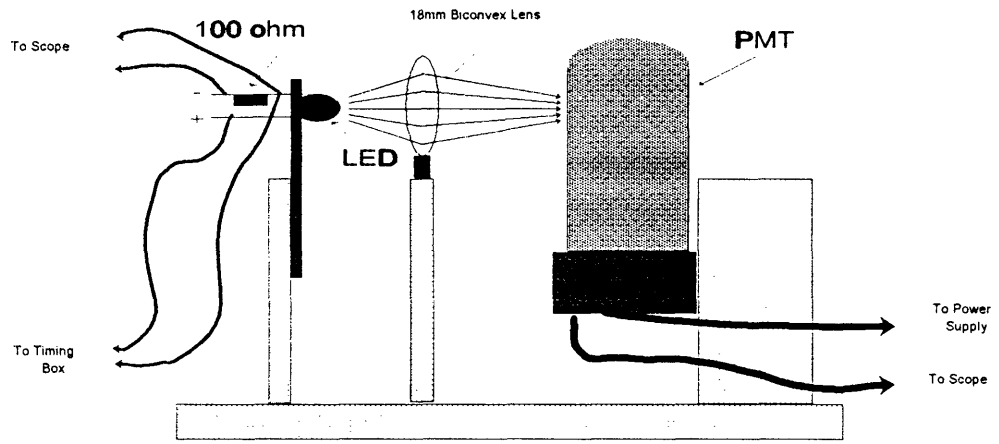

Figure 21 - PMT Calibration

Facing the LED mounted on the card was the sensing end of the PMT. Using a very short focal length lens (19 mm) to image the LED onto the sensing surface of the PMT, we can measure the response (signal gain) of the PMT to the LED as a function of time and voltage applied to the PMT. We could thus check the gain of one PMT versus its twin's as shown in Figure 22.

The SPEX 270M spectrometer is a commercial spectrometer with 3.1 nm resolution per millimeter slit width. It has the interchangeable gratings, which for this experiment as set for 1200 lines per inch at 600 nm. We tested the spectrometer by passing a green HeNe laser through the optical transport system to the spectrometer the front side exit where a video camera was. Knowing that the green HeNe's wave-

length is 543.5 nm, we saw that the spectrometer thought the light was at 544.5 nm.

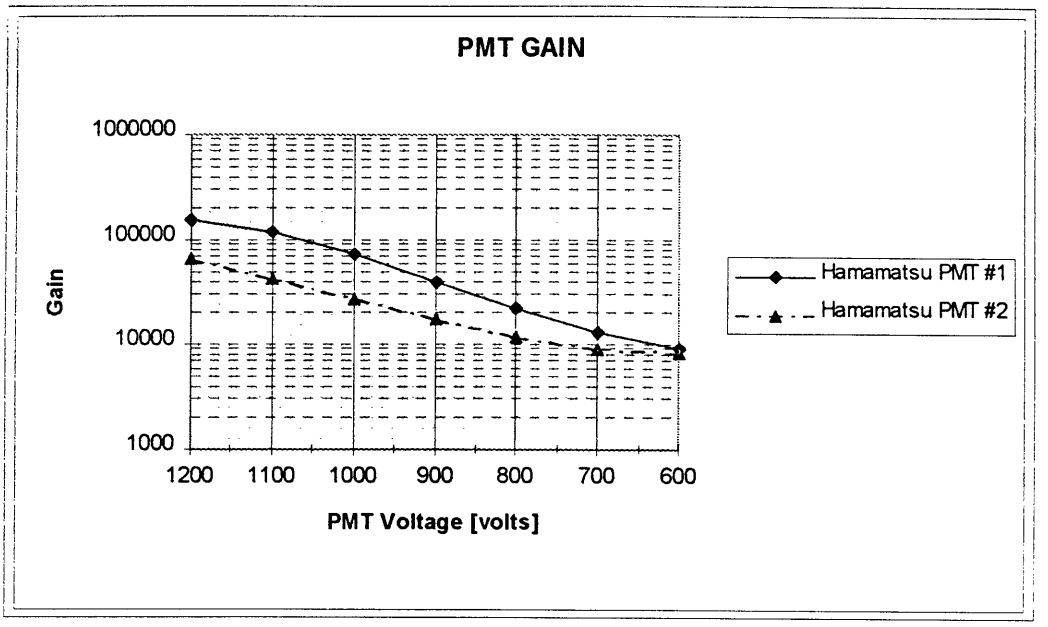

Figure 22 Empirical PMT Gain Curve

Since the slit width with set for 50 microns, the error was quite small, down to its diffraction limit. The spectrometer is electronically controlled in slit width increments of 12.5 microns and to 0.1 nm in grating setting. The output can be directed to either the PMT or the video camera.

3.6 The Linear Accelerator

The Accelerator Test Facility at Brookhaven is still in the final development stages. It was designed to be a high brightness, low emittance device[30]. The accelerator is an advanced design rf linear accelerator. The charge for the experiment was on the order of 50 pC, while design specs are for 1 nC. The accelerator is designed to operate at 50 MeV but during our run operated at 41 MeV. During the initial runs, the beam emittance has generally been poor. . The emittance is designed for 4.5 mm-

[30] Bachelor et al, pp. 160-161.

mrad but has been operating at much greater values. A large beam energy spread has led to a large cross sectional area of the beam coming out of the upstream turning dipole immediately in front of the wiggler. The electrons are created with a frequency quadrupled YAG laser illuminating a magnesium cathode. The YAG laser is quadrupled so as to obtain photon energies above the 3.6 volt work function of magnesium. The laser pulse, design for 6 ps but measured at 11 ps FWHM, produces 200 μJ. The cathode has an internal acceleration of 100 MeV/m over the rf length of 7.857 cm. The electrons then enter two accelerating cells of 25 MeV each and acquire a total acceleration up to 50 MeV, ideally. A continuing problem with arcing inside the klystron and laser stability problems have exacerbated the acceleration and emittance problems. Further, probable space charge effects at the cathode, due to too much incident laser energy, are under investigation to increase the beam's current, for this run at ≈5 amps. Throughout the accelerating process and afterwards, the electrons are focused and monitored throughout their journey down to the wiggler by a series of beam profile monitors situated upstream of the wiggler.

CHAPTER IV

ANALYSIS OF EXPERIMENTAL RESULTS

In this chapter we will examine the experimental results and contrast them with the theoretical predictions. We will cover:

1. ideal beam spectrum,
2. energy spread effects,
3. broad beam effects,
4. off axis emissions (collection effects),
5. combined effects, and
6. estimation of beam charge.

4.1 The Conduct of the Experiment

We will first examine the data collected during the run held in January, 1994. Using the experimental setup described in Chapter III, we took sample points of the data at 5 and 10 nanometer increments over the range for which we saw a signal. Each data point is the eight-shot average of the wiggler's pulses as seen by the PMT at a particular wavelength setting on the spectrometer. A typical PMT signal is below in Figure 23. We can see that the signal with the wiggler's magnetic field on is considerably stronger than with it off.

The data [see Worksheet 1, Appendix B] are the average of four spectral scans. We can combine the scans because the signals are normalized, thus for a given beam energy (both scans had the same beam energy) the individual data points are independent of the one next to it. Normalizing the data and merging them together with

equal weighting, I arrive at Figure 24 as the spectrum for the raw data. Each data point

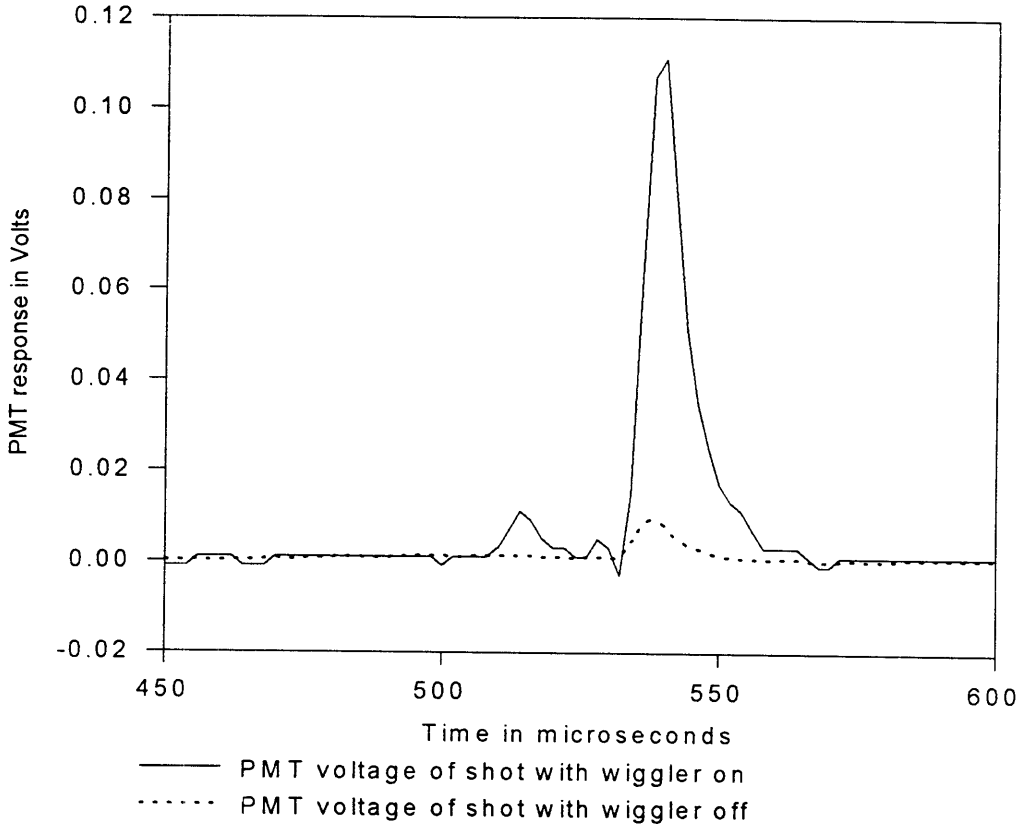

Figure 23 - Typical PMT Signal on Spectrometer

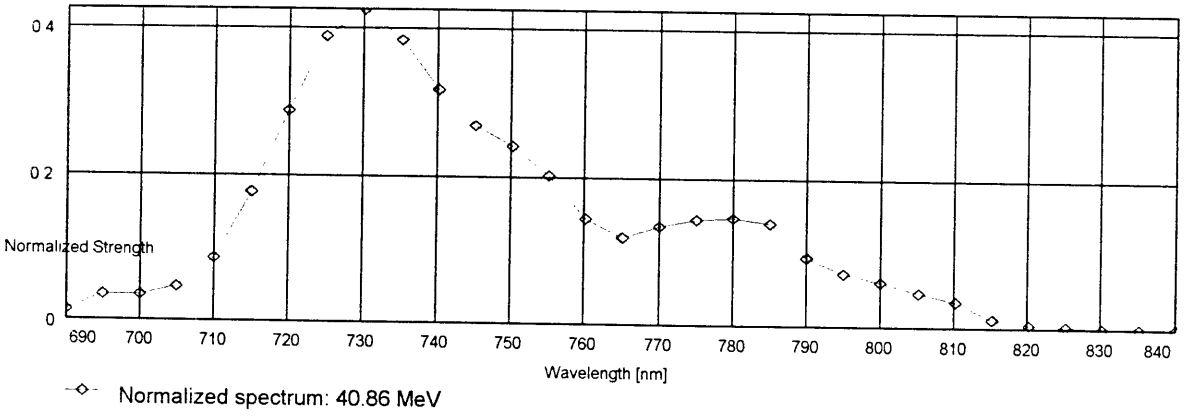

Figure 24 - Raw data spectrum

is 5 nm away from its neighbor in the averaged spectrum. We can expect the spectrum to be continuous over the wavelengths.

4.2 Optical Path Effects

An important factor to be considered is the effect on the measured spectrum due to the mirrors and lenses used in the experiment. This experiment was originally intended to use a 50 MeV beam, creating light in the 550 nm range. All the optics in the beam transport path were designed with this in mind. But on the day of our run, the beam energy was only 40.86 MeV with a resonant wavelength near the 730 nm range. Being on the edge of visible light, our observed wavelength range of 690 - 840 nm exceeds the design specs of the mirrors and to a much lesser extent the lenses.[31] Therefore, the raw spectrum must be compensated for the deleterious effects of our optics.

In Chapter 3, I covered the testing of the mirrors for their reflectivity in this range. By applying the correction derived from those tests, I can adjust the spectrum accordingly (see Worksheet 1, Appendix B). We noticed during the run that signals at wavelengths longer than approximately 780 nm created only a few millivolts of signal compared to the tens and hundreds of millivolts at shorter wavelengths. These readings were probably unreliable. From the reflectivity curves of the mirror, we can conclude that the longer wavelengths have been severely attenuated as demonstrated by the intermittent signals. It is very possible that there is a long, broad shoulder at longer wavelengths than what the empirical results show. Figure 25 compares the measured spectrum to the spectrum obtained by the application of the mirror corrections.

---

[31] According to the manufacturer's (Optics for Research) chart, the lenses are 99.5% transmittal at 690 nm and 98.5% at 850 nm. Relative to the effects of the mirrors, the lenses' effects are negligible.

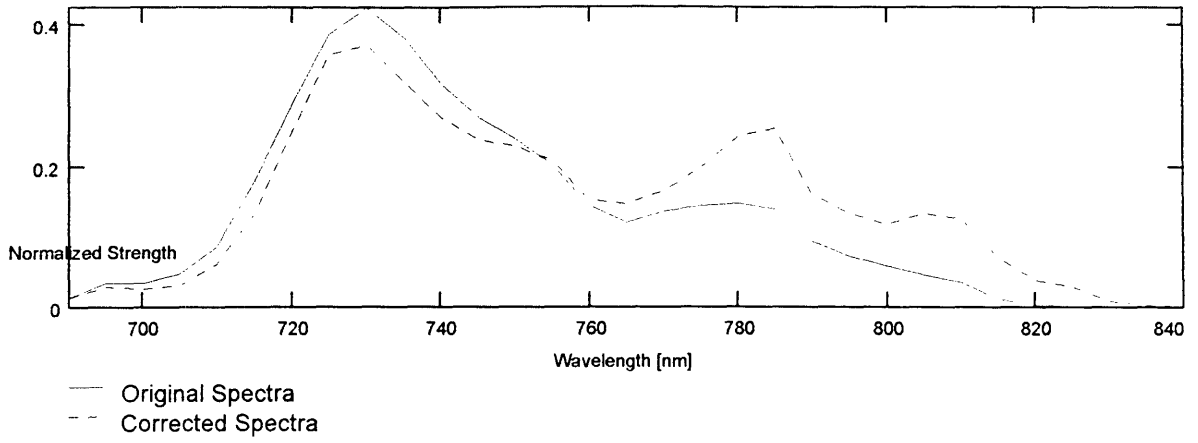

Figure 25 - Mirror adjusted spectrum

The basic form of the spectrum has not changed considerably, but the longer wavelength values are increased significantly the longer wavelength values. I consider this to be the spectrum for the rest of this analysis.

We have come to a point where we must compare the actual results to those theoretically predicted. For simplicity,, my theoretical calculations assume a perfectly collimated beam and ignore all forms of transverse electron motion. I will discuss the validity of this assumption in the next two sections.

4.3 Betatron Oscillations

Betatron oscillations occur when the electron enters into the wiggler slightly off axis. It induces a focusing motion to the electron moving tranversely to the wiggler axis. This sinusoidal motion is betatron oscillation. See Appendix A. In our wiggler, though, the period of betatron oscillation is six times the length of the wiggler. In other words, an off axis electron in the wiggler will only travel one-sixth of a betatron period, corresponding to a shift of only a hundred microns. Therefore, we will neglect betatron

oscillations.

4.4 Transverse Momentum

Transverse momentum results in betatron oscillation. This is illustrated in Figure 26. It is related to betatron oscillation because the electron is now subject to the influences of betatron oscillation, however the electron does not just have the slight magnetic field difference effects but also a strong momentum component in the $\hat{y}$ direction. There are two effects from transverse moving electrons. The first is that the $1/\gamma$ cone is not centered on the axis but is angled away from the axis along the path of the electron moving further off axis. The second is that as the electron travels down the wiggler it moves further and further away from the axis due to its initial momentum, thus it keeps changing a_w throughout its travel. That in turn changes the resonant wavelength more and more into longer wavelengths. The two effects broaden the observed spectrum - the first because we observe the electron's emitted radiation off axis (according to the electron direction of travel) and the second because a_w continues to grow throughout the electron's travel.

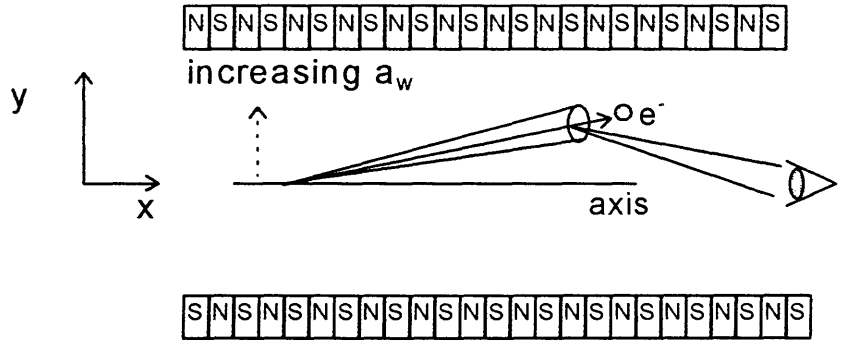

Figure 26 - Transverse Motion showing off axis emission with increasing a_w

The transverse momentum effect will contribute to spectral broadening but is probably

small in comparison to the effects described below. Beginning with the ideal spectrum, I will cover the numerical analysis of the spectrum.

4.5 The Ideal Spectrum

Let's examine the spectrum from an ideal beam (see Worksheet 3, Appendix B). By ideal, I mean that the electron beam is monoenergetic, travels directly down the center of the wiggler on axis, is very narrowly focused, and we observe the light looking directly down the axis over a very small solid angle.

Due to the $\frac{\sin x}{x}$ nature of the ideal spectrum, we will observe a spectrum of the shape shown in Figure 27. It is a symmetric function, narrowly defined near the resonant frequency for that beam energy. Of course, a real beam must have some finite physical dimension and some finite energy spread, the effects of which I will now examine.

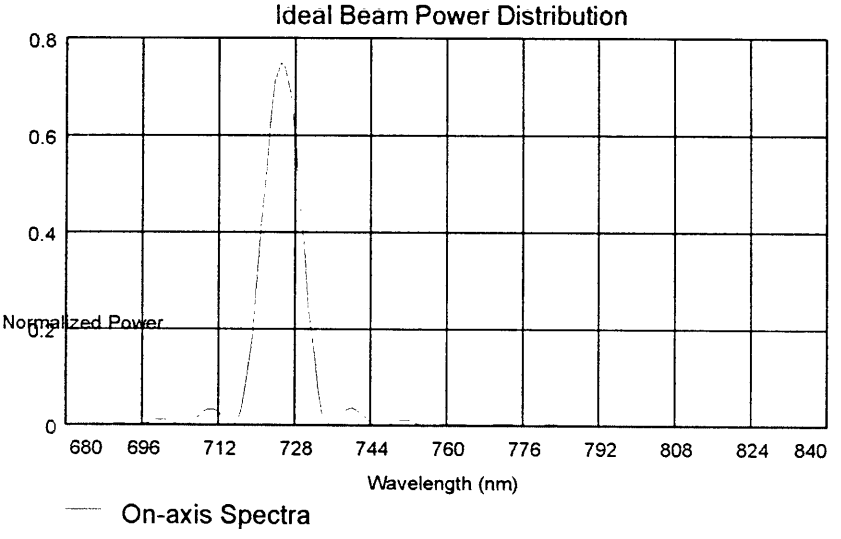

Figure 27 - Ideal Spectrum

4.6 Energy Spread Effects

Let's take into account the effect of the nearly 0.6 MeV momentum spread in the beam. See Worksheet 4, Appendix B. The spread is determined by the momentum slits in the accelerator. As the beam makes its first turn in the accelerator system, it passes a turning dipole. Higher energy electrons' trajectories do not get bent as much as lower ones do. With these electrons passing through a small window with a variable width, the operator can chose a range of electron momentum that passes through. For our runs, that width corresponded to nearly 0.6 MeV. I assume that the energy spread is gaussian in shape.

The effect of the energy spread is manifested in the change it induces in γ. Thus for the spontaneous emission, it appears as

$$\lambda(\gamma)_{resonant} = \frac{\lambda_w}{2\gamma^2}\left[1+\frac{a_w(y)^2}{2}\right].$$

So the effect of higher momentum would be to shorten the resonant wavelength by γ^2

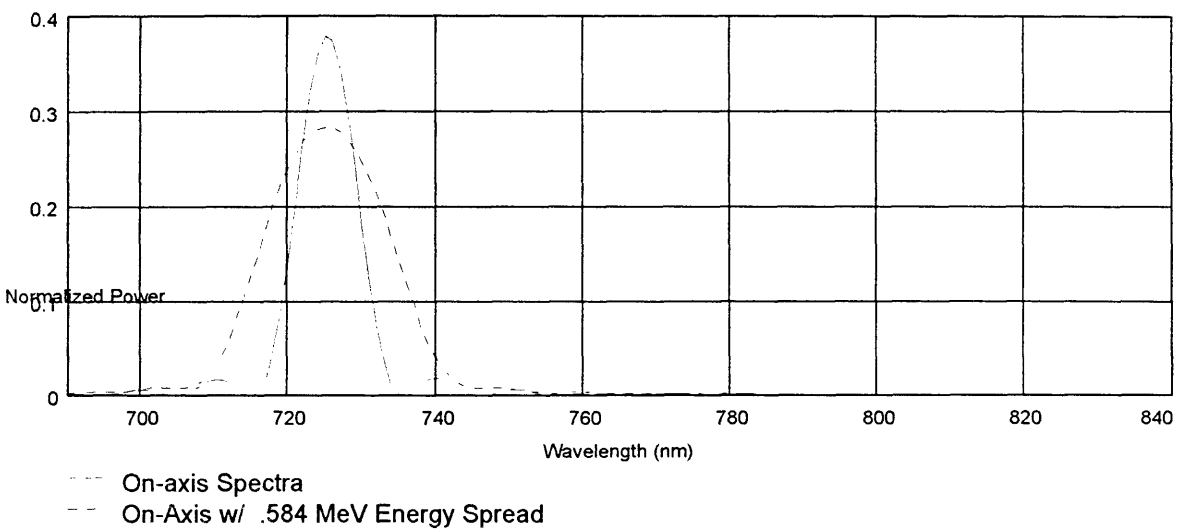

Figure 28- Ideal beam with energy spread

and vise versa. Thus a gaussian momentum distribution symmetrically broadens the monoenergetic spectrum as shown in Figure 28. This cannot be the sole cause of the actual spectrum.

4.7 Broad Beam Effects

Now let's suppose the beam is still monoenergetic but now has a cross section of either cylindrical or gaussian form.

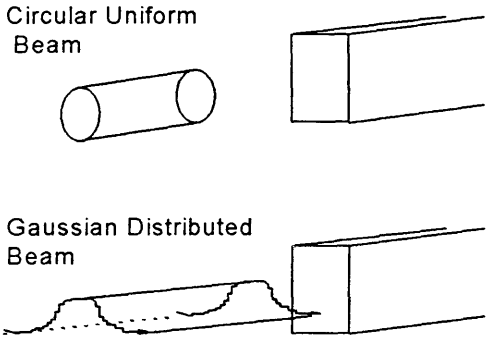

Figure 29 - Broad beam distribution diagram

The broadened beam affects the a_w term. An off-axis electron encounters a stronger magnetic field. Thus the resonant wavelength will shift to longer wavelengths since

$$a_w(y) = \frac{eB_w}{m_e c k_w}\left[1 + \frac{1}{2}(k_w y)^2\right],$$

$$\lambda(y)_{resonant} = \frac{\lambda_w}{2\gamma^2}\left[1 + \frac{a_w(y)^2}{2} + \gamma^2\theta^2\right],$$

where y is the distance from the axis. If taken in the aggregate where we allow the electrons to be distributed as a gaussian cross section going into the wiggler, the spectrum will broaden due to this effect. This is shown in Figure 30. Now let's assume that an electron has equal probability of being on axis as it does being on 0.5 mm from the axis or even 1 mm from the axis. Then the spectrum becomes Figure 31. The apparent

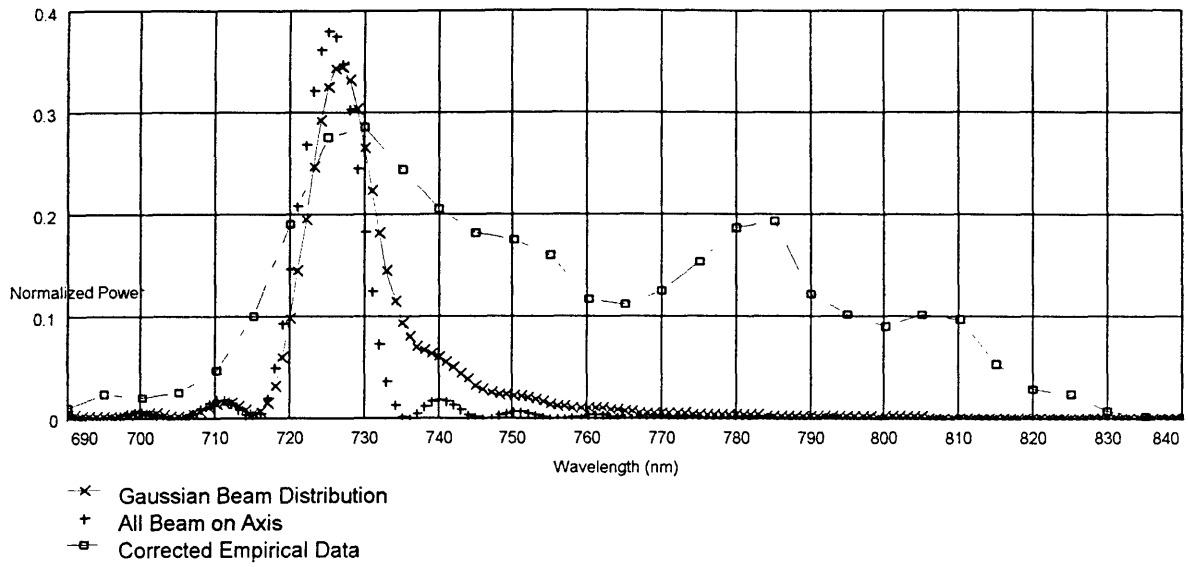

Figure 30 - Gaussian Distribution on an Ideal Spectrum

effect of broad electron distributions is to slightly broaden the emission toward the red, adding a small shoulder to the spectrum. In contrast to our results, this effect alone

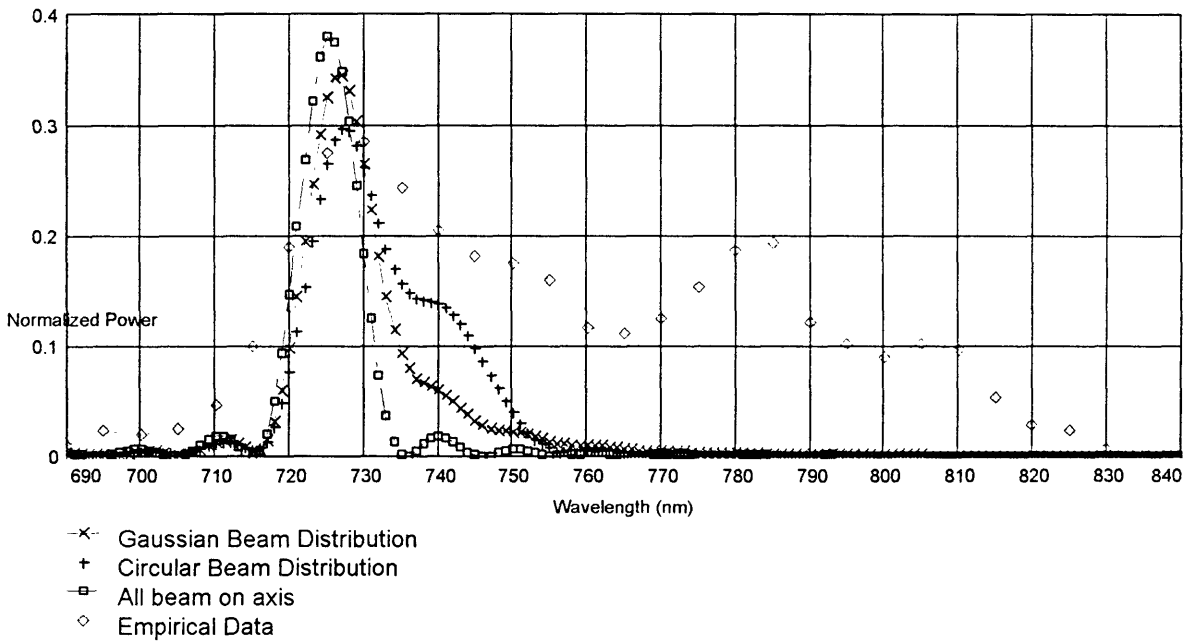

Figure 31 - Circular Distribution

cannot account for the broadness in the spectrum we obtained.

4.8 Broad Beam Effects and Energy Spread Coupling

We so far have looked at energy spread effects and broad beam effects. Let's examine the emission into a finite solid angle of collection.

Earlier I mentioned that the beam goes through a turning dipole after which the momentum range is selected. It would appear that higher momentum electrons are on one side of the beam while lower ones are on the other. Thus the position of the electron is momentum dependent. If that distribution is maintained to the wiggler, we would end up with the hybrid effects of high energy electrons displace on one side of the axis going to low energy ones on the other and propagating that way through the wiggler as seen in Figure 32. Surely this would broaden the spectrum as well.

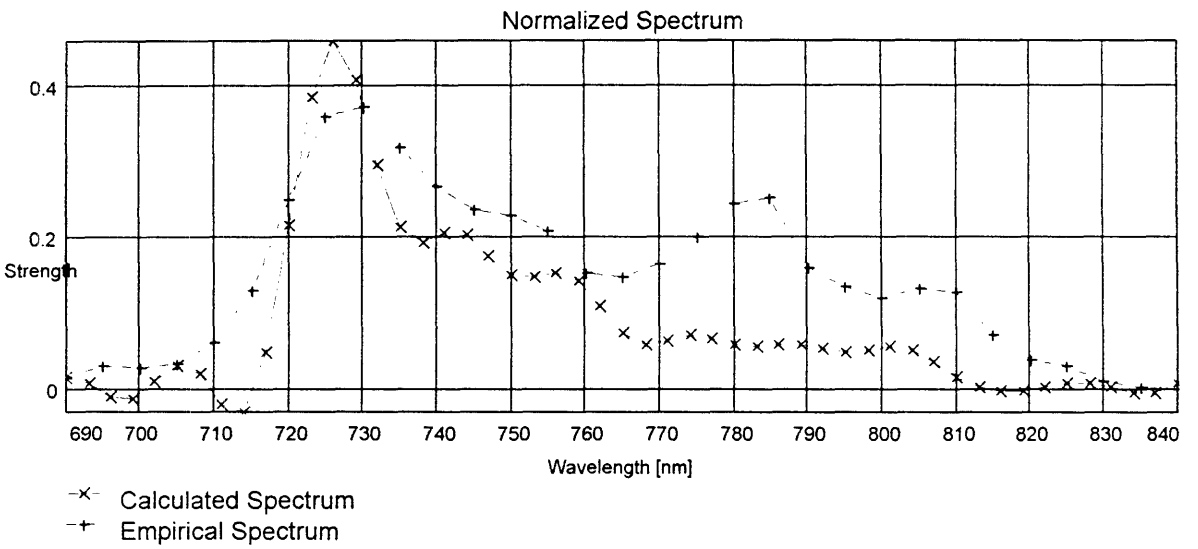

Figure 32 - Energy/Position Spectrum

This is somewhat unrealistic since the beam goes through one more dipole which should collect the beam and not leave it dispersed.

4.9 Off Axis Emission

In the ideal beam case, we assumed that the light was collected looking only along the axis. Let's now assume that the light we observe comes in a solid cone toward us as in Figure 33. See Worksheet 5, Appendix B. This is reasonable since our collection system actually does not observe the light strictly along the axis but has a physical aperture.

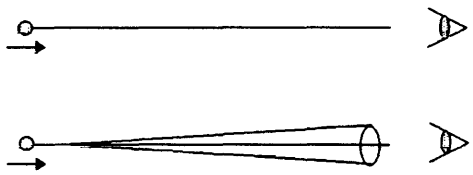

Figure 33 - On Axis Versus Off Axis Collection Cone

By seeing the emission slightly off axis, we see that the radiation is more red as the angle increases. This is due to the effect stated in Chapter III, where the viewed radiation is given by:

$$\lambda(\theta)_{\text{resonant}} = \frac{\lambda_w}{2\gamma^2}\left[1+\frac{a_w^2}{2}+\gamma^2\theta^2\right]$$

where θ is the angle from the axis. This will broaden our spectrum. In Chapter 3, we found the spectrum as a function of this angle. It is

$$I = \frac{e^2 a_w^2 \gamma^2 N_w^2}{2\pi\varepsilon_o c\left[1+\frac{a_w^2}{2}+\gamma^2\theta^2\right]}\left[\frac{\sin x}{x}\right]F, \text{where}$$

$$F = \left[\sum_{k=0}^{\infty} -1^k J_{2k}(\alpha)\left[J_k(\xi)-J_{k+1}(\xi)\right]\right]^2$$

$$\alpha = \frac{2^{\frac{3}{2}} a_w \gamma\theta \cos\phi}{1 + \frac{a_w^2}{2} + \gamma^2\theta^2}$$

$$\xi = \frac{1}{2} \frac{a_w^2}{\left(1 + \frac{a_w^2}{2} + \gamma^2\theta^2\right)}$$

Taking into consideration only the solid cone having a half angle of 4 mrad, we can calculate a spectrum that looks like Figure 34. Notice how a large shoulder exists on the spectrum. This comes from the collective effects of radiation viewed from off axis. If we plot the resonant frequency as a function of viewing angle we end up with Figure 35.

The horseshoe shape comes from the shifting of light to the red at greater viewing angles. If we now turn the diagram sideways looking only at wavelength vs. intensity and add up all the values for each wavelength, we get the figure below. Com

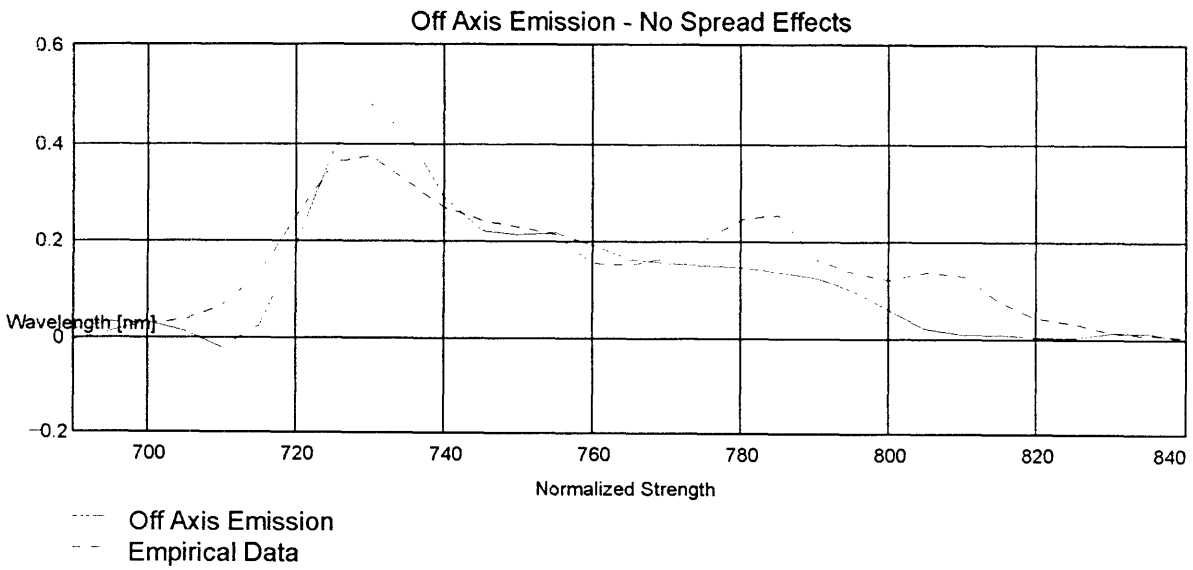

Figure 34 - Off Axis Emission only

pared to the actual spectrum, we can see a great deal of resemblance. But there are a few problems with it; we still have assumed no energy spread and no broad beam effects.

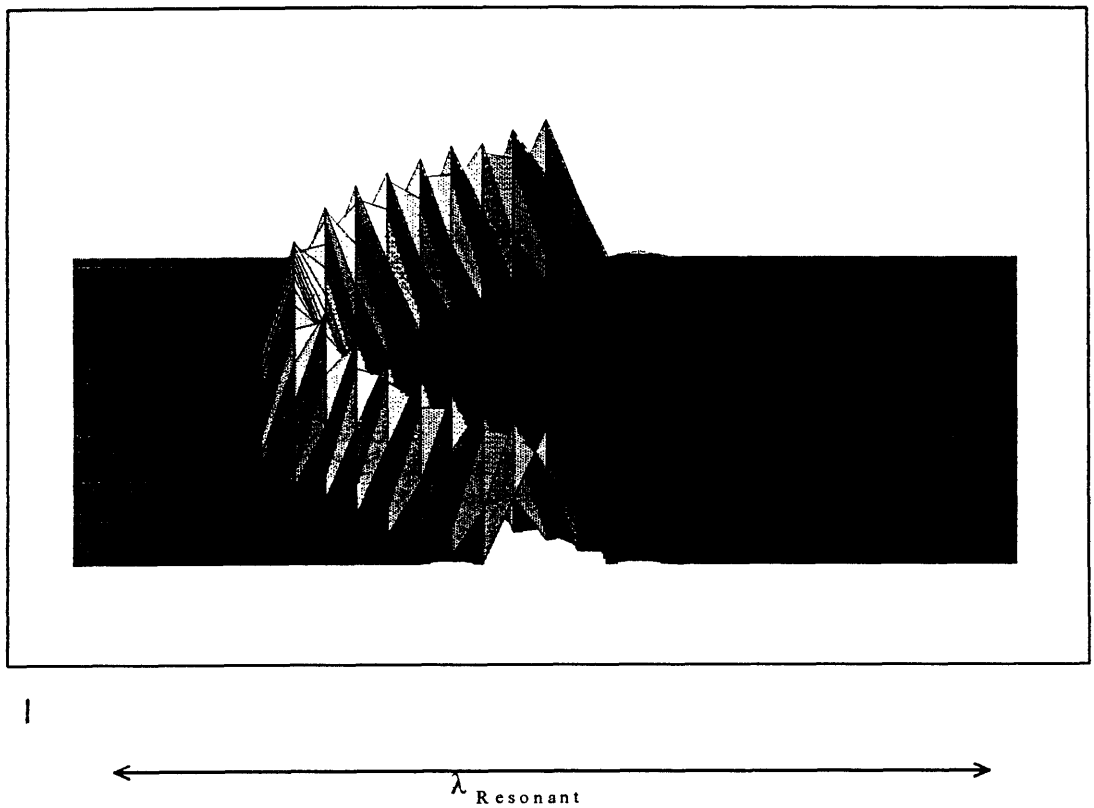

Figure 35 - Depiction of wavelength vs. viewing angle

4.10 Off Axis Emission with Energy Spread

Once again, let's assume that the beam energy is gaussian distributed. By modulating γ in the above equation, the spectrum, shown in Figure 36, is

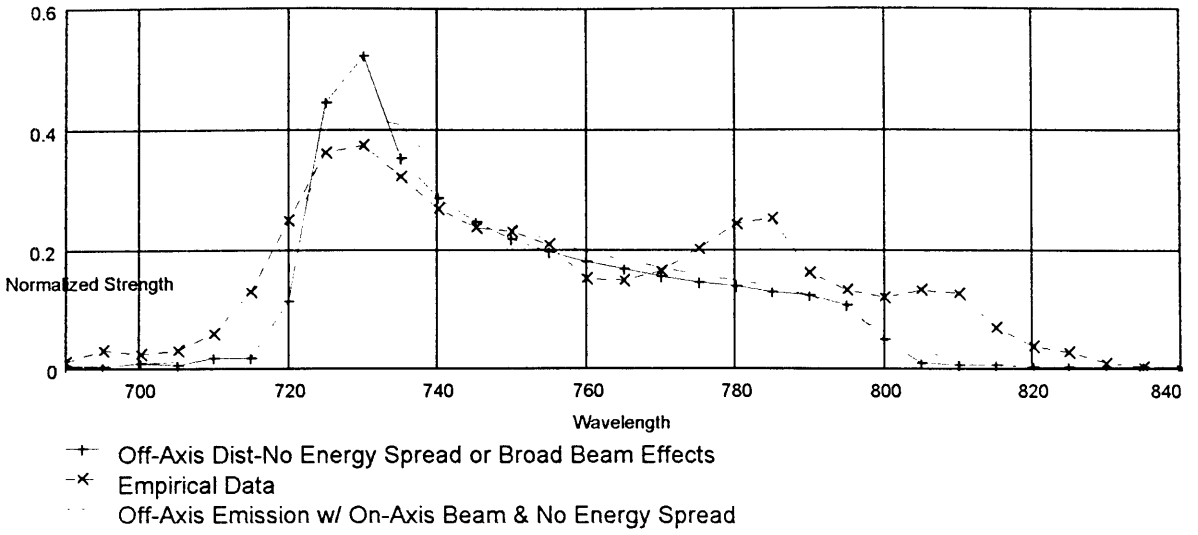

Figure 36 - Off Axis with Energy Spread

Note that it is centered on the actual spectrum but is relatively narrow. The factor of the range in momentum simply broadens the spectrum.

4.11 Off Axis Emission with Energy Spread and Broad Beam Effects

We still need to account for the physical extent of the beam. Adding the broad beam factor yields Figure 37. We see that the beam is broadened and shifted more to the red. This is due to the cumulative effects of off-axis propagation of the electrons. It has the effect of shifting the spectrum toward the red, since moving to one side of the axis or the other moves the resonant frequency to longer wavelengths.

The shape of the off axis emission with energy spread and broad beam effects assumes the form of the actual spectrum quite well. Since we can only speculate as to the distribution of electron positions and energy, this seems a reasonable estimation of what happened.

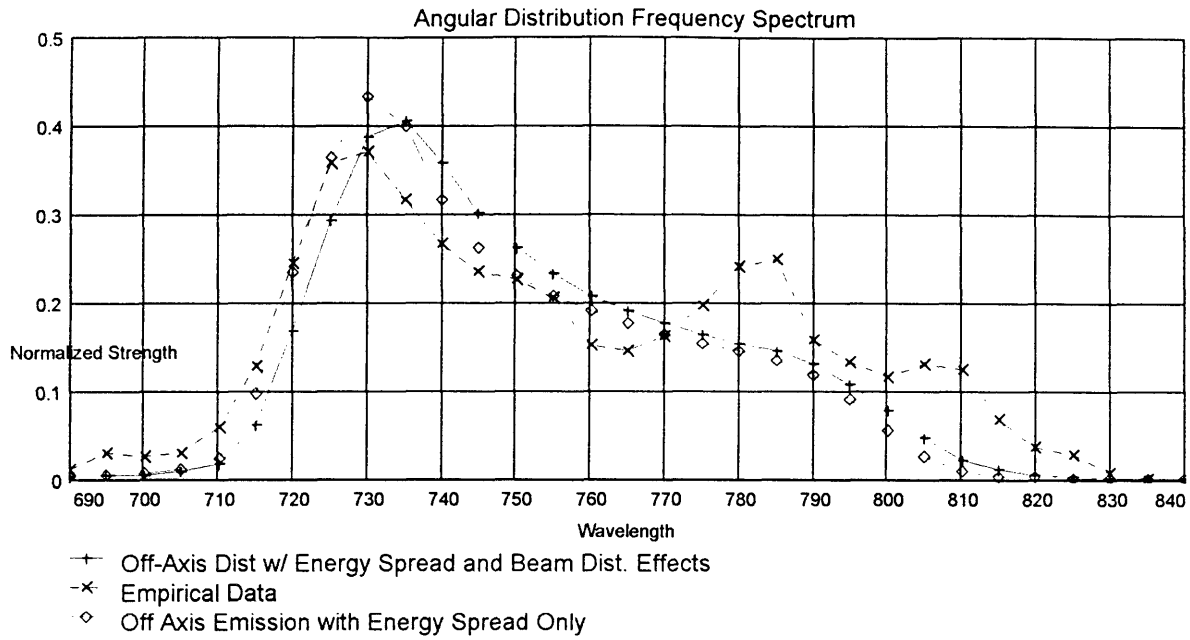

Figure 37 - Off Axis Emission with Energy Spread and Broad Beam Effects

4.12 Beam Charge Calculations

The signal on the normalizing PMT can give us an indication of the amount of charge applied to the wiggler. In the charge worksheet in Appendix B, we can see when all losses and effects are considered, we estimate the charge for this experiment to have been about 8.5 pC, which is a reasonable number supported by the estimation of the ATF staff.

4.13 Summary

In Chapter II, we saw that the off-axis emission effects would probably dominate the spectral broadening. We can see here that this forecast bears out to be true. Whereas the energy spread effect just spreads out the spectrum equally and the broad beam effects shift the spectrum to the red, it is the off axis emission that really expands

the spectrum.

This leads to an interesting note. If we can cut down the collection angle, that is to say limit the off-axis emission seen by the measuring system, we could isolate the combined effects of energy spread and broad beam effects. This may be possible by physically cutting down the aperture to the collection system. By doing this, though, we would need much brighter light, or in other words much more charge through the wiggler, since we would be seriously restricting the light seen by the PMTs. In turn, this may lead to an establishment of beam emittance depending upon the spectrum seen by the measuring system.

CHAPTER V

FUTURE DIRECTIONS

Presently the Accelerator Test Facility is undergoing upgrades and servicing. Upgrades to the YAG laser, photocathode, accelerator cells, and many other improvements will increase the possible accelerator to 100 MeV and lower the emittance. These two improvements will aid considerably in the production of a more narrow spectrum. With the testing of the accelerator, we can determine by established methods the emittance. By comparing the emittance with the spontaneous spectrum, we can determine the relationship between emittance and the dimensions of the spectrum. Additionally, the increase in beam energy will allow us to use the optics in the regime for which they were designed, alleviating the need to adjust the experimental spectrum for mirror losses.

Concurrently, improvements on the wiggler system are underway. The capacitor/pusler bank is ready for the upgrade to four large capacitors capable of handling 600 volts. This will aid in shot-to-shot stability, higher repetition rates, and occupy less physical space in the experimental hall.

The wiggler itself needs improvement, but it will take about a man-month in order to achieve the desired results. Prior to tuning the wiggler, the field error was 4%. By adjusting the resistive wires, the error was 0.12%. Earlier I mentioned the weakness in period 34's magnetic field and that replacing it would be a monumental undertaking. The next step in the wiggler's evolution will be to remove all the magnets and test them individually under controlled conditions for their field characteristics. By establishing a very small range of acceptable field values, we can selectively choose only those few magnets whose fields are very close to each other. Reinstalling the new sets of

matched magnets, we potentially could start out with an unadjusted field error of only a percent and ultimately tuning the magnet to a fraction of the 0.12% from before. The more uniform field without problems of weak magnets will allow us to tune the wiggler for higher repetition rate, ultimately limited by the ability of the supporting systems - the cooler or power supply - to keep up.

As mentioned in Chapter 4, we can install a smaller aperture to limit the off axis emissions seen by the measuring system. This would allow us to isolate energy spread and broad beam effects and may lead to a relation of emittance versus spectrum.

CHAPTER VI

CONCLUSIONS

This thesis has discussed the experimental theory, setup, results, and comparative analysis. Focusing on the results first, we note that the spectrum occurs in the theoretically predicted range. The peak strength occurs at 725 nm, and the shape of the spectrum resembles that which the theory predicts. The principle broadening mechanisms appear to be the collective effects of off-axis emission, broad beam distribution, and energy spread. All three effects can be minimized but never eliminated because we must deal with physical systems. The comparative shapes of the predicted versus actual spectra are quite similar and have a difference of 5 nm, which is well within the potential error of our techniques. As predicted the off axis emissions dominate the spectral broadening.

The question of charge and emittance for now cannot be answered. We lack the empirical evidence to point to a conclusion. I can only speculate that the beam charge was on the order of 8.5 C. The emittance will have to wait until we can compare it to a known value, hopefully by applying a relation between spectrum and emittance.

CHAPTER VII

REFERENCES

Batchelor, Kenneth, et al, "Status of the Visible Free Electron Laser at Brookhaven Accelerator Test Facility", Nuclear Instruments and Methods in Physics Research, A318, pp. 159-164, 1992.

Brau, Charles, Free Electron Lasers, Boston, Academic Press, 1990

Friedman, A., et al, "Spontaneous and Stimulated Emission from Quasifree Electrons", Reviews in Modern Physics, Vol. 60, No. 2, pp. 471-535, April, 1988.

Jacobs, Stephen, et al, Free Electron Generators of Coherent Radiation, Addison-Wesley Publishing Company, 1980.

Luchini, P. and Hans Motz, Undulators and Free Electron Lasers, Oxford Science, Oxford, 1990.

Marshall, Thomas, Free Electron Lasers, New York, MacMillan, 1985.

Murphy, JB, and C. Pellegrini, "Introduction to the Physics of the Free Electron Laser", Laser Handbook, Vol. 6, Elsevier Science Publishers, 1990.

Pellegrini, C., "Free Electron Lasers", Encyclopedia of Applied Physics, Vol. 8, VCH Publishers, 1994.

Sisson, David, "Analysis of the MIT Microwiggler Magnetic Field", Bachelor's Thesis, MIT Library, 1994.

Stoner, Richard, "A Planar Electromagnet Microwiggler for Free Electron Lasers", IEEE Transactions on Plasma Science, Vol. 18, No. 3, pp. 387-391, June 1990.

Stoner, Richard, "Radiation from Relativistic Electrons in a Periodic Structure", PhD Thesis, MIT, 1994.

BIOGRAPHICAL NOTE

James C. Blastos was born May 3, 1963, in Augsburg, Germany. The son of a US Army officer and registered nurse, he grew up in Kansas, Alaska, Virginia, and Seoul, South Korea. He graduated from Seoul American High School, Seoul, Korea in 1981 and entered the United States Military Academy at West Point later that summer.

Graduating from West Point in 1985, he was commissioned into the Army as a Second Lieutenant in the US Army Aviation branch. He attended flight school at FT Rucker, AL; graduated from the US Army Airborne School and US Army Air Assualt School; completed the AH-1S attack helicopter transition course; and was assigned to the Attack Helicopter Battalion of the 25th Infantry Division (Light) at Schofield Barracks, HI.

During his assignment, he was an attack helicopter platoon leader, battalion intelligence officer, flight operations officer, and Commander, B Company, 25th Aviation Battalion (Attack).

While in Hawaii, he attended Chaminade University. He graduated in 1991 with a Masters in Business Administration.

He was assigned back to FT Rucker to attend the Aviation Officer Advance Course and became an honor graduate. After serving as a special projects officer, he attended the Combined Arms and Service Staff School at FT Leavenworth, KS, and was assigned for schooling at MIT.

Upon graduation from MIT, he will be an instructor in the Department of Physics at West Point. He intends to attend the Naval Experimental Test Pilot Program and ultimately join the NASA program as a mission specialist.

APPENDIX A

BETATRON OSCILLATIONS

Beginning with Maxwell's equations,

$$\left.\begin{aligned}\nabla\times\vec{B}&=\frac{4\pi}{c}\vec{J}\\ \nabla\bullet\vec{B}&=0\end{aligned}\right\}\Rightarrow\nabla\left(\nabla\bullet\vec{B}\right)-\nabla^2\vec{B}=\frac{4\pi}{c}\nabla\times\vec{J}$$

$$-\nabla^2\vec{B}=\frac{4\pi}{c}\nabla\times\vec{J}$$

and in free space, $\vec{J}=0$. This leaves us to solve $\nabla^2\vec{B}=0$ with the condition that $\nabla\bullet\vec{B}=0$. The Poisson equation leads to a magnetic field of $\vec{B}=B_o\left[\cos k_w z\cosh k_w x\,\hat{x}-\sin k_w z\sinh k_w x\,\hat{z}\right.$, where k_w can take on the values of $k_w=\frac{2\pi}{\lambda_w}n$ and n in an integer to force the solution to be periodic with period λ_w. We will consider on n=1 for the primary mode. Solving for the acceleration,

$$\frac{d\vec{v}}{dt}\approx\frac{e}{mc\gamma}\left(\beta_{\|}c\,\hat{z}+\frac{K_w}{\gamma}c\sin k_w\beta_{\|}ct\,\hat{y}\right)\times B_o\left(\cos k_w z\cosh k_w x\,\hat{x}-\sin k_w z\sinh k_w x\,\hat{z}\right).$$

The $\hat{y}\times\hat{x}$ term yields axial "jitter" motion; the $\hat{z}\times\hat{x}$ term yields wiggler motion; and the $\hat{y}\times\hat{z}$ term yields motion transverse to the plane of the wiggler field. We can obtain the equation of motion by averaging over a wiggler period

$$\left\langle\frac{dv}{dt}\right\rangle=-K_w^2\frac{c^2}{\gamma^2}k_w\left\langle\sin^2 k_w\beta_{\|}ct\right\rangle\sinh k_w x$$

$$=-K_w^2\frac{c^2}{2\gamma^2}k_w\sinh k_w x$$

$$\ddot{x}\approx-K_w^2\frac{c^2}{2\gamma^2}k_w^2 x$$

This gives us the equation of motion for the electron through the wiggler. If we define

the betatron frequency as $\Omega_\beta \equiv \frac{K_w c k_w}{\sqrt{2}\gamma}$, the equation of motion can be condensed to a familiar form of $\ddot{x} = -\Omega_\beta^2 x$.

We must consider just how much does betatron motion effect the spectrum. An indication of this is

$$\Delta z_\beta = \beta_\parallel c \frac{2\pi}{\Omega_\beta} = \frac{\sqrt{2}\beta_\parallel \gamma}{K_w} \lambda_w \approx 430 \lambda_w .$$

For a 70-period wiggler, only 1/6th of a betatron period takes place inside the wiggler, thus its effect within the wiggler is quite small.

APPENDIX B

MATHEMATICAL ANALYSIS WORKSHEETS OF EXPERIMENTAL RESULTS AND SIMULATIONS

There are 11 analytical worksheet for this thesis. They are:

1. Experimental Data Results,
2. Mirror Correction Calculations,
3. Ideal and Broad Beam Distribution Analysis,
4. Ideal Beam with Energy Spread Effects,
5. Energy Spread and Broad Beam Coupling Spectrum,
6. Off-Axis Emission Spectrum,
7. Off-Axis Emission with Energy Spread Effects,
8. Off-Axis Emission with Energy Spread and Broad Beam Effects,
9. Off-Axis Emission with Variable Collection Angle Effects,
10. Beam Charge Calculations, and
11. Summary Graphics Worksheet.

EXPERIMENTAL DATA RESULTS

This worksheet reads in the raw data from the experiment. The data are found in two files. Since each data point is normalized, and therefore independent, we can expand the data by interpolating from both files.

From a spreadsheet, in which we have already normalized and averaged scans 10, 11, 12, and 13, import the data.

data := READPRN(column)

$\lambda := data^{<0>}$ joint := $data^{<15>}$

a := 0..length(λ) − 1 b := 1..length(λ) − 2

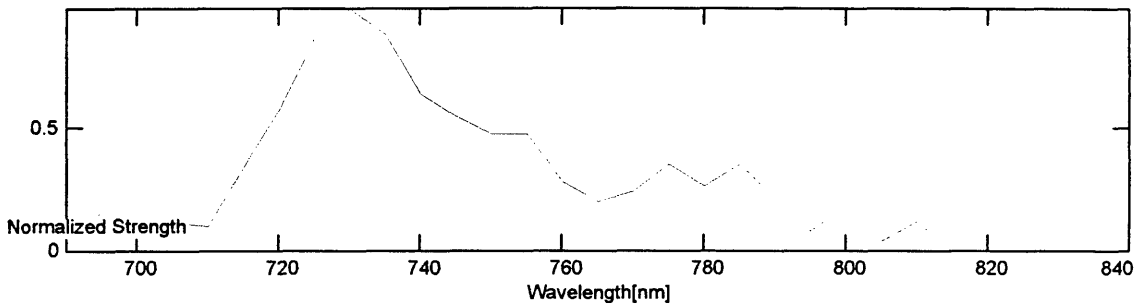

In this section, we take the next neighbor average.

$$joint_b := \frac{joint_{b-1} + joint_b + joint_{b+1}}{3}$$

$$Sum := \sqrt{\sum_a (joint_a)^2} \qquad joint := \frac{joint}{Sum} \qquad \sum_a (joint_a)^2 = 1$$

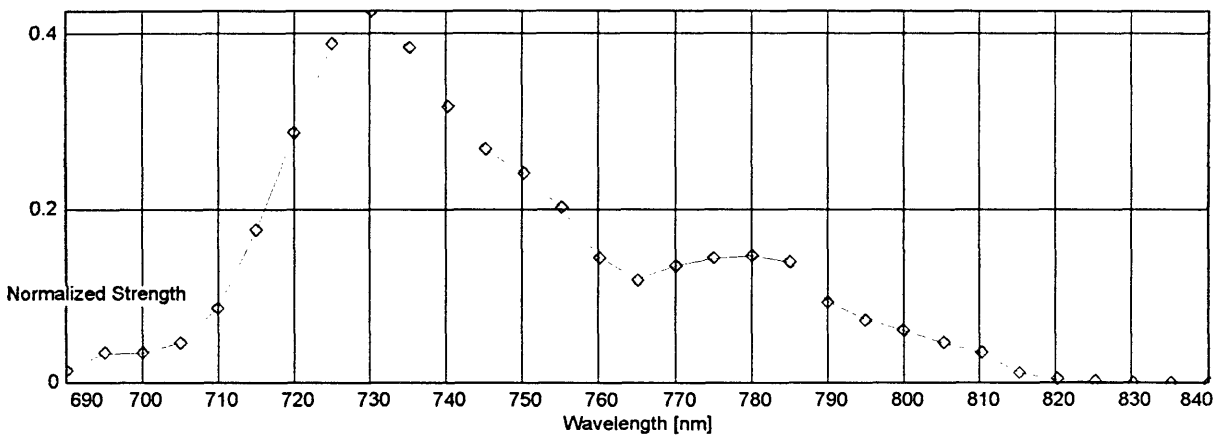

Worksheet #2, Appendix B

MIRROR CORRECTION CALCULATIONS

This worksheet takes the raw spectral signals from the mirrors used in the experiment and contrasts them to aluminum mirrors, which have a relatively flat response in this range. Then apply the corrections to the spectral data for a corrected spectra for mirror effects. The lens transmittance in this range is virtually 99% throughout the range and would not these normalized results.

data := READPRN(lensdata) i := 0..30

$\lambda := data^{<0>}$ $m7p5 := data^{<3>}$ $m7p10 := data^{<6>} \cdot 2$ $m5s10 := data^{<9>}$

$m2p5 := data^{<1>}$ $m3s5 := data^{<4>}$ $alp10 := data^{<7>} \cdot 2$ $m6s10 := data^{<10>}$

$m4p5 := data^{<2>}$ $m3s10 := data^{<5>} \cdot 2$ $als10 := data^{<8>} \cdot 2$

$m3s := \frac{m3s5 + m3s10}{2}$ $m7p := \frac{m7p5 + m7p10}{2}$

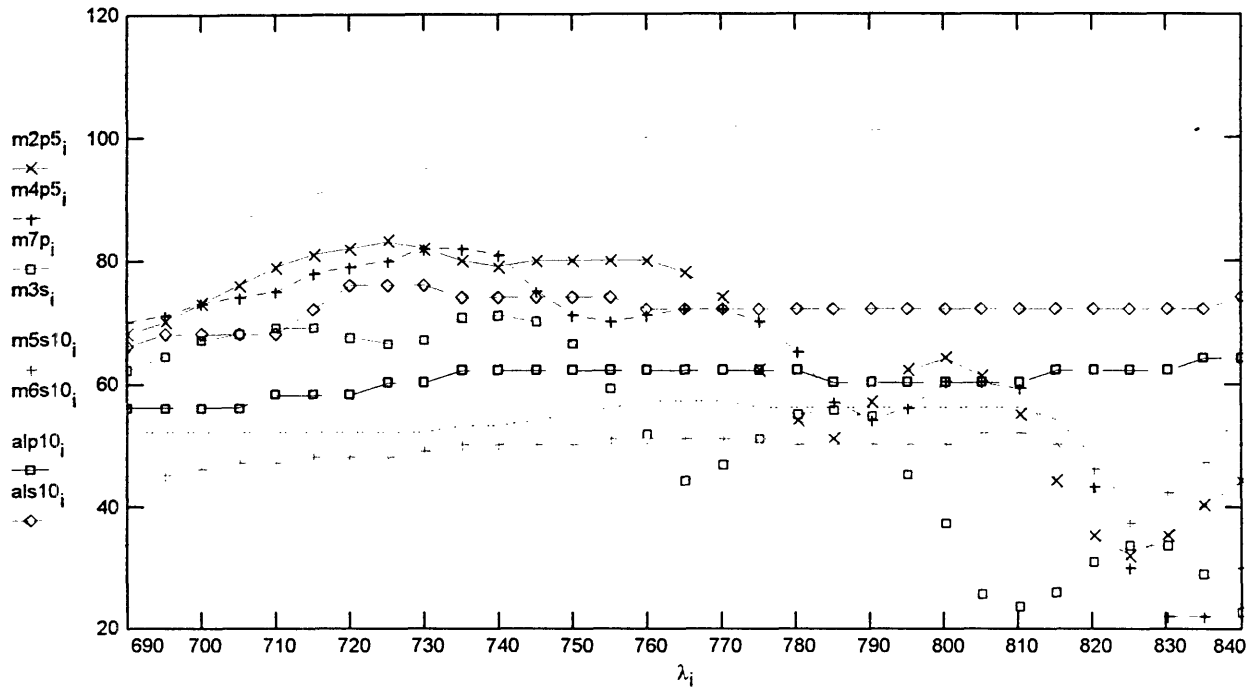

$Ss_{11} := READPRN(s11)$ $d := 0..length(Ss_{11}) - 1$ Read in empirical data

$p_i := \frac{m2p5_i \cdot m4p5_i \cdot m7p_i}{(alp10_i)^3}$ $p_{max} := max(p)$ $p := \frac{p}{p_{max}}$ Calculate P polarlization factor

$s_i := \left[\frac{m3s_i \cdot m5s10_i \cdot m6s10_i}{(als10_i)^3}\right]$ $s_{max} := max(s)$ $s := \frac{s}{s_{max}}$ Calculate S polarization factor

$s_{11_d} := \frac{Ss_{11_d}}{p_d \cdot s_d}$ $sum := \sqrt{\sum_d (s_{11_d})^2}$ $s_{11} := \frac{s_{11}}{sum}$ Adjust spectrum for mirror effects

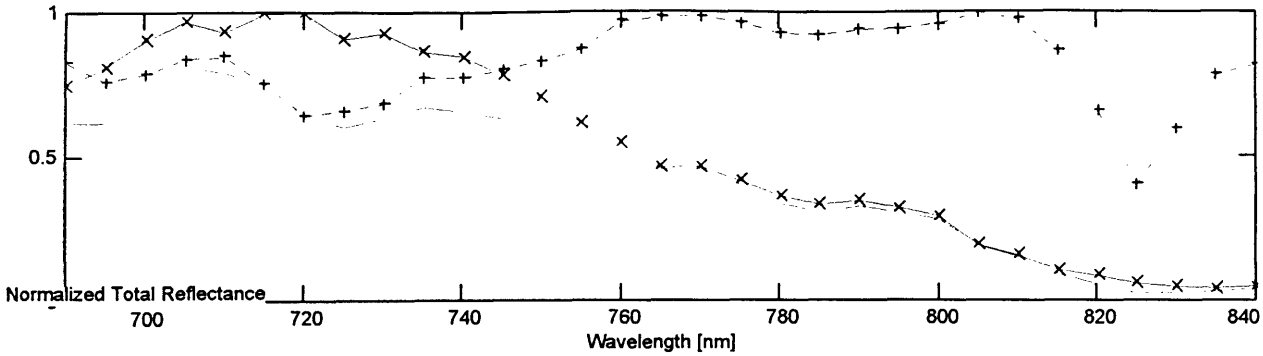

Horizontally Polarized
Vertically Polarized
Product of Hor and Ver Polarization Corrections

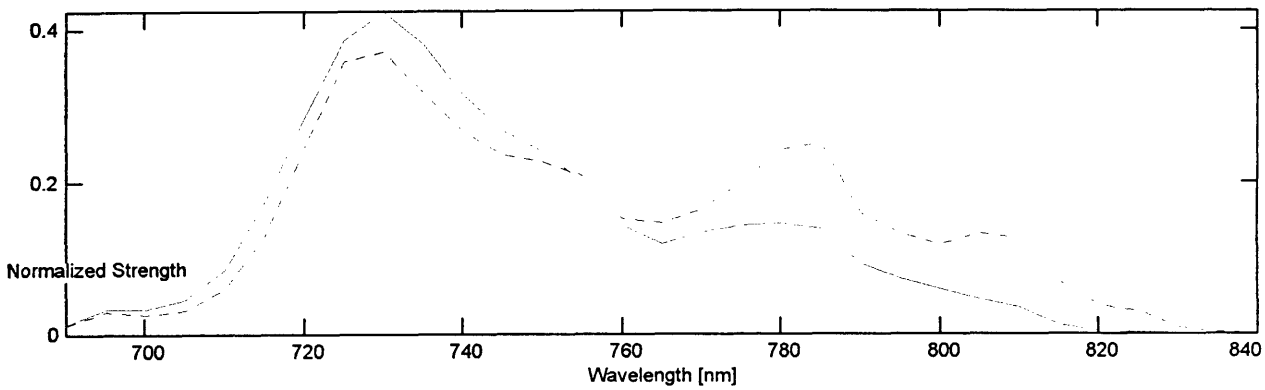

Original Spectra
Corrected Spectra

Worksheet #3, Appendix B

IDEAL AND BROAD BEAM DISTRIBUTION ANALYSIS

This worksheet calculates the spectrum change considering a circular and gaussian electron distribution with no energ spread or off axis emission.

$N_w := 70$ Number of periods in the wiggler $\quad i := 0..40 \quad j := 0..150$

$a_{w0} := .329$ On axis wiggler parameter

$\lambda_w := 8.8$ Wiggler period [mm] $\quad k_w := \frac{2\cdot\pi}{\lambda_w}$

$c := 3\cdot 10^8$ Speed of Light [m/s]

$E_o := .511$ Electron Rest Energy [MeV]

$E := 40.86$ Beam Energy [MeV]

$$\gamma_0 := \sqrt{\left(\frac{E}{E_o}\right)^2 + 1} \qquad \gamma_0 = 79.967$$

$\lambda_{L_j} := (690 + j\cdot 1)\cdot 10^{-6}$ Emitted wavelength in mm for range study

$y_i := i\cdot .05$ Distance from wiggler axis in mm.

$$a_{w_i} := a_{w0}\cdot\left[1 + \frac{1}{2}\cdot(k_w\cdot y_i)^2\right]$$ Off-axis wiggler parameter

$$\lambda_{R_i} := \frac{\lambda_w}{2\cdot\gamma_0^2}\cdot\left[1 + \frac{(a_{w_i})^2}{2}\right]$$ Off-axis resonant wavelength [mm] $\quad d\lambda_{i,j} := \lambda_{L_j} - \lambda_{R_i}$

$$P_{i,j} := \frac{2\cdot N_w^2\cdot e^2\cdot\gamma_0^2\cdot\frac{(a_{w_i})^2}{2}}{c\cdot\left[1 + \frac{(a_{w_i})^2}{2}\right]^2}\cdot\left[\frac{\sin\left(\pi\cdot N_w\cdot\frac{d\lambda_{i,j}}{\lambda_{R_i}}\right)}{\pi\cdot N_w\cdot\frac{d\lambda_{i,j}}{\lambda_{R_i}}}\right]^2$$

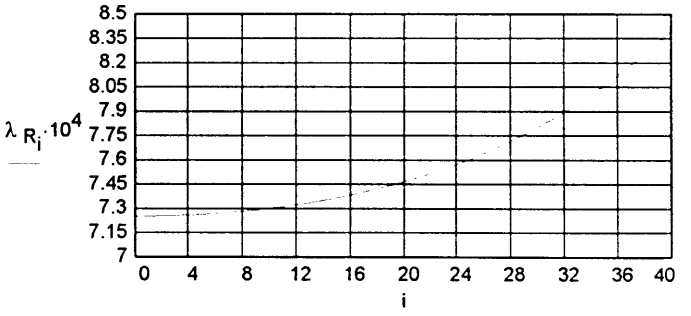

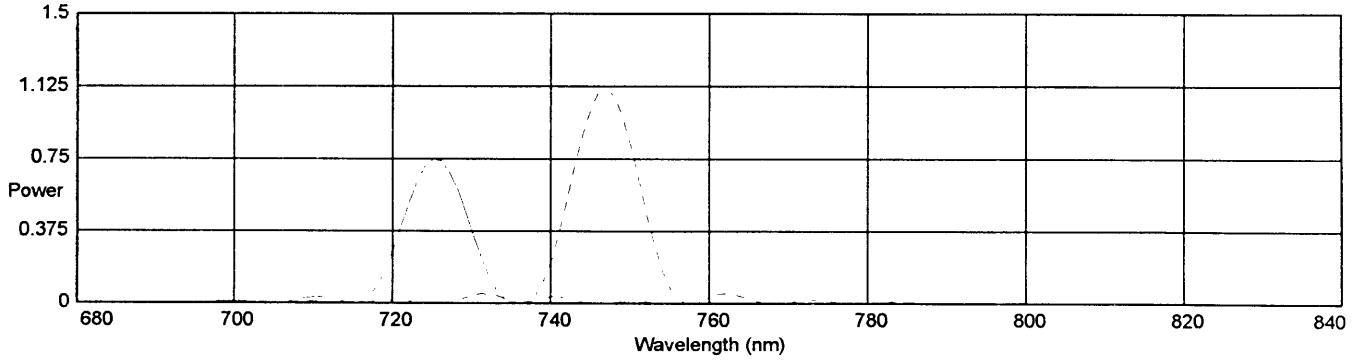

On-axis Spectra

Spectra if the beam is .1mm off axis

$$sum3 := \sqrt{\sum_j (P_{0,j})^2} \qquad P_{0,j} := \frac{P_{0,j}}{sum3}$$

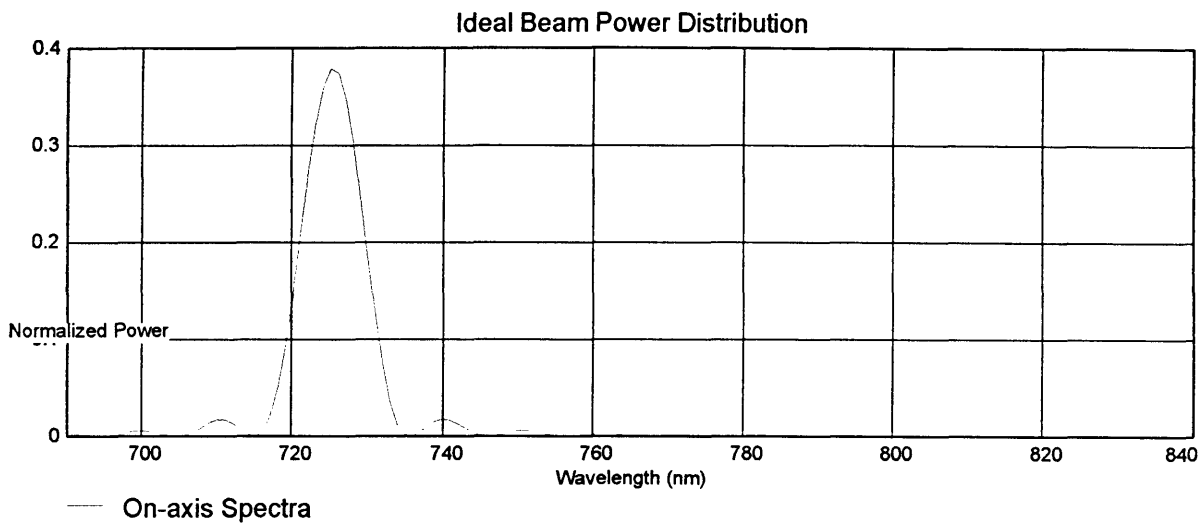

Now average over a distribution from all of the various different positions, assuming a circular distribution

$$k := 0..20 \qquad Power_j := \sum_k P_{k,j} \qquad sum := \sqrt{\sum_j (Power_j)^2} \qquad Power_j := \frac{Power_j}{sum} \qquad \sqrt{\sum_j (Power_j)^2} = 1.000$$

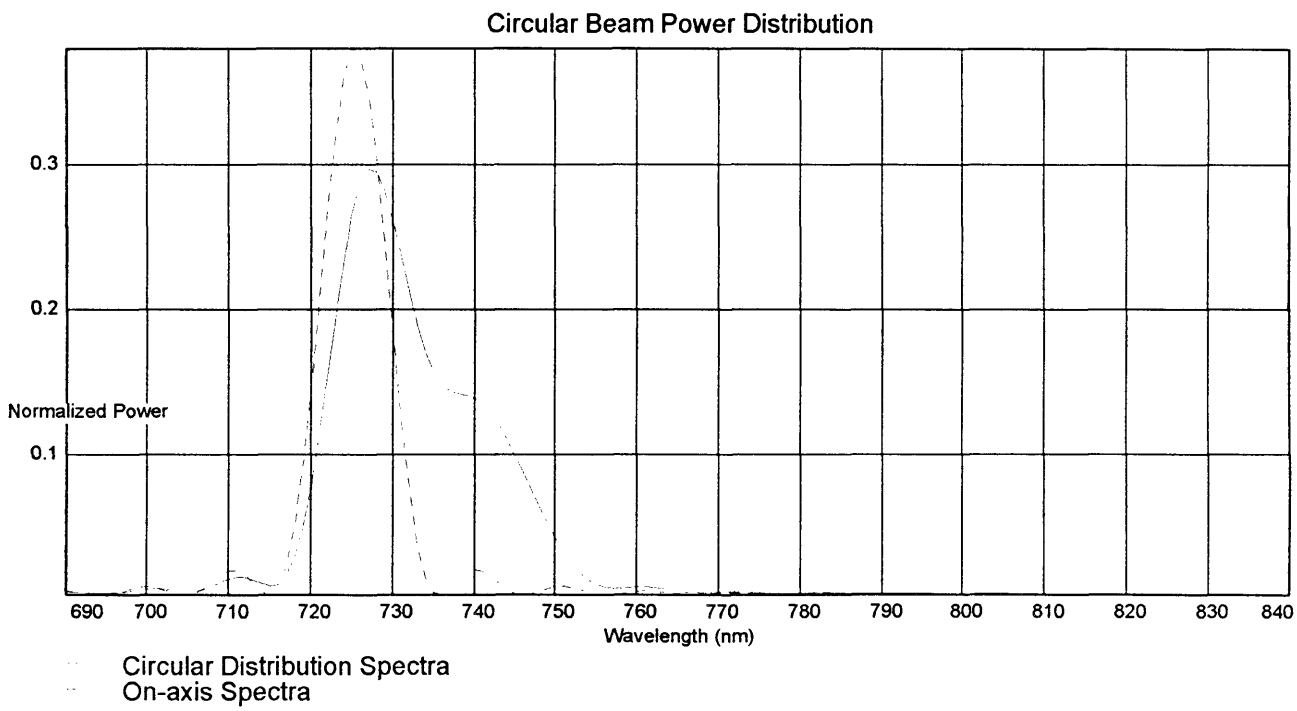

Worksheet #3, Appendix B

Look at a gaussian beam distribution

$k := 0 .. \text{length}(y)$ $\text{length}(y) = 41.000$

$$Pow_j := \sum_i \exp\left[-\frac{(y_i)^2}{.5}\right] \cdot P_{i,j} \qquad sum1 := \sqrt{\sum_j (Pow_j)^2} \qquad Pow_j := \frac{Pow_j}{sum1}$$

$s_{11} := \text{READPRN}(\text{cors11})$ $\lambda_{11} := \text{READPRN}(\text{lambda11})$ $z := 0 .. \text{length}(\lambda_{11}) - 1$

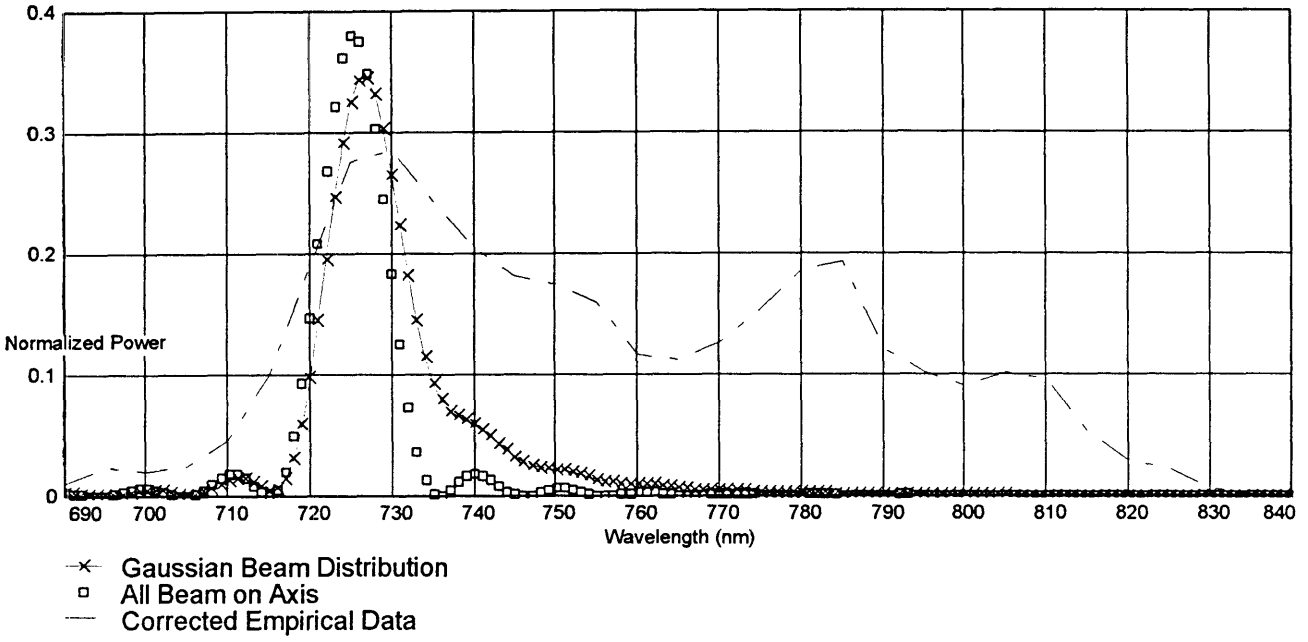

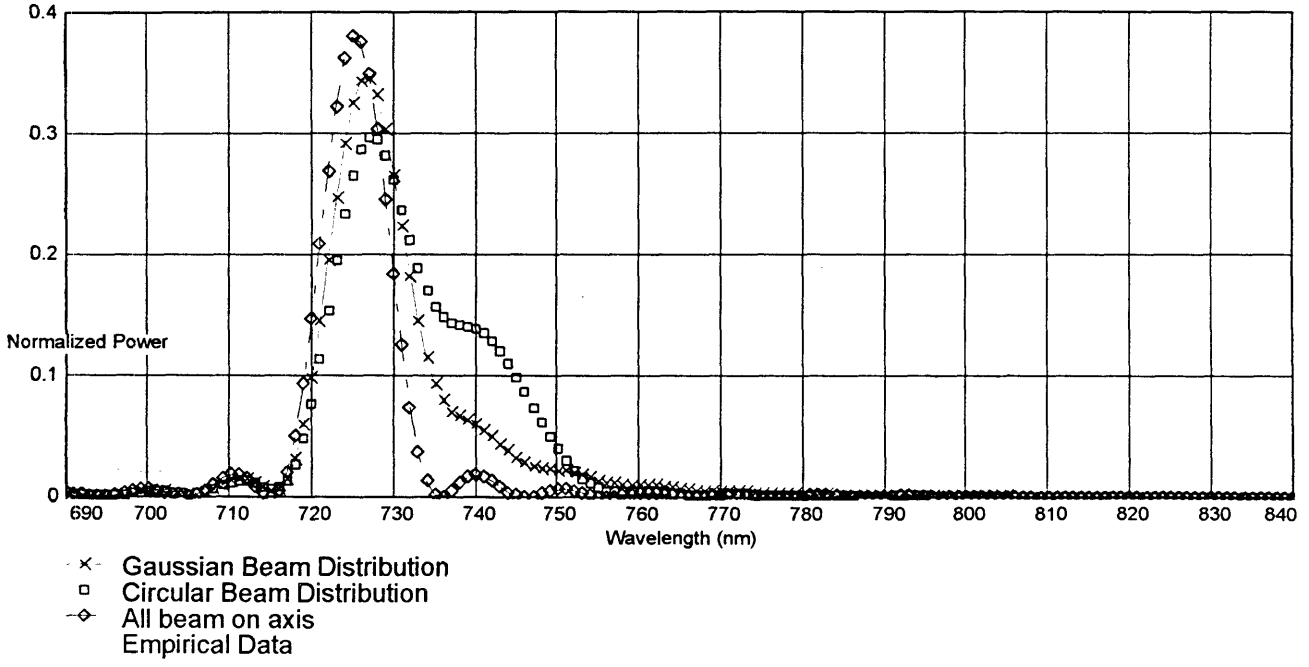

IDEAL BEAM WITH ENERGY SPREAD

This worksheet calculates the spectrum change considering an ideal distribution with energy spread or off axis emission. Notice that the energy spread just evenly spreads out the spectrum.

$N_w := 70$ Number of periods in the wiggler

$i_{max} := 40$

$a_{w0} := .329$ On axis wiggler parameter

$i := 0..i_{max}$ $j := 0..150$

$\lambda_w := 8.8$ Wiggler period [mm] $k_w := \frac{2\cdot\pi}{\lambda_w}$

$c := 3\cdot 10^8$ Speed of Light [m/s]

$E_o := .511$ Electron Rest Energy [MeV]

$E := 40.86$ Beam Energy [MeV]

$\delta E := .584$

$$dE_i := -\frac{\delta E}{2} + i\cdot\frac{\delta E}{i_{max}}$$

$$\gamma_i := \sqrt{\left(\frac{E + dE_i}{E_o}\right)^2 + 1}$$

$\lambda_{L_j} := (690 + j\cdot 1)\cdot 10^{-6}$ Emitted wavelength in mm for range study

$$\lambda_{R_i} := \frac{\lambda_w}{2\cdot(\gamma_i)^2}\cdot\left[1 + \frac{(a_{w0})^2}{2}\right]$$ Off-axis resonant wavelength [mm] $d\lambda_{i,j} := \lambda_{L_j} - \lambda_{R_i}$

$$P_{i,j} := \frac{2\cdot N_w{}^2\cdot e^2\cdot(\gamma_i)^2\cdot\frac{(a_{w0})^2}{2}}{c\cdot\left[1 + \frac{(a_{w0})^2}{2}\right]^2}\cdot\left[\frac{\sin\left(\pi\cdot N_w\cdot\frac{d\lambda_{i,j}}{\lambda_{R_i}}\right)}{\pi\cdot N_w\cdot\frac{d\lambda_{i,j}}{\lambda_{R_i}}}\right]^2$$

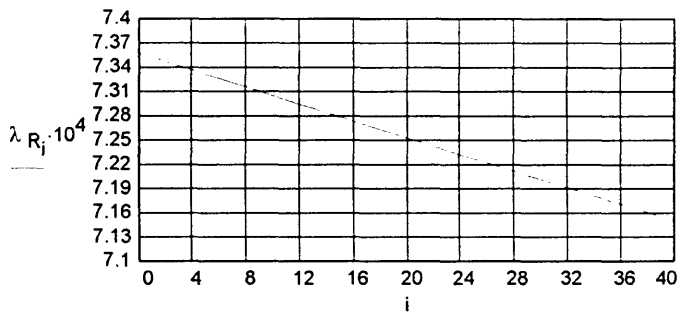

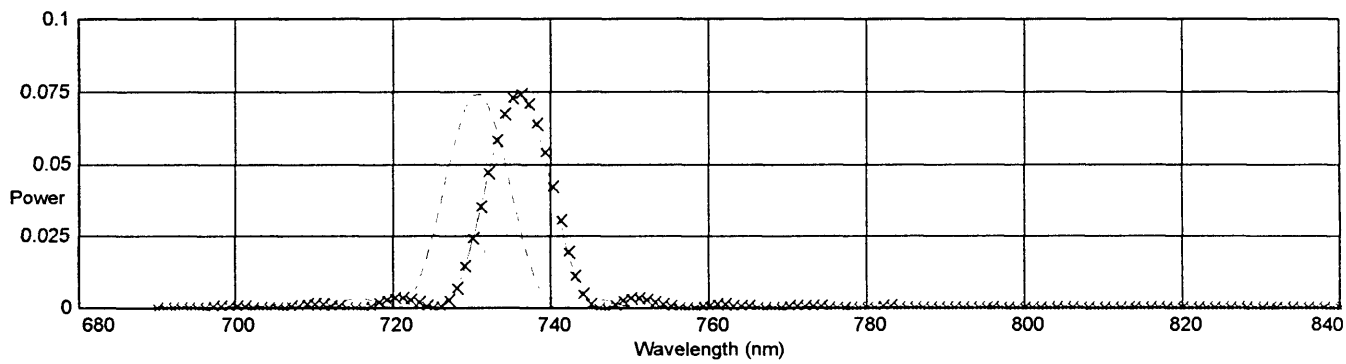

$$sum3 := \sqrt{\sum_j (P_{20,j})^2} \qquad P_{20,j} := \frac{P_{20,j}}{sum3} \qquad X_j := \sum_i P_{i,j} \qquad sum := \sqrt{\sum_j X_j} \qquad X := \frac{X}{sum}$$

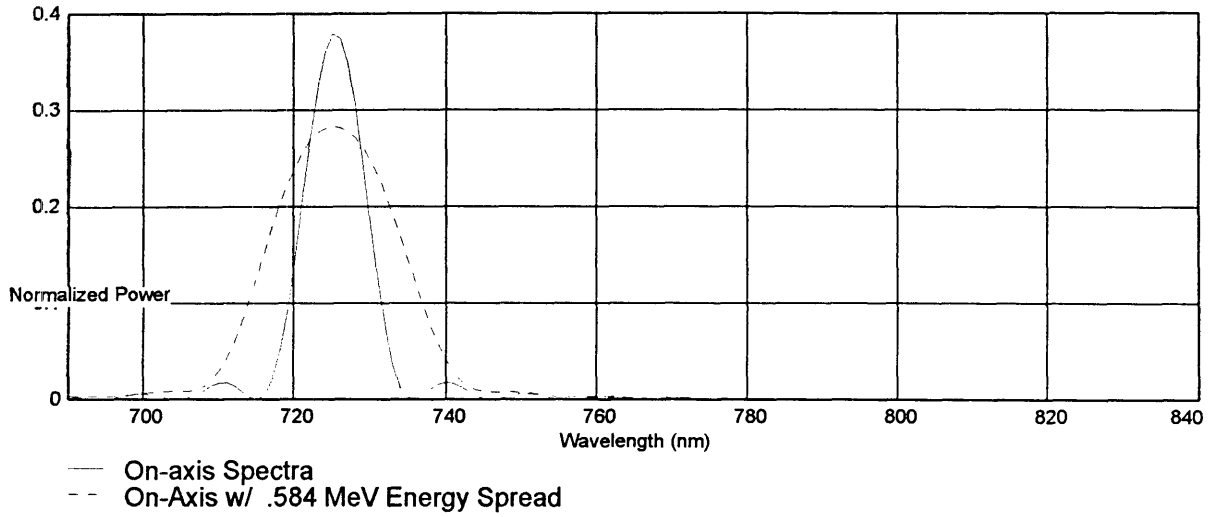

Worksheet #5, Appendix B

BEAM POSITION AND ENERGY COUPLING SPECTRUM

This worksheet calculates the spectrum if we assume that the energy and position are related. If the electrons' angles of incidence coming out of the last dipole to the wiggler are tied to the electron energy, the electrons will enter into the wiggler with higher energy electrons displaced off axis on one side with the lower energy electron will be on the other.

DECLARATION OF VARIABLES

$B_w := .4$ Wiggler Magnetic Field [T]

$N_w := 70$ Number of periods in the wiggler

$\lambda_w := .0088$ Wiggler period [m] $k_w := \frac{2\cdot\pi}{\lambda_w}$

$c := 3\cdot10^8$ Speed of Light [m/s]

$E_o := .511$ Electron Rest Energy [MeV]

$I := 22.75$ Dipole Current Setting [amps]

$dI := .325$ Momentum Slit Current Range [amps]

$Cal := 1.796$ Dipole Current to MeV Calibration

$e := 1.602\cdot10^{-19}$ Electron Charge [C]

$m_e := 9.1\cdot10^{-31}$ Electron Mass [kg]

$c := 3\cdot10^8$ Speed of Light [m/s]

$d\lambda_j := j\cdot3\cdot10^{-9}$ Wavelength Step [m]

$f_{start} := 690\cdot10^{-9}$ Starting Frequency for 150 nm scan [m]

Definition of Range Variables

$i_{max} := 40$ $i := 0..i_{max}$ Y Off-axis radius

$j_{max} := 50$ $j := 0..j_{max}$ Wavelength range

$m_{max} := 30$ $m := 0..m_{max}$ Energy range

$r := 0..j_{max}$

CALCULATION OF WIGGLER PARAMETERS

$a_{w0} := \frac{e\cdot B_w}{m_e\cdot c\cdot k_w}$ $a_{w0} = 0.329$ On-axis Wiggler Parameter

$y_m := -r_{axis} + 2\cdot m\cdot\frac{r_{axis}}{m_{max}}$ Stepped distance away from axis [m]

SELECT RANGE VARIABLES FOR WAVELEGTH AND BEAM RADIUS

$\delta E := Cal\cdot dI$ $\delta E = 0.584$ Energy Spread [MeV] $FWHM := \delta E$

$E := Cal\cdot I$ $E = 40.859$ Beam Energy [MeV]

$dE_m := -\delta E + m\cdot\frac{2\cdot\delta E}{m_{max}}$ Gives energy spread range of +/- dE MeV of the beam energy stepped over m starting at low energies to high $\frac{2\cdot\delta E}{m_{max}} = 0.039$

Worksheet #5, Appendix B

$$\gamma_m := \sqrt{\left(\frac{E + dE_m}{E_o}\right)^2 + 1} \qquad a_{w_m} := a_{w0}\cdot\left[1 + \frac{(k_w \cdot y_m)^2}{2}\right]$$ Off-axis wiggler parameter

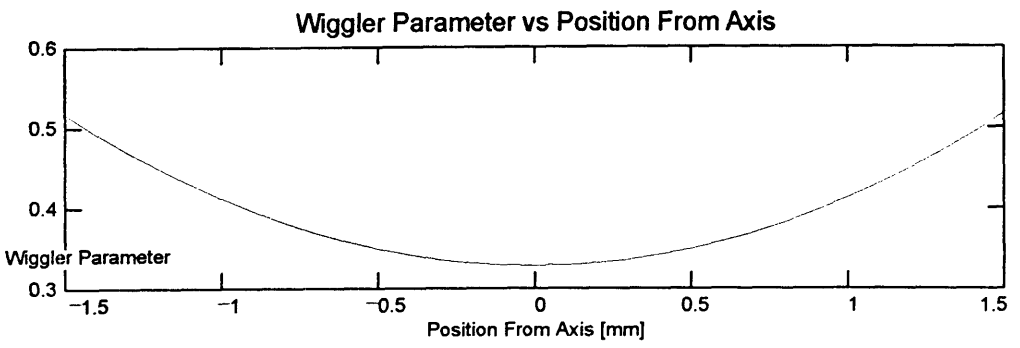

$$\lambda_{R_m} := \frac{\lambda_w}{2\cdot(\gamma_m)^2}\cdot\left[1 + \frac{(a_{w_m})^2}{2}\right] \qquad \omega_{R_m} := \frac{2\cdot\pi\cdot c}{\lambda_{R_m}}$$ Yields range of resonant frequencies for the range in beam energy.

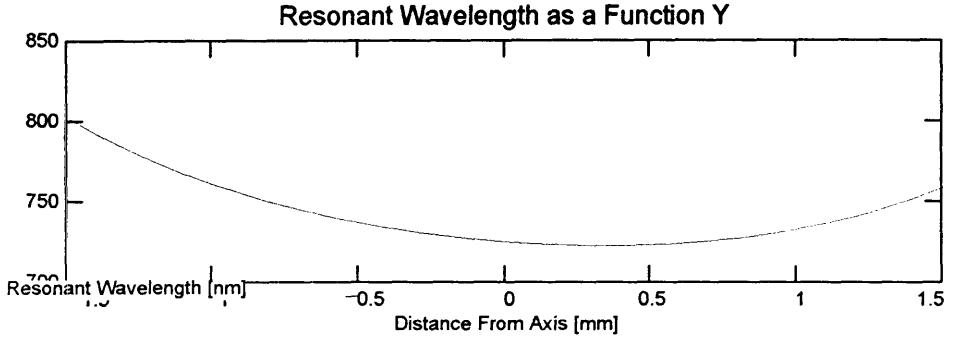

$\lambda_{L_j} := (f_{start} + d\lambda_j)$ Emitted wavelength in m for range study $\omega_j := \frac{2\cdot\pi\cdot c}{\lambda_{L_j}}$ Corresponding frequency

$$P_{j,m} := \frac{\frac{(a_{w_m})^2}{2}}{\left[1 + \frac{(a_{w_m})^2}{2}\right]}\cdot\left[\frac{\sin\left(2\cdot\pi\cdot N_w\cdot\frac{\omega_j - \omega_{R_m}}{\omega_{R_m}}\right)}{2\cdot\pi\cdot N_w\cdot\frac{\omega_j - \omega_{R_m}}{\omega_{R_m}}}\right]^2$$

$\lambda_{L_j} := \lambda_{L_j}\cdot 10^9$

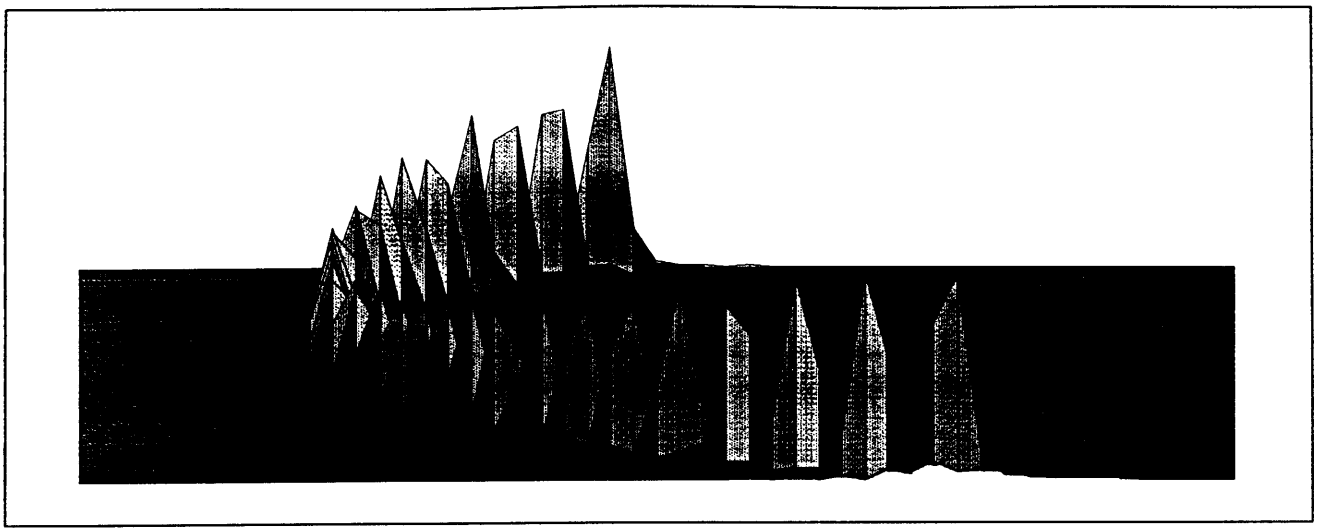

P

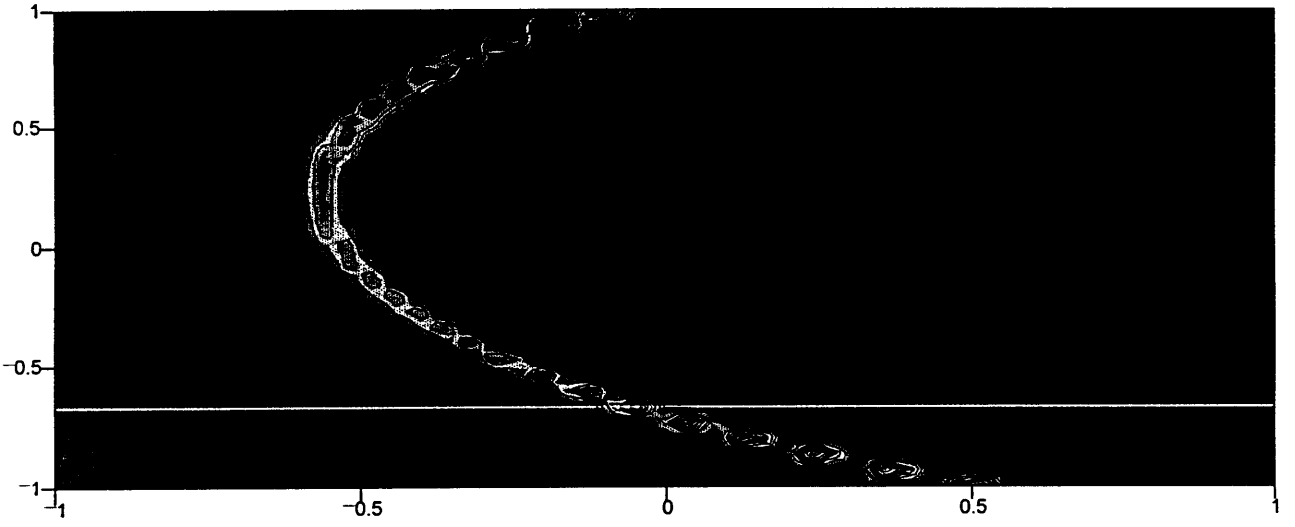

P

$Pow_j := \sum_m P_{j,m}$ $XPow_m := \sum_j P_{j,m}$ $v_j := j$

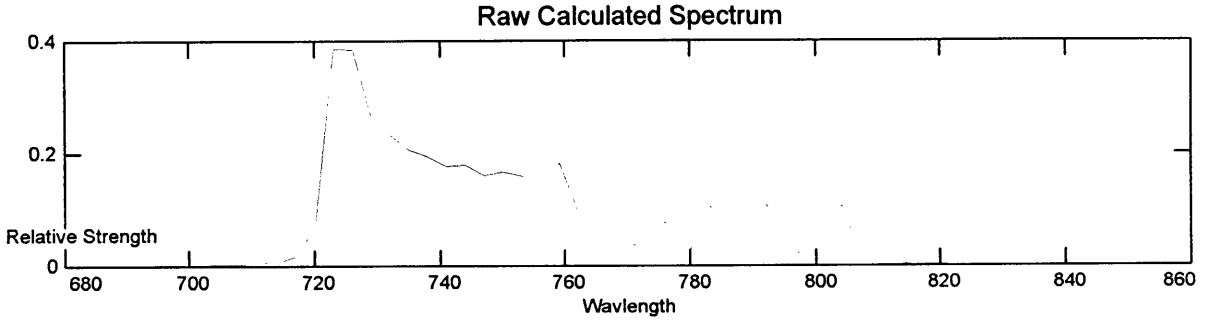

Worksheet #5, Appendix B

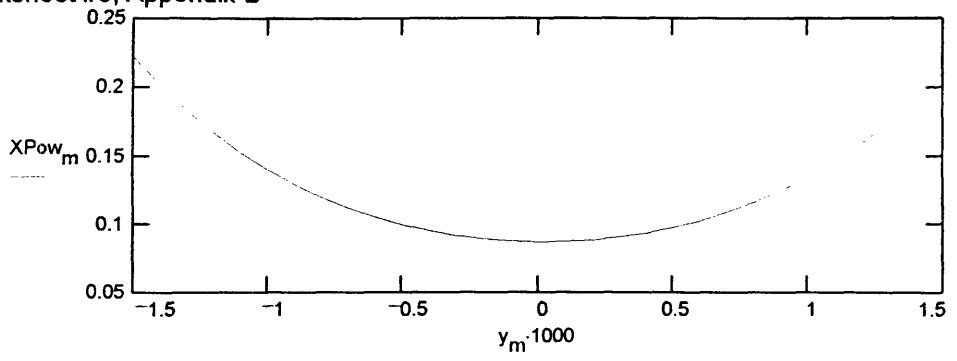

$$\text{Beam}_{dist_m} := \exp\left[-\frac{(dE_m + offset)^2}{FWHM}\right] \qquad YPow_j := \sum_m \text{Beam}_{dist_m} \cdot P_{j,m}$$

Temper Spectrum with Estimate of Beam Distribution

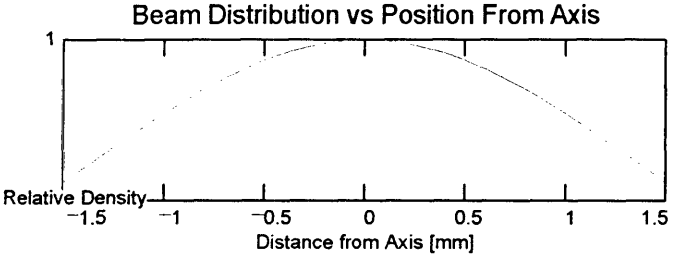

Low Energy High Energy

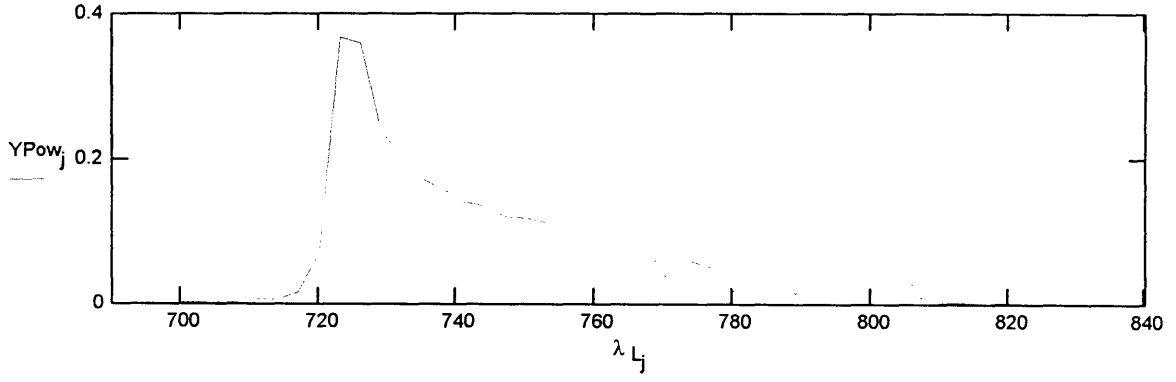

$f1 := cfft(YPow)$ $q := 10..40$ $f1_q := 0$ Remove middle harmonics from FFT of the Distribution

$f1_u := cfft(YPow)$

Worksheet #5, Appendix B

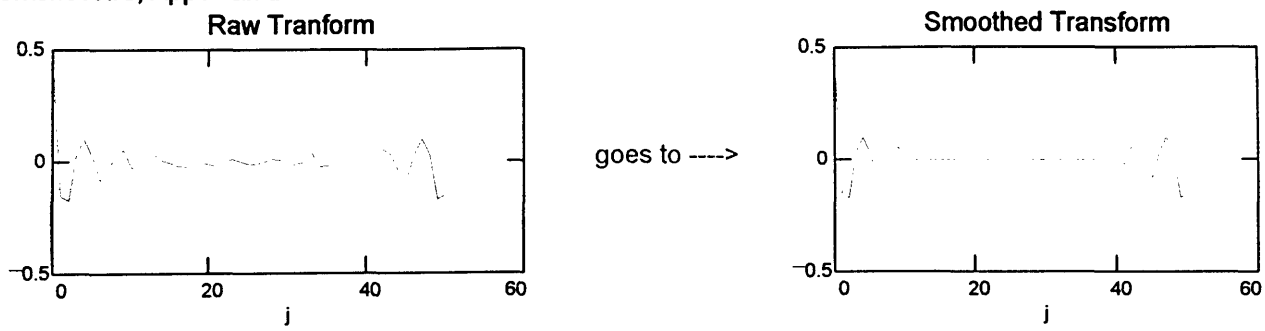

$k3 := Re(icfft(f1))$ Return back to spectrum domain.

$s_{11} := READPRN(cors11)$ $\lambda := READPRN(lambda11)$ $d := 0..length(\lambda) - 1$

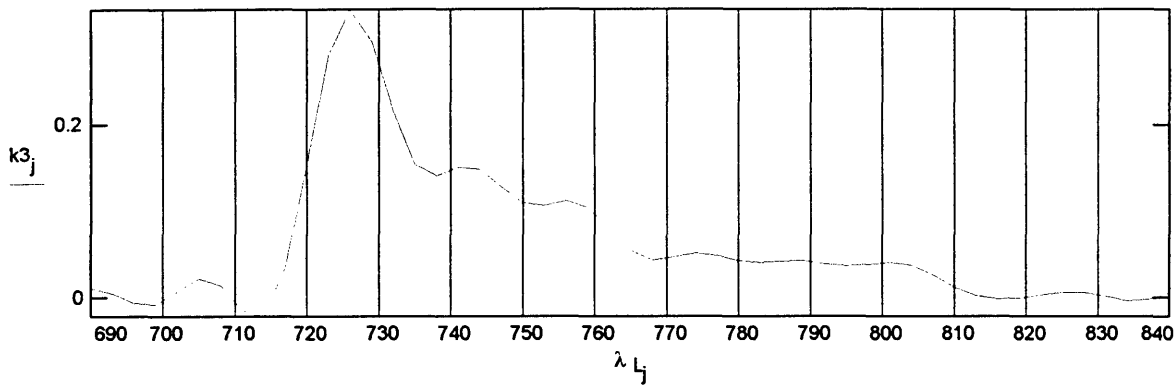

$r_{axis} \equiv .0015$ E-beam Radius from Axis [m] $offset \equiv 0$ Shifts energy distribution center

$K3 := \sqrt{\sum_j (k3_j)^2}$ $k3_j := \frac{k3_j}{K3}$ Normalize the curve $\sum_j (k3_j)^2 = 1$ Check Normalization

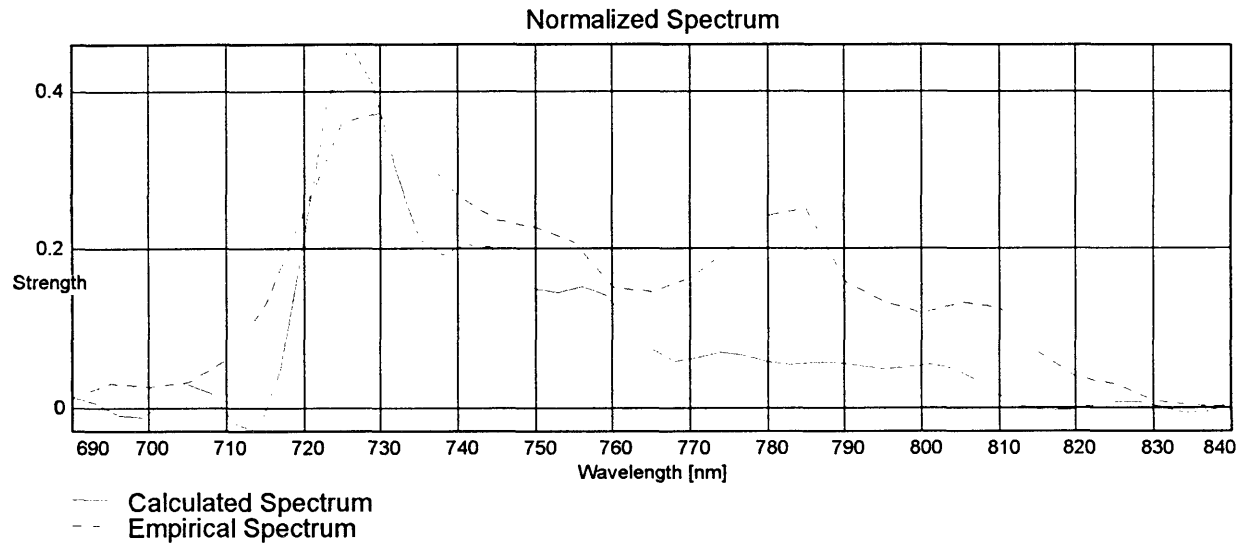

OFF AXIS EMISSION WITH NO ENERGY OR BEAM EFFECTS

This worksheet calculates the off axis emission with no energy spread or beam distribution.

DECLARATION OF VARIABLES

$B_w := .4$ Wiggler Magnetic Field [T]

$N_w := 70$ Number of periods in the wiggler

$\lambda_w := .0088$ Wiggler period [m] $k_w := \frac{2\cdot\pi}{\lambda_w}$

$c := 3\cdot10^8$ Speed of Light [m/s]

$E_o := .511$ Electron Rest Energy [MeV]

$I := 22.75$ Dipole Current Setting [amps]

$Cal := 1.796$ Dipole Current to MeV Calibration

$e := 1.602\cdot10^{-19}$ Electron Charge [C]

$m_e := 9.1\cdot10^{-31}$ Electron Mass [kg]

$c := 3\cdot10^8$ Speed of Light [m/s]

$\varepsilon_o := 8.85\cdot10^{-12}$ Permitivity of Free Space [C^2/N^*m^2]

$\delta\lambda := 5$ Wavelength Step Function [nm]

$\phi_{div} := 2\cdot\pi$ Rotation Angle

$\theta_{div} := 4\cdot10^{-3}$ Horizontal Half-angle

$f_{start} := 690$ Starting Frequency [nm]

Definition of Range Variables

$j_{max} := 30$	$j := 0..j_{max}$	Wavelength Step
$k_{max} := 10$	$k := 0..k_{max}$	Set bessel fn add range
$m_{max} := 40$	$m := 0..m_{max}$	Set phi range
$n_{max} := 40$	$n := 0..n_{max}$	Set theta range

CALCULATION OF WIGGLER PARAMETERS

$a_{w0} := \frac{e\cdot B_w}{m_e\cdot c\cdot k_w}$ $a_{w0} = 0.329$ On-axis Wiggler Parameter

$E := I\cdot Cal$ $E = 40.859$ Beam Energy $\gamma := \sqrt{\left(\frac{E}{E_o}\right)^2 + 1}$ $\gamma = 79.965$

CALCULATION OF ANGULAR STEP FUNCTION

$\delta\theta := \frac{2\cdot\theta_{div}}{n_{max}}$ $\delta\phi := \frac{\phi_{div}}{m_{max}}$ Sets step angle

$\theta_n := -\theta_{div} + \delta\theta\cdot n$ $\phi_m := \delta\phi\cdot m$ Sets range of angles

$\lambda_{L_j} := \left(f_{start} + \delta\lambda\cdot j\right)\cdot10^{-9}$ Emitted wavelength range [m]

CALCULATION OF FREQUENCY SPECTRUM

$$\alpha_{m,n} := \frac{2^{1.5} \cdot a_{w0} \cdot \gamma \cdot \theta_n \cdot \cos(\phi_m)}{1 + \frac{a_{w0}^2}{2} + \gamma^2 \cdot (\theta_n)^2} \qquad \xi_n := \frac{1}{2} \cdot \frac{a_{w0}^2}{1 + \frac{a_{w0}^2}{2} + \gamma^2 \cdot (\theta_n)^2}$$

$$F\,odd_{n,m} := \left[\sum_k (-1)^k \cdot Jn(2 \cdot k, \alpha_{n,m}) \cdot (Jn(k, \xi_n) - Jn(1 + k, \xi_n)) \right]^2$$

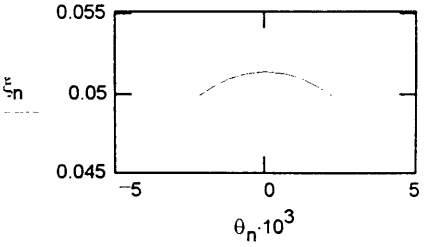

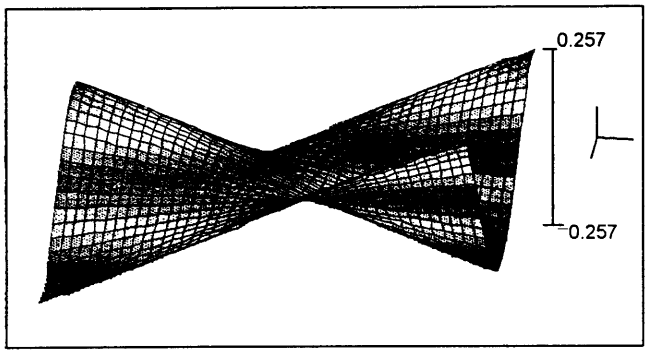

α

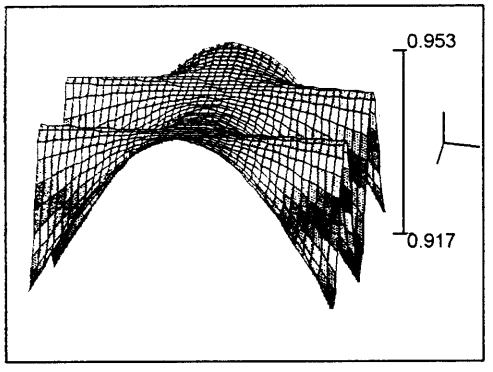

F odd

$$\lambda_{R_n} := \frac{\lambda_w}{2 \cdot \gamma^2} \cdot \left[1 + \frac{a_{w0}^2}{2} + \gamma^2 \cdot (\theta_n)^2 \right]$$ Resonant Frequencies [m]

$d\lambda_{j,n} := \lambda_{L_j} - \lambda_{R_n}$ Calculates the difference in sample frequency and resonant frequency

$F_n = \sum_m F\,odd_{n,m}$ Sum over all azimuthal angles

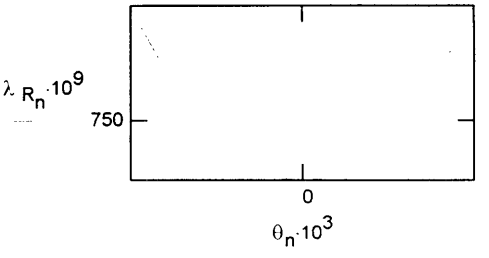

$$I_{n,j} := \frac{e^2 \cdot a_{w0}^2 \cdot \gamma^2 \cdot N_w^2}{2 \cdot \pi \cdot \varepsilon_o \cdot c \cdot \left[1 + \frac{a_{w0}^2}{2} + \gamma^2 \cdot (\theta_n)^2\right]^2} \cdot \left[\frac{\sin\left(\pi \cdot N_w \cdot \frac{d\lambda_{j,n}}{\lambda R_n}\right)}{\left(\pi \cdot N_w \cdot \frac{d\lambda_{j,n}}{\lambda R_n}\right)}\right]^2 \cdot F_n$$

Power Distribution Function

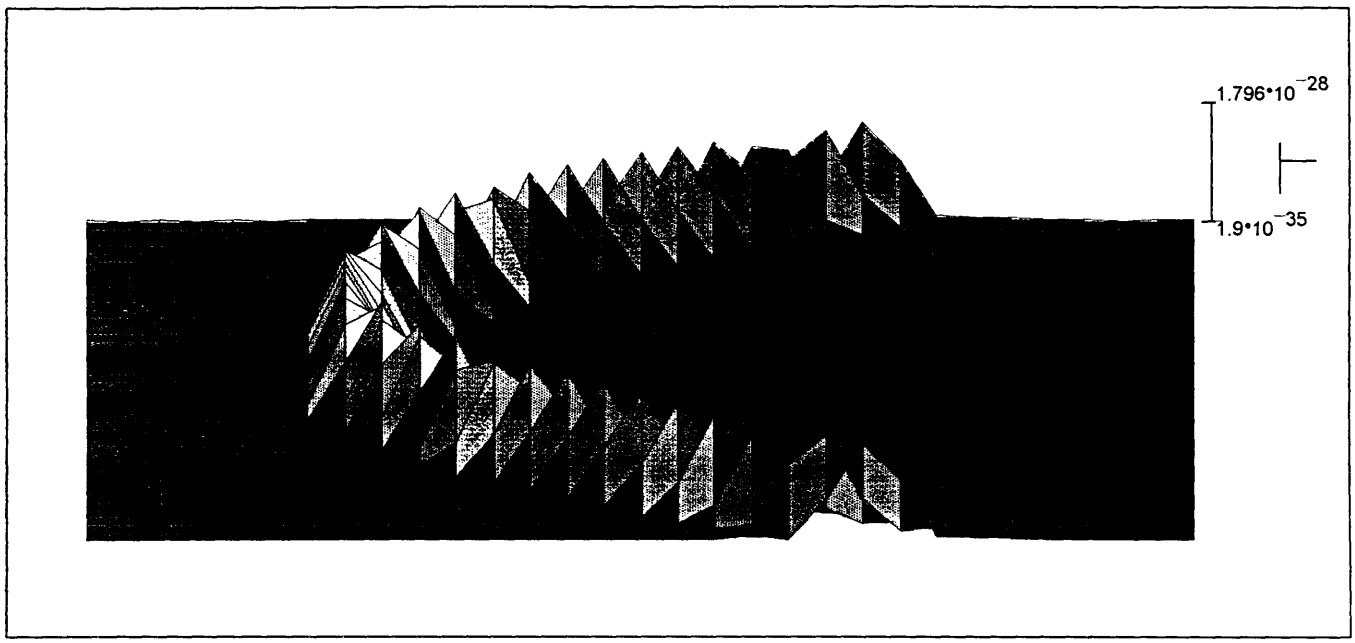

I

$P_j := \sum_n I_{n,j}$ Sum over the solid cone angles

$p := \sqrt{\sum_j (P_j)^2}$ $P_j := \frac{P_j}{p}$ $\sum_j (P_j)^2 = 1$ Normalize and Check

f := cfft(P) Take fourier transform and remove higher order jitter and return to spectrum domain

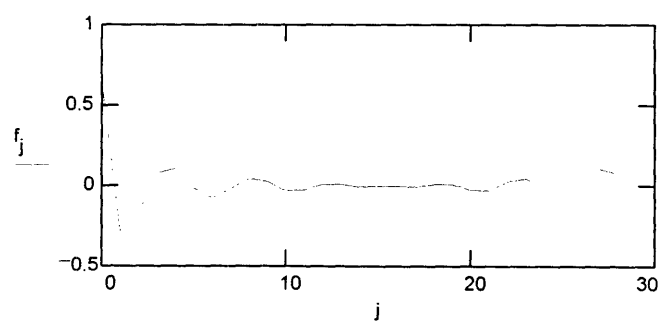

i := 7..23

$f_i := 0$

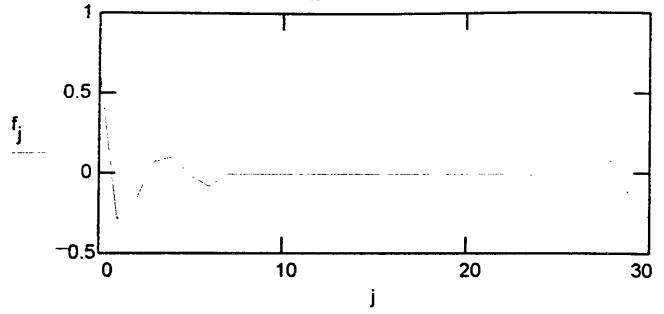

$P := Re(icfft(f))$ $s_{11} := READPRN(cors11)$

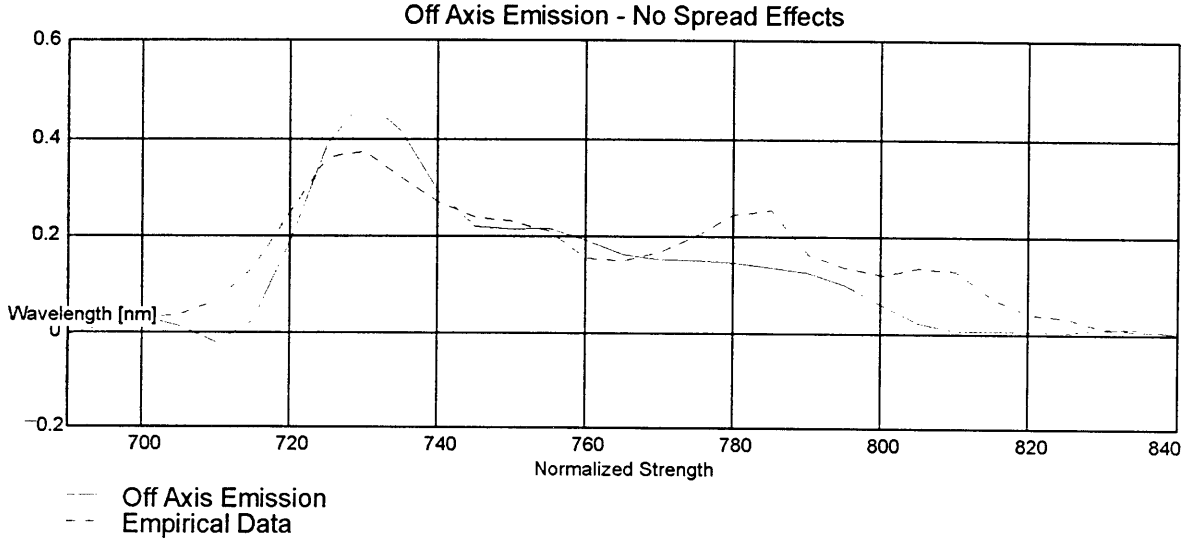

OFF AXIS EMISSION WITH ENERGY SPREAD EFFECTS

This worksheet calculates the off axis emissions with energy spread but with no beam distribution. Line P5 is the off-axis distribution at 40.86 MeV. PTOT is the off-axis average spectrum with all energies included.

DECLARATION OF VARIABLES

$E_o := .511$ Electron Rest Energy [MeV]

$I := 22.75$ Dipole Current Setting [amps]

$dI := .325$ Energy Spread

$Cal := 1.796$ Dipole Current to MeV Calibration

$j_{max} := 30$ $j := 0..j_{max}$ Wavelength Step

CALCULATION OF WIGGLER PARAMETERS

$E := I \cdot Cal$ $E = 40.859$ Beam Energy $s_{max} := 10$ $s := 0..s_{max}$

$\delta E := Cal \cdot dI$ $\delta E = 0.584$ Energy Spread [MeV] $FWHM := \delta E$

$dE_s := -\frac{\delta E}{2} + s \cdot \frac{\delta E}{s_{max}}$ Gives energy spread range of +/- dE MeV of the beam energy stepped over m starting at low energies to high

$DIST_s := \exp\left[-\frac{(dE_s)^2}{.2 \cdot FWHM}\right]$ Assume gaussian distribution of electrons for a given energy focused on the mean value, E.

$\lambda_L := READPRN(lambda11)$ $P5 := READPRN(P5) \cdot DIST_5$

$P0 := READPRN(P0) \cdot DIST_0$ $P6 := READPRN(P6) \cdot DIST_6$

$P1 := READPRN(P1) \cdot DIST_1$ $P7 := READPRN(P7) \cdot DIST_7$

$P2 := READPRN(P2) \cdot DIST_2$ $P8 := READPRN(P8) \cdot DIST_8$

$P3 := READPRN(P3) \cdot DIST_3$ $P9 := READPRN(P9) \cdot DIST_9$

$P4 := READPRN(P4) \cdot DIST_4$ $P10 := READPRN(P10) \cdot DIST_{10}$

$PTOT_j := (P0_j + P1_j + P2_j + P3_j + P4_j + P5_j + P6_j + P7_j + P8_j + P9_j + P10_j)$

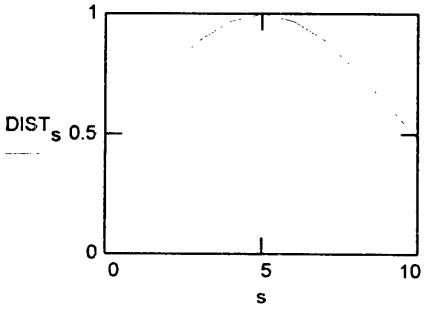

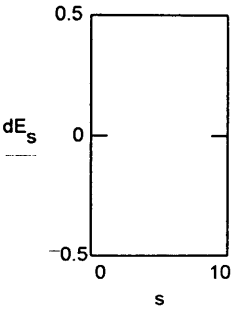

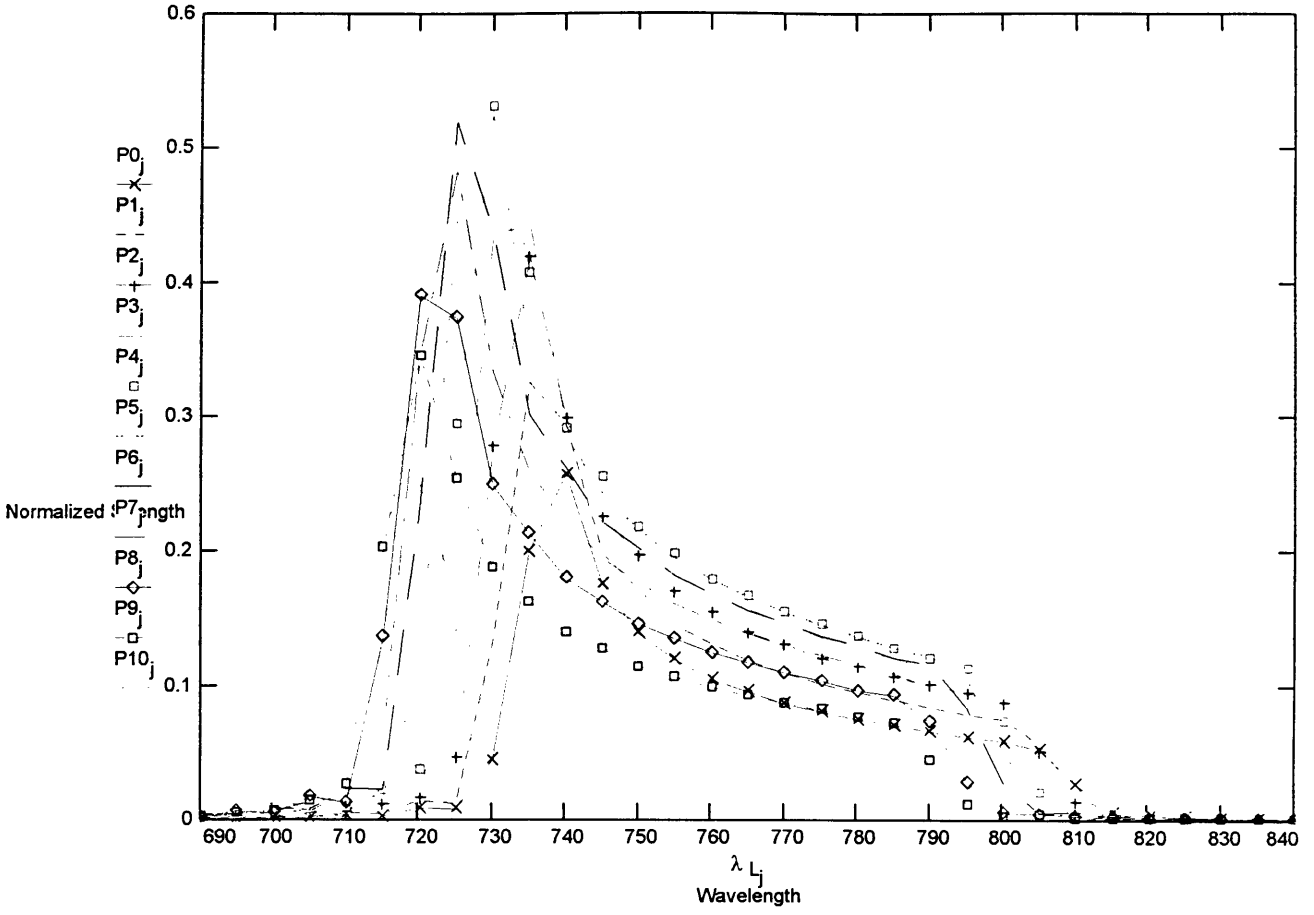

$$sum := \sqrt{\sum_j (PTOT_j)^2} \qquad PTOT := \frac{PTOT}{sum} \qquad s_{11} := READPRN(cors11)$$

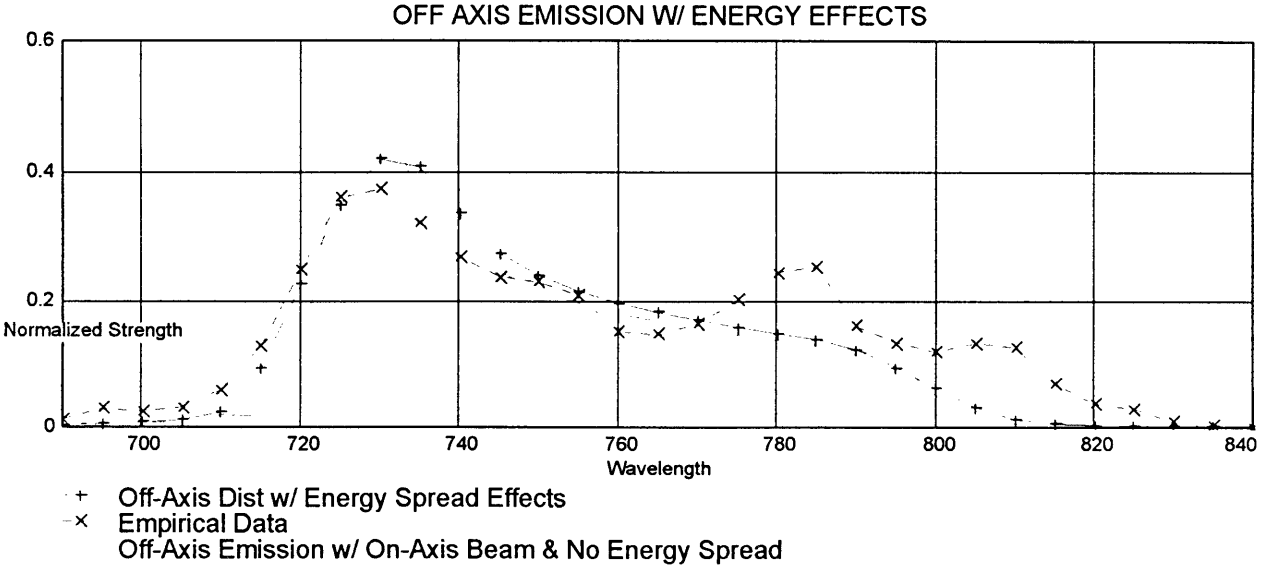

OFF AXIS EMISSION WITH ENERGY SPREAD AND BROAD BEAM EFFECTS

This worksheet calculates the off axis emissions with energy spread and beam distribution.

DECLARATION OF VARIABLES

$s_{max} := 20$ $\quad s := 0..s_{max}$

$y_{max} := .001$

$FWHM := .0005$

$$y_s := -y_{max} + \frac{s \cdot 2 \cdot y_{max}}{s_{max}}$$

$$DIST_s := \exp\left[-\frac{(y_s \cdot 10)^2}{.08 \cdot FWHM}\right]$$

Taking the results derived in FREQDIS1, we assume that the position distribution of the electrons is gaussian. Reading the in the results from FREQDIS1, we can relate the relative spectral intesity due to the position of the electrons and come up with the projected spectrum for off axis emission with energy spread and broad beam effects.

From FREQDIS1, we can see that a_w has a parabolic shape to it. So we only need to calculate the first half of the positions since the second half is only a reflection of the first. Note that P10 is the spectrum where y=0 and all the beam travels down the axis.

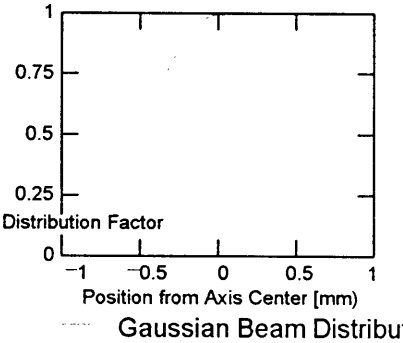

Gaussian Beam Distribution

$\lambda_L := READPRN(spectrum)$

$P0 := READPRN(PTOT0) \cdot DIST_0$ $\quad P5 := READPRN(PTOT5) \cdot DIST_5$

$P1 := READPRN(PTOT1) \cdot DIST_1$ $\quad P6 := READPRN(PTOT6) \cdot DIST_6$

$P2 := READPRN(PTOT2) \cdot DIST_2$ $\quad P7 := READPRN(PTOT7) \cdot DIST_7$

$P3 := READPRN(PTOT3) \cdot DIST_3$ $\quad P8 := READPRN(PTOT8) \cdot DIST_8$

$P4 := READPRN(PTOT4) \cdot DIST_4$ $\quad P9 := READPRN(PTOT9) \cdot DIST_9$

$j := 0..length(\lambda_L) - 1$ $\quad P10 := READPRN(PTOT10) \cdot DIST_{10}$

$$PTOT_j := (P0_j + P1_j + P2_j + P3_j + P4_j + P5_j + P6_j + P7_j + P8_j + P9_j + P10_j)$$

$$sum := \sqrt{\sum_j (PTOT_j)^2} \qquad PTOT := \frac{PTOT}{sum} \qquad \sqrt{\sum_j (PTOT_j)^2} = 1$$

$s_{11} := READPRN(cors11)$

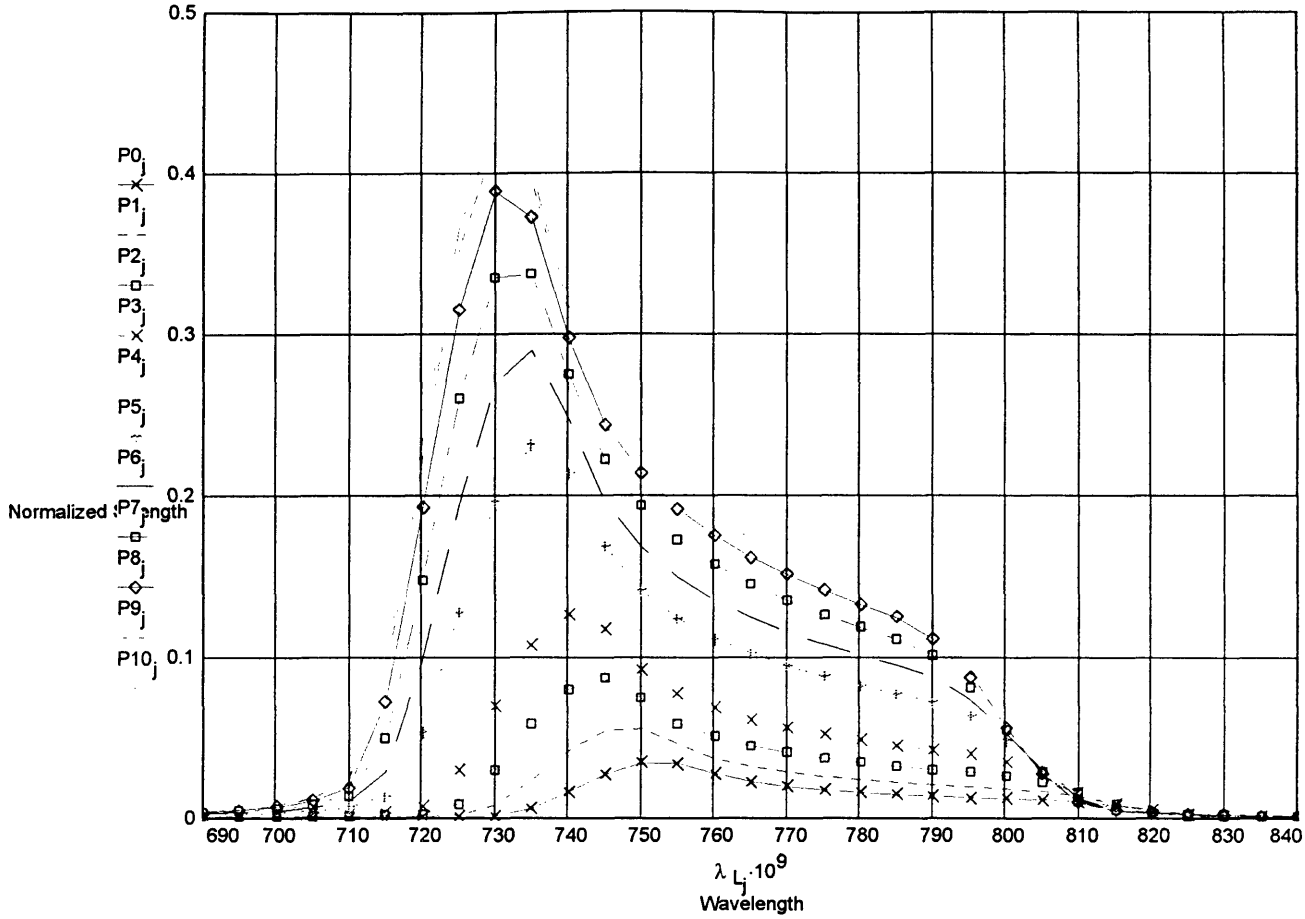
0.5
0.4
0.3
0.2
0.1
0
P0j
P1j
P2j
P3j
P4j
P5j
P6j
P7j
P8j
P9j
P10j
Normalized Strength
690 700 710 720 730 740 750 760 770 780 790 800 810 820 830 840
λ Lj·10^9
Wavelength

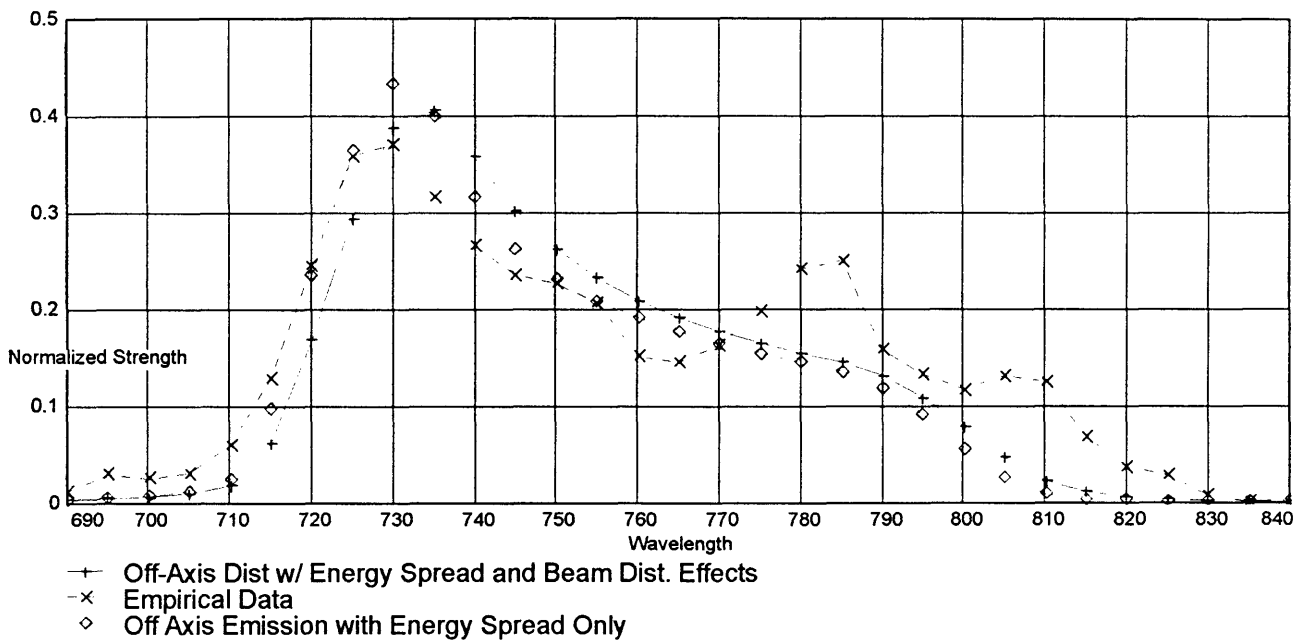
0.5
0.4
0.3
0.2
0.1
0
Normalized Strength
690 700 710 720 730 740 750 760 770 780 790 800 810 820 830 840
Wavelength
Off-Axis Dist w/ Energy Spread and Beam Dist. Effects
Empirical Data
Off Axis Emission with Energy Spread Only

OFF AXIS EMISSION WITH VARIABLE COLLECTION ANGLE EFFECTS

This worksheet calculates the spectrum if we collect from half angles from 0 to 5 mrad.

DECLARATION OF VARIABLES

$B_w := .4$ Wiggler Magnetic Field [T]

$N_w := 70$ Number of periods in the wiggler

$\lambda_w := .0088$ Wiggler period [m] $k_w := \frac{2\cdot\pi}{\lambda_w}$

$c := 3\cdot10^8$ Speed of Light [m/s]

$E_o := .511$ Electron Rest Energy [MeV]

$I := 22.75$ Dipole Current Setting [amps]

$dI := .325$ Beam Energy Spread [amps]

$Cal := 1.796$ Dipole Current to MeV Calibration

$e := 1.602\cdot10^{-19}$ Electron Charge [C]

$m_e := 9.1\cdot10^{-31}$ Electron Mass [kg]

$\varepsilon_o := 8.85\cdot10^{-12}$ Permitivity of Free Space [C^2/N^*m^2]

$\delta\lambda := 1$ Wavelength Step Function [nm]

$\phi_{div} := 2\cdot\pi$ Azimuthal Rotation Angle

Definition of Range Variables

$n_{max} := 40$	$n := 0..n_{max}$	Set theta range
$m_{max} := 40$	$m := 0..m_{max}$	Set phi range
$k_{max} := 10$	$k := 0..k_{max}$	Set bessel fn add range
$j_{max} := 150$	$j := 0..j_{max}$	Wavelength Step
$s_{max} := 10$		
$i_{max} := 20$		

$i := 10$

$f_{start} := 690$ Starting Frequency [nm]

$y_{max} := .001$ Max Displacement from Wiggler Axis [m]

$$y_i := -y_{max} + \frac{i\cdot y_{max}}{i_{max}}\cdot 2$$

$a_{w0} := \frac{e\cdot B_w}{m_e\cdot c\cdot k_w}$ $a_{w0} = 0.329$ On-axis Wiggler Parameter

$$a_w := a_{w0}\cdot\left[1 + \frac{1}{2}\cdot(k_w\cdot y_i)^2\right]$$

$\delta E := Cal\cdot dI$ $\delta E = 0.584$ Energy Spread [MeV] $FWHM := \delta E$

$E := Cal\cdot I$ $E = 40.859$ Beam Energy [MeV]

CALCULATION OF ANGULAR STEP FUNCTION

$\delta\theta := \frac{2\cdot\theta_{div}}{n_{max}}$ $\quad \delta\phi := \frac{\phi_{div}}{m_{max}}$ Sets step angle

$\theta_n := -\theta_{div} + \delta\theta\cdot n$ $\quad \phi_m := \delta\phi\cdot m$ Sets range of angles

$\lambda_{L_j} := (f_{start} + \delta\lambda\cdot j)\cdot 10^{-9}$ Emitted wavelength range [m]

CALCULATION OF WIGGLER PARAMETERS

$s := 5$ $\quad dE_s := -\frac{\delta E}{2} + s\cdot\frac{\delta E}{s_{max}}$ $\quad \gamma := \sqrt{\left(\frac{E + dE_s}{E_o}\right)^2 + 1}$ $\quad \alpha_{n,m} := \frac{2^{1.5}\cdot a_w\cdot\gamma\cdot\theta_n\cdot\cos(\phi_m)}{1 + a_w^2 + \gamma^2\cdot(\theta_n)^2}$

$\xi_n := \frac{1}{2}\cdot\frac{a_w^2}{1 + a_w^2 + \gamma^2\cdot(\theta_n)^2}$ $\quad F_n := \sum_m\left[\sum_k(-1)^k\cdot Jn(2\cdot k,\alpha_{n,m})\cdot(Jn(k,\xi_n) - Jn(1+k,\xi_n))\right]^2$

$\lambda_{R_n} := \frac{\lambda_w}{2\cdot(\gamma)^2}\cdot\left[1 + \frac{a_w^2}{2} + (\gamma)^2\cdot(\theta_n)^2\right]$ $\quad d\lambda_{j,n} := \lambda_{L_j} - \lambda_{R_n}$

$I_{j,n} := \frac{e^2\cdot a_w^2\cdot\gamma^2\cdot N_w^2}{2\cdot\pi\cdot\varepsilon_o\cdot c\cdot\left[1 + \frac{a_w^2}{2} + \gamma^2\cdot(\theta_n)^2\right]^2}\cdot\left[\frac{\sin\left(\pi\cdot N_w\cdot\frac{d\lambda_{j,n}}{\lambda_{R_n}}\right)}{\left(\pi\cdot N_w\cdot\frac{d\lambda_{j,n}}{\lambda_{R_n}}\right)}\right]^2\cdot F_n$ $\quad IP_j := \sum_n I_{j,n}$ $\quad p := \sqrt{\sum_j(IP_j)^2}$ $\quad P0_j := \frac{IP_j}{p}$

$\sum_j(P0_j)^2 = 1$

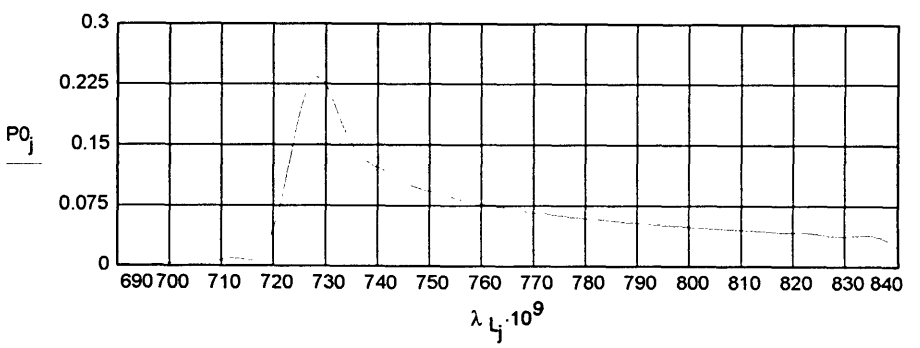

WRITEPRN(angle5) := P0

Due to some programming limitations, we have to manually change the collection angles, writing them in order "Angle0" to "Angle5".

$\theta_{div} \equiv 5\cdot 10^{-3}$ Horizontal Half-angle

BEAM CHARGE CALCULATIONS

This worksheet calculates the beam energy based on the PMT response and tracking losses through the system.

$i_{max} := 30$

$i := 0..i_{max}$ Step Function

$d\lambda := 5$ Wavelength Step

$Lens := .99$ Lens Loss

$BS := .5$ Beam Splitter

$d\theta := 4 \cdot 10^{-3}$ Observation Half-Angle

$T := 20 \cdot 10^{-9}$ Scope Trace Time [sec]

$E := I \cdot dI$ $E = 40.859$

$\gamma := \sqrt{\left(\frac{E}{E_o}\right)^2 + 1}$ $\gamma = 79.965$

$s_{11} := READPRN(cors11)$

$ptot := READPRN(ptot)$

$mirror := READPRN(mirtot)$

$\lambda := READPRN(lambda11)$

$\Omega := 50$ Termination Resistance

$I := 22.75$ Dipole Current Setting [amps]

$dI := 1.796$ Current to MeV Calibration

$F := .9$ Blue Filter Tranmission

$G := 1.7 \cdot 10^5$ Measured PMT Gain @ 1200 V

$V := .990$ Scope Voltage

$E_o := .511$ Electron Rest Energy [MeV]

$d\% := \frac{.02}{i_{max}}$ Quantum Efficiency Slope

$QE_i := .12 - i \cdot d\%$ Quantum Efficiency

$Scale := \frac{87}{.47}$ Scaling Factor for Normalization

$$Q := \frac{V \cdot T}{Lens^4 \cdot F \cdot BS \cdot \left[\frac{d\theta}{\left(\frac{1}{\gamma}\right)}\right]^2 \cdot G \cdot \Omega \cdot d\lambda \cdot \left(\sum_i \frac{s_{11_i}}{Scale} \cdot QE_i \cdot mirror_i\right)} \cdot 10^{12}$$

Q = 7.683 pico-coulombs

A note of explaination is required. Ideally, we want the PMT to be right next to the wiggler as the light comes out. The next best thing is to place the PMT in the optical path, which we've done, track the losses through the system, make the PMT measurements, and adjust the results accordingly.

Worksheet #11, Appendix B

SUMMARY GRAPHICS WORKSHEET

This worksheet is a summary of all graphs. We can see the evolution of Chapter 4.

λ := READPRN(lambda11)

s_{11} := READPRN(s11)

$CorS_{11}$:= READPRN(cors11)

Ideal := READPRN(ideal)

Circ := READPRN(circ)

Gaussian := READPRN(gaussian)

IdealEnergy := READPRN(enideal)

OffAxis := READPRN(offaxis)

i := 0.. length(λ) − 1

OffAxisEn := READPRN(ofaxisen)

OffAxisEnPs := READPRN(ofaxenps)

Angle0 := READPRN(angle0)

Angle1 := READPRN(angle1)

Angle2 := READPRN(angle2)

Angle3 := READPRN(angle3)

Angle4 := READPRN(angle4)

Angle5 := READPRN(angle5)

j := 0.. length(Ideal) − 1

λ_L := READPRN(lam)

Empirical Results

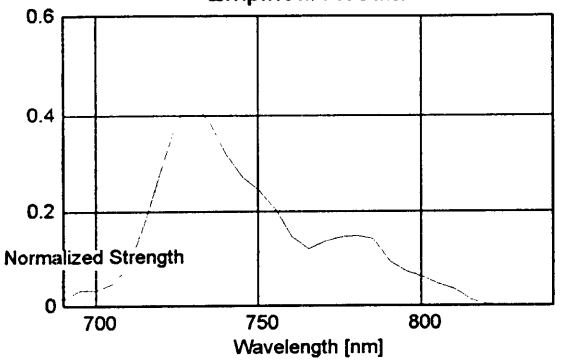

Mirror Corrected Empirical Results

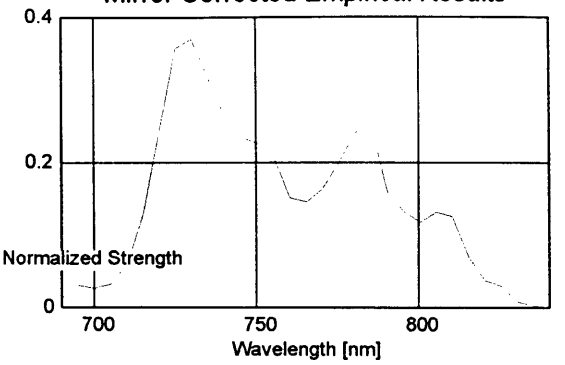

Ideal/Circular/Gaussian Distribution

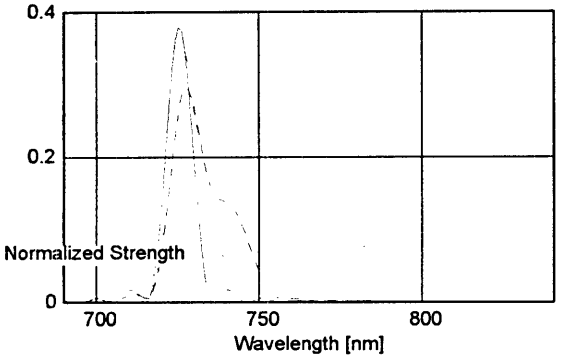

Ideal Spectrum with Energy Spread Effect

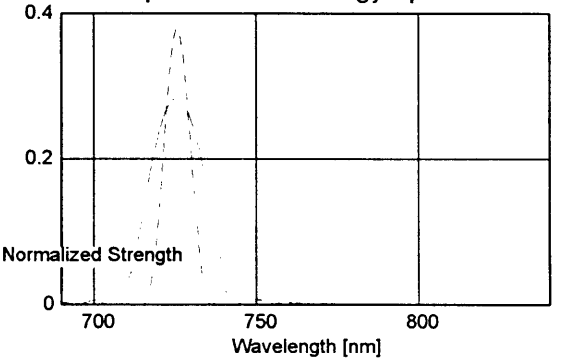

Off-Axis Spectrum w/ No Effects

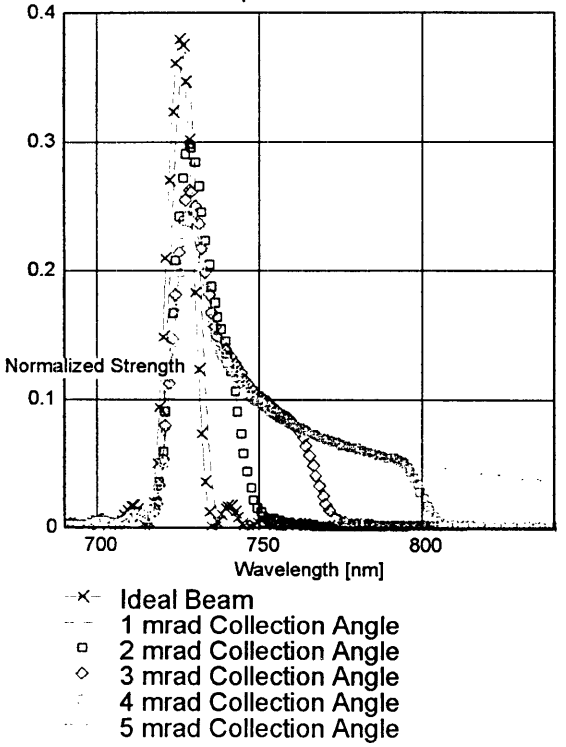

4 mrad Off-Axis w/ Energy Spread

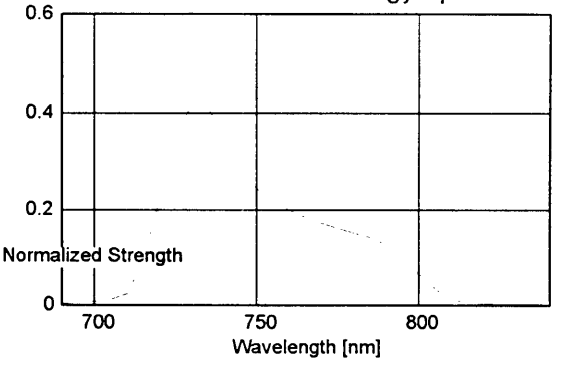

4 mrad Off-Axis w/ Energy & Beam Effects